

OCT 26 1962



Technical Note

98

SYNOPTIC RADIO METEOROLOGY

B. R. BEAN, J. D. HORN,
AND L. P. RIGGS



U. S. DEPARTMENT OF COMMERCE
NATIONAL BUREAU OF STANDARDS

THE NATIONAL BUREAU OF STANDARDS

Functions and Activities

The functions of the National Bureau of Standards are set forth in the Act of Congress, March 3, 1901, as amended by Congress in Public Law 619, 1950. These include the development and maintenance of the national standards of measurement and the provision of means and methods for making measurements consistent with these standards; the determination of physical constants and properties of materials; the development of methods and instruments for testing materials, devices, and structures; advisory services to government agencies on scientific and technical problems; invention and development of devices to serve special needs of the Government, and the development of standard practices, codes, and specifications. The work includes basic and applied research, development, engineering, instrumentation, testing, evaluation, calibration services, and various consultation and information services. Research projects are also performed for other government agencies when the work relates to and supplements the basic program of the Bureau or when the Bureau's unique competence is required. The scope of activities is suggested by the listing of divisions and sections on the inside of the back cover.

Publications

The results of the Bureau's research are published either in the Bureau's own series of publications or in the journals of professional and scientific societies. The Bureau itself publishes three periodicals available from the Government Printing Office: The Journal of Research, published in four quarterly volumes, presents complete scientific and technical papers, the Technical News Bulletin presents summary and preliminary reports on work in progress; and Basic Radio Propagation Predictions provides data for determining the best frequencies to use for radio communications throughout the world. There are also five series of non-periodical publications: Monographs, Applied Mathematics Series, Handbooks, Miscellaneous Publications, and Technical Notes.

A complete listing of the Bureau's publications can be found in National Bureau of Standards Circular 460, Publications of the National Bureau of Standards, 1901 to June 1947 (\$1.25), and the Supplement to National Bureau of Standards Circular 460, July 1947 to June 1957 (\$1.50), and Miscellaneous Publication 160, July 1957 to June 1960 (Includes Titles of Papers Published in Outside Journals 1950 to 1959) \$2.00, available from the Superintendent of Documents, Government Printing Office, Washington 25, D. C.

NATIONAL BUREAU OF STANDARDS

Technical Note

98

OCTOBER 1962

SYNOPTIC RADIO METEOROLOGY

B. R. Bean, J. D. Horn, and L. P. Riggs

NBS Boulder Laboratories
Boulder, Colorado

NBS Technical Notes are designed to supplement the Bureau's regular publications program. They provide a means for making available scientific data that are of transient or limited interest. Technical Notes may be listed or referred to in the open literature.

Contents

	Page
ABSTRACT	iv
1. Introduction	1
2. Background	1
3. Refractive Index Parameters	11
4. A Synoptic Illustration	16
5. Surface Analysis in Terms of N_o	18
6. Constant Pressure Chart Analysis	21
7. Vertical Distribution of the Refractive Index Using A Units . .	22
8. Summary	25
References	27

ABSTRACT

A survey of some of the advances in the field of synoptic radio meteorology is presented. The development of representative refractive index profiles for major air mass types is reviewed. Included is a description of several refractive index parameters currently in use by radio meteorologists. Two reduced-to-sea-level index forms developed at the National Bureau of Standards are used to illustrate the three-dimensional structure of a broad-scale storm system traversing the North American continent.

SYNOPTIC RADIO METEOROLOGY

B. R. Bean, J. D. Horn, and L. P. Riggs

1. Introduction

The variation of refractive index structure in the troposphere may be related to synoptic tropospheric disturbances. Within the scope of the synoptic field are time-wise and space-wise variations in the atmosphere from microscale fluctuations to broad-scale systems of continental dimensions.

The microscale fluctuations of the refractive index are those that one would expect to observe at a particular point along a radio path. They reflect detailed terrain and weather conditions in the immediate vicinity of the transmitter or receiver site.

Mesoscale variations, by way of contrast, are those which cover tens of kilometers and thus encompass a substantial portion of a radio path. Examples of this type of variation are land-sea breeze effects and convection cells of thunderstorm activity.

Large-scale weather systems, affecting vast areas, perhaps even on a continental scale, fall under the classification of macroscale variation. Examples of this type of activity in the atmosphere are sweeping air mass changes and frontal systems traversing thousands of kilometers on the earth's surface. A detailed analysis of such a system is given as an illustration later in this technical note.

2. Background

The radio refractive index, n , may be defined in terms of its scaled-up value, $N = (n-1)10^6$, from the Smith-Weintraub relation [1953]:

$$N = \frac{77.6}{T} \left(P + \frac{4810 e}{T} \right), \quad (1)$$

where P is the observed pressure in millibars (mb),

T is the observed temperature in $^{\circ}\text{K}$, and

e is the partial pressure of water vapor in mb. The Smith-Weintraub constants yield an overall accuracy of ± 0.5 percent in N for the frequency range 30 Mc - 30 kMc. For practical work in radio meteorological studies, (1) may be simplified to a two-term expression

$$N = D + W, \quad (2)$$

where D, the "dry term", is given by

$$D = 77.6 \frac{P}{T} \quad (3)$$

and W, the "wet term", by

$$W = 3.73 \times 10^5 \frac{e}{T^2} . \quad (4)$$

The problem of determining the vertical and horizontal distribution of the radio refractive index has engaged the attention of radio meteorologists for the better part of two decades [Sheppard, 1946; Gerson, 1948; Perlat, 1948; Randall, 1954; Misme, 1957; Hay, 1958].

By analysis of current synoptic conditions from standard weather charts, one may ascertain the characteristics of an air mass appearing over a given region and, likewise, may predict with reasonable accuracy the air mass type and consequent changes in atmospheric structure expected over a particular locale in, say, 24 hours. Then, from a knowledge of air mass profile characteristics [Bean, Horn, and Riggs, 1959] one may estimate the departures of refractive index (and radio ray bending) from normal for a certain region. The bending predictions permit an estimate of refraction errors and the introduction of appropriate corrections for radio range and elevation angle errors in radio navigational equipment.

VHF-UHF radio field strengths beyond the normal radio horizon will also differ from air mass to air mass. It has been known for many years that the seasonal cycle of VHF radio field strengths received far beyond the normal radio horizon was correlated with the refractive index [Pickard and Stetson, 1950a; b; Bean, 1956; Onoe, 1958] and that significant changes in field strength level are observed from air mass to air mass [Hull, 1935; 1937; England, Crawford, and Mumford, 1938]. Speaking about signal level on a 60 Mc/s beyond-the-horizon radio path near Boston, Massachusetts, Hull [1935] states that during the winter low signal levels prevail during the presence over the path of fresh polar air. Periods of high signal level occur when a cold, dry polar air mass is overrun by warm, moist air of tropical maritime origin. Hull's analysis represents early recognition of refraction and reflection phenomena on a synoptic scale. Later work on seasonal changes of fields and N represents, in a way, a summary of synoptic conditions over a period of time. Gerson [1948] was one of the first to consider the variation of the radio refractive index, n , in terms of seasonal and air mass changes. Gerson divided n into two parts, one density-sensitive and the other moisture-sensitive. This division is equivalent to the wet- and dry-term separation of $N = (D + W)$ in equation (2). Gerson was able to measure seasonal thermal changes by variation in the dry term and seasonal moisture changes by observed variation in the wet term. His graphs show a sinusoidal variation of the dry term with a warm season trough and a cool season crest, indicating density changes in inverse proportion to the temperature. The wet term component of n , on the other hand, was observed to attain its maximum during the warm season when the dry term was at its minimum. In arctic and antarctic locales the surface variation of the wet term was found to be quite small, while in temperate and tropical climates there was a sizable annual variation of the moisture

component. Yerg in 1950 showed that even during the long cold arctic night vertical variations in moisture made significant contributions to the N profile. Apparent ducting gradients, obtained by neglecting the wet term at low temperatures, may in actuality be only slightly more refractive than standard.

Continuing his investigation, Gerson next turned to the analysis of refractive index changes within various air masses. Using air mass data available in the meteorological literature of the day, he charted mean refractive index profiles for different air mass types. The largest initial values and also the largest vertical gradients of n occurred with tropical maritime air. The air mass with the weakest gradients and, therefore, the poorest refraction properties was found to be the polar continental type. Common to all of Gerson's air mass refractive index graphs is an approximately exponential decrease of n with respect to height. In 1933 Schelleng, Burrows, and Ferrell attempted to remove this systematic n -decrease with height by utilizing a correction factor of linear form. However, this method of correction leads to serious over-estimation of refraction effects that becomes steadily more pronounced within increasing altitude (in the more modern problem of satellite telecommunications). [Bean, 1962]

The work of Hay [1958] confirmed and extended the observations Gerson had made concerning air mass profiles. Measuring air mass characteristics at Maniwaki, Quebec, Hay concluded that each large-scale air mass type in central Canada had a distinctive refractive index profile. Hay determined the height distribution of N for four basic air masses by fitting a second degree polynomial to each of the four sets of air mass data, indicating that an average N profile cannot be approximated effectively by a linear curve except over small height increments. Hay obtained further discrimination by constructing a "dry-term" curve for

each air mass. The dry-term curves display a smaller standard deviation than the total N curves for all air masses except the continental arctic, which is normally very dry. The largest variations in total N are due to fluctuations in the wet term. The saturation vapor pressure is approximately an exponential function of the temperature, so that during the warm season normal temperature changes cause the saturation vapor pressure, and therefore the wet term, to vary sharply.

Hay's discussion [1958] of the use of N profiles to estimate correction for radio ray refraction includes a table of mean effective earth's radius factors calculated within 95 percent probability limits for each of four air masses.

Misme [1957] has studied synoptic radio meteorology in connection with telecommunications networks in France and North Africa. His discussions include considerations of vertical gradients of the refractive index and atmospheric reflection of radio waves.

A reasonable question at this point is to what extent are model exponential atmospheres applicable to various climatic zones around the earth. While it is readily apparent that individual profiles vary widely from any sort of exponential norm, there is an increasing amount of experimental evidence [Misme, Bean, and Thayer, 1960] which shows that long-term averages of synoptic refractive index variations do tend toward an exponential form with respect to height. Indeed, the five-year mean N profiles of figures 1 and 2, representing arctic and tropical climates respectively, bear out this contention by showing close agreement with models developed from mid-latitude data. The examples verify the results obtained by Gerson [1948] for various air masses.

In 1954 Randall investigated the relationship of surface meteorological data to surface N (N_s) and to field strength in the FM frequency band. The results described were drawn from a very limited data sample that

covered less than a month during the summer of 1947. Within the framework of this specialized study, however, Randall found that polar continental air masses were associated with low field strengths and low N_s , while tropical maritime air masses were associated with high field strengths and high N_s , as shown in figure 3. Randall advanced the hypothesis that the observed field strength changes were due to the existence of characteristic N profiles typical of each air mass type. Randall was curious also as to the behavior of N and radio fields during the passage of fronts and squall lines. Figure 4 shows the results of his investigation and indicates that definite field strength changes may occur during frontal and squall line passage. Caution should again follow in the interpretation of these results since they represent but a single example of frontal and squall line passage.

Gray [1957] made studies of the correlation of N and the gradient of N with path losses at UHF frequencies for observing points representative of various climatic areas around the world and concluded that changes in trans-horizon telecommunications were strongly dependent on atmospheric changes.

Recently Gray [1961] considered radio propagation and related meteorological conditions over the Caribbean Sea. Utilizing the effective earth's radius factor as a representative index, he developed an empirical curve of annual median scatter loss versus effective propagation distance for both Caribbean and temperate regions. Effective distance as defined by Gray is the angular distance in radians multiplied by the radius of the earth modified for normal refraction. Gray reports that the refractive gradient in the first 100 meters is in general the determining factor in median scatter loss for transhorizon telecommunications, as one would expect from earlier refraction studies [Bean and Thayer, 1959a].

Other studies on refraction problems during the past decade have led to systematic computation of refraction effects, and to significant applications such as the evaluation of radar elevation angle errors in differing air masses and climates [Schulkin, 1952; Fannin and Jehn, 1957]. Schulkin advanced a practical and very fundamental method for numerical calculation of atmospheric refraction (radio ray bending) from radiosonde data. Figure 5, after Schulkin, gives mean angular bendings for radio rays passing completely through the earth's atmosphere for two extremes of air mass type. Fannin and Jehn concluded that a particular refractive index profile depends on air mass type and the climatic controls of season and latitude. Their conclusion was substantiated by mean N profiles for thirty-four weather observing sites located in or near four distinct air mass source regions about the world. These data show that a definite difference does exist in the profiles of various air masses. Refraction effects were found to be largest in tropical maritime air masses, intermediate in polar continental and polar maritime, and least in tropical continental air masses. Fannin and Jehn also published graphs showing day-to-day variations in profiles (representing the effects of air mass changes over a given observing station) and graphs of diurnal profile variations.

Bean, Horn, and Riggs [1960] demonstrated that radio ray refraction within the lower layers of an air mass is mirrored by the difference between the observed refractive index structure and that of a standard atmosphere. Figure 6 shows a graph of bending, τ , plotted with a modified refractive index profile representative of summertime tropical maritime air. It is apparent that near the ground bending departures reflect refractive index profile departures from standard. Figure 7 presents a series of graphs of departures of refractive index and bending from normal for each air mass and emphasizes the close relation between the two. This affords the synoptic radio meteorologist a set of standard reference profiles for

the study of a given air mass or the confluence of contrasting air masses at a frontal zone.

Arvola [1957] discussed the changes in refractive index profiles caused by migratory weather systems. He examined a series of synoptic situations that gave rise to greater-than-normal refraction in the mid-western portion of the United States during November, 1951. Ridges and accompanying subsidence effects generally gave rise to strong N gradients and enhanced signal strength over a 200 km link broadcasting at 71.75 Mc. Refractive gradients were stronger in the warmer air masses and at the times when moist air was present below the inversion created by the subsidence mechanism. Strong gradients which appeared behind a squall line later weakened with the approach of a cold front. After the passage of this front, stratification in the cold air again increased the gradient.

Subsequent investigations of polar continental air across central North America have made use of reduced-to-sea-level forms of the radio refractive index as synoptic parameters. The reduced forms are sensitive indicators of synoptic changes and afford a clearer picture of storm structure than that obtained using analyses in terms of unreduced N or B units (defined by equation 6).

Jehn [1960a] at the University of Texas used a form of the potential refractive modulus, ϕ , (see equation 11) developed by Lukes [1944] and Katz [1951] to account for the height dependence feature of the refractive index. (When referenced to the 1000 mb level, ϕ is termed K by Jehn.) Articles by Jehn on synoptic climatology in 1960 [b] and 1961 use composite analysis techniques to study the synoptic properties of the Texas-Gulf cyclone and the Central-United-States type of cold outbreak.

In another application of the potential refractive modulus, Flavell and Lane [1962] utilized Katz's K unit to study tropospheric wave propagation

Field strength measurements on VHF-UHF transhorizon radio links over the British Isles were analyzed with cross sections in terms of K and regional charts of ΔK (the difference between K at the surface and at the 850 mb level). These charts show features similar to those obtained by the use of N_o or A , as defined by equations 5 and 7 respectively.

Flavell and Lane recorded a series of measurements on a 500 km path at 877 Mc on which the received signal was ordinarily below the noise level. The singular occasions on which the received signal could be measured at the normal times of radiosonde ascent all exhibited a symmetric variation of ΔK over the transmission path. These results lend credence to the hypothesis that synoptic disturbances play an important role in transhorizon telecommunications.

Moler and Arvola [1956] advanced the hypothesis that the vertical gradient of the refractive index is affected by broad-scale vertical motion in the troposphere and suggested that moisture and temperature stratification is modified principally by changes in vertical velocity. This latter work was extended [Moler and Holden, 1960] by a study of mesoscale centers of horizontal air mass convergence and divergence in the troposphere. Horizontal convergence takes place in a low pressure area, where the winds around the low have a predominant component toward a local vortex at the center. Upward vertical motion results from the pile-up of air in the vortex region. In a high pressure area winds have a predominant component away from the center of the high (divergence) and subsiding air descending from higher levels takes the place of air transported outward from the center. Local convergence implies upward vertical motion in the lower levels of the troposphere, while local divergence implies downward vertical motion in the lower levels. It follows that local convergence centers (small-scale low pressure cells) produce updrafts in the atmosphere that result in considerable mixing and the destruction

of atmospheric layers. Centers of divergence (small-scale high pressure cells) create strong temperature and humidity inversions by the motion of subsiding air. Such inversions produce large vertical refractive index gradients that partially reflect microwaves traveling through this meteorological environment [Gossard and Anderson, 1956]. In a well-mixed atmosphere, on the other hand, the primary propagation mechanism is believed to be scattering by turbulent fluctuations of the refractive index [Megaw, 1950; Booker and Gordon, 1950].

Sea level measurements studied by Moler and Holden [1960] showed N_s to be essentially invariant during the period of observation, yet signal levels varied by more than 60 db. Since scattering theory would account for a rise in signal level of only about 13 db, Moler and Holden concluded that refractive layering and thermal stability over the oceans, principally functions of vertical wind velocities, contribute significantly to the high signal levels. These conclusions are similar to the findings of Saxton [1951] and Flavell and Lane [1962] that high signal levels from a distant transmitter may well be the consequence of refractive layering and subsequent reflection of radio energy by turbulent eddies and the effects of superrefraction of radio waves produced by departures from normal of the height variation of the tropospheric refractive index.

A knowledge of the vertical motion of the atmosphere becomes at this point central to the problem of refractive layering. The relative magnitude and direction of the vertical component of the wind velocity may be estimated by a method outlined by Moler and Holden [1960].

In the same article Moler and Holden give a description of the large signal enhancement and deep fading that occurs as the propagation mechanism varies between partial reflection and scattering on a trans-horizon radio path along the California coastline. Reflection occurs when strong refracting layers are present within a kilometer of the surface,

typifying meteorological conditions generally associated with the subsidence inversion frequently found along the California coast.

Figure 8 shows the sea level pressure chart and a series of streamline analyses by Moler and Holden depicting mesoscale centers of convergence and divergence for a day in March along the southern California coast. Figure 9 shows the X-band signal level received at Point Loma, San Diego (SD) from Santa Barbara (SB) during the same day. As the centers of convergence along the radio path weaken, refractive layers are formed and the signal level rises sharply during the middle of the day. Later the signal level lowers again with the regeneration of convergence centers and the destruction of stratified layers during the afternoon hours.

3. Refractive Index Parameters

Later in this Technical Note the analysis of a synoptic disturbance in the troposphere will be described in detail. Certain reduced forms of the refractive index that will be useful in the ensuing discussion will be developed here.

Figure 10 shows contours of the mean value of N at the surface, N_s , determined from eight years of data for August, 0200 local time. Miniature circles indicate the sixty-two observing stations from which N data were available. It is evident that coastal areas display high values of N_s as compared with inland locations. Low values of N_s are apparent along the Appalachian mountain chain and in the great mountain systems and intermountain plateaus of the western United States. There is a marked similarity between the N_s contours on figure 10 and the elevation contours of figure 11. N_s , as a sensitive indicator of changes in atmospheric density, displays a strong elevation dependence. To remove this effect a reduced-to-sea-level expression, N_o , is introduced:

$$N_o = N_s \exp \frac{z}{H^*} , \quad (5)$$

where z is height in km and $H^* = 7.0$ km is the scaled height. Scale height is the height at which the mean value of N has decreased to a fraction, $1/e$, of its initial value where

$$e = 1 + \frac{1}{1!} + \frac{1}{2!} + \dots \doteq 2.71828 \dots$$

A scale height of 7.0 km is in close agreement with $H^* = 7.01$ km for the NACA standard atmosphere with 80 percent relative humidity and $H^* = 6.95$ km obtained from climatic studies utilizing over two million observations of the variation in N over the first km above the surface of the earth [Bean and Thayer, 1959a]. The N_o contours of figure 12 utilize the same data as figure 10. The use of N_o produces a simpler map with a smaller range of variation. Additionally, N_s may easily be estimated from the smooth and slowly-varying contours of N_o if the station elevation is known. Numerous tests have shown that N_s may be more accurately estimated from charts of N_o than from charts of N_s itself, by a factor of four or five to one [Bean, Horn, and Ozanich, 1960].

The attempt to find a workable method to compensate for the decrease of N with increasing height has brought about the development of various model atmospheres. [Bean and Thayer, 1959a; Bean, 1962.] Specifically, CRPL model refractive index atmospheres were developed by Bean and Thayer in 1959 [a]. The steps in this development that are relevant to synoptic studies are outlined briefly.

Vertical refractive index cross sections are standard working charts for synoptic studies. Such charts constructed from observed values of N suffer from a serious shortcoming in that the natural decrease of N with respect to height effectively masks contrasts between air masses in the lower troposphere. An idealized synoptic example depicting the confluence of contrasting air masses is presented in figures 13 and 14.

When these idealized systems are analyzed in terms of N as in figures 15 and 16, the most prominent feature is the laminar structure of the N field.

Early attempts to compensate for the decrease of N with increasing height used the constant gradient of the effective earth's radius theory, $1/4a$, where a is the radius of the earth. As an illustration, the strong elevated layer found during the summer in southern California was studied in terms of a linearly-corrected expression, B, given by

$$B = N(z) + (39.2)z, \quad (6)$$

where $N(z)$ is the value of N at height z in kilometers [Smyth and Trolese, 1947]. Since N tends to be an exponential function of height rather than the linear function assumed by the effective earth's radius theory, the B-unit approach overcorrects when z is greater than about one km. This point is illustrated by figures 17 and 18, where the N data of figures 15 and 16 are plotted in terms of B units. Note that the overcorrection produces a cross-section in which N increases with height from a value of 310 at the surface to 360 at 5 kilometers. A function of exponential form was designed to account for the systematic decay of density with height that characterizes the terrestrial atmosphere, as given by [Bean, Riggs, and Horn, 1959]

$$A = N(z) + 313 \left[1 - \left\{ \exp \left(-\frac{z}{7.0} \right) \right\} \right]. \quad (7)$$

The quantity A enables one to discern departures of N structure from the model atmosphere

$$N = 313 \exp \left\{ -\frac{z}{7.0} \right\}. \quad (8)$$

Further, the radio-ray bending,

$$\tau_{1,2} \doteq - \int_{n_1}^{n_2} \cot \theta \, dN \cdot 10^{-6}, \quad (9)$$

where θ is the local elevation angle of the radio ray to spherically stratified surfaces of constant N , may be approximated by [Bean and Dutton, 1960]

$$\tau_{1,2} \doteq - \int \frac{\cot \theta (10^{-6})}{n} dA(z, 313) + \tau(z, 313). \quad (10)$$

The term $\tau(z, 313)$ is the bending in the average atmosphere given by (8), while the integral term represents the departures in bending produced by various synoptic and air mass effects. The values of bending in the average atmosphere are tabulated [Bean and Thayer, 1959b] and approximate methods of calculating the integral term in (10) to within a few percent have been given [Bean and Dutton, 1960].

In figures 19 and 20 the frontal cross sections, previously analyzed in terms of N and B , are plotted in A units. The range of refractivity values on the new charts is reduced from more than 60 to about 25 N units, and a pattern emerges that displays sharp contrasts for air mass differences associated with the frontal zone. Note that for the warm front case (figure 20) the A values increase with height until they reach a maximum associated with the upgliding warm moist air overriding the frontal surface. The region of precipitation in advance of the front is shown as an area of high surface N . In the cold front case (figure 19) the push of warm air aloft by the encroaching cold air is evidenced by the "dome" of high A value just before the front. Stratification in the cold air due to inversion effects, although impossible to detect in the N charts, is clearly shown on the A unit charts.

" A " units are used in subsequent cross-section analyses presented in this article in order to throw frontal discontinuities and air mass differences into sharp relief. The Potential Refractivity Chart of figure 21 facilitates the rapid conversion of N to A . This simplification eliminates the necessity of using exponential tables for each individual calculation

of A and thus lends considerable ease to the preparation of charts of the new parameter. The N_o and A corrections do substantially the same thing; the primary distinction is that A is a non-linear "add-on" correction while N_o is a multiplicative one. The disparity between N_o and A is tabulated in table I.

Table I

Differences Between N_o and A at Various Elevations ($N_o - A$)

Elevation (km)	Value of N at z = 0				
	250	300	313	350	400
1	-10	-2	0	5	13
2	-21	-5	0	7	29
3	-49	-22	0	5	31
4	-48	-29	0	30	68

These figures were obtained by taking the value of A (for example, 300), subtracting the "add-on" correction for, say, 3 km ($300 - 109 = 191$) and "reducing" this number ($N = 191$) to zero elevation by the N_o "reduction",

$$N_o = N \exp \left(\frac{3}{7} \right).$$

The $N = 313$ exponential atmosphere is adopted for a single reference atmosphere. The large discrepancies of table I may be avoided for practical applications by choosing a model near the mean value of N for the site under study.

The A unit has the additional advantage that while it is a convenient method for height reduction the ray bending is also readily recoverable from it, requiring only a knowledge of the altitude of the observed refractive index measurement and the local elevation angle of the radio ray. The potential refractive modulus of I. Katz [1951],

$$\phi = \frac{c}{\theta} \left[P_o + b \frac{e_o}{\theta} \right], \tag{11}$$

where θ is the potential temperature and e_0 the potential vapor pressure, is also in current use. The values of b and c of equation (11) are the Smith-Weintraub [1953] constants, $b = 4810$ and $c = 77.6$. The potential refractive modulus has been employed by Jehn [1960] to study polar waves over North America. N cannot accurately be recovered from ϕ for bending calculations unless additional information is available: namely, observed temperature and vapor pressure. The concept of the potential refractive modulus arose out of the earlier refractive modulus, M , [Kerr, 1951] which is defined by

$$M = \left[n - 1 + \frac{z}{a} \right] \times 10^6 = N(z) + \left[\frac{z}{a} \right] \times 10^6, \quad (12)$$

where z = height above the earth's surface and a = earth's radius.

The M unit came into being out of an approach similar to that which led to the development of the B unit. The condition $\frac{dn}{dz} = -\frac{1}{a}$ (a radio duct) implies an effective earth of infinite radius (effective earth's radius factor, $k = \infty$) [Schelleng, Burrows, and Ferrell, 1933]. The M unit is designed so that $\frac{dM}{dz} = 0$ when $k = \infty$. M units are employed from time to time in radio meteorological analysis. The Canterbury Project [1951], for example, used M unit analyses in the study of ranges of over-water radar signals near New Zealand.

4. A Synoptic Illustration

The specialized field of synoptic radio meteorology attempts a description of the variations in atmospheric refraction that arise from large scale weather changes such as the passage of a polar front or the movement of an air mass over a particular geographic region. The term air mass is used to describe a portion of the troposphere that has at the surface generally homogeneous properties. Although no air mass is in fact homogeneous, the advantages of the air mass concept as a convenient fiction are evident in the cataloguing of meteorological observations

for climatic or synoptic purposes.

The region of interaction between the cold air of the poles and the warm air of the tropics is referred to as the polar front and is generally located between 30° and 60° N or S. From time to time a section of the polar front is displaced poleward by a flow of warm tropical air while an adjacent section is simultaneously displaced toward the equator by a flow of polar air. The interaction of the flow of polar and tropical air results in the formation of a "wave" that moves along the polar front, often for thousands of kilometers. An example of a fully developed polar front wave is shown in figure 22(a), as it might appear on a weather map. Across the Great Plains and eastern seaboard of the United States the polar front wave normally moves along the line AB in figure 22(a). An idealized space cross section along the line AB is shown in figure 22(b). The warm tropical air that flows into the warm sector of the wave overrides the cool air before the wave to form the transition zone denoted as a warm front. The cold front represents the transition between the generally humid air of the warm sector that has been forced upward and the advancing cold polar air. Squall lines are drawn to represent belts of vigorous vertical convection, intense thunder showers, and sharp wind shifts that frequently precede fast-moving cold fronts. The fronts shown on a daily weather map represent the ground intersection of the transition zones between various air masses.*

As a representative example of the application of refractive index parameters to a synoptic situation, a large-scale outbreak of continental polar air which occurred over the U. S. during February, 1952, was

* A critical appraisal of recent meteorological thinking on fronts, air masses, squall lines, etc., is given in Dynamic Meteorology and Weather Forecasting, by Godske, Bergeron, Bjerknes, and Bundgaard, American Meteorological Society and Carnegie Institute of Washington, D. C., 1957.

analyzed in terms of N_0 and A [Bean and Riggs, 1959; Bean, Riggs, and Horn, 1959].

For this synoptic illustration the reduced expression, N_0 , was used in preparing constant level charts of the storm at the same levels and times as those used in the daily weather map series of the U. S. Weather Bureau. The A unit, on the other hand, was employed to construct vertical cross sections through the frontal system to give a three-dimensional picture of the synoptic changes taking place.

5. Surface Analysis in Terms of N_0

A pronounced cold front developed and moved rapidly across the central and eastern United States during the period 18 to 21 February 1952.

Prior to February 18, a polar maritime air mass had been moving slowly eastward across the Great Basin and Rocky Mountain regions. This system included a slow-moving cold front extending from northern Utah southward into Arizona, and a quasi-stationary front extending northeastward into Wyoming. With the outbreak of polar continental air east of the Rocky Mountains, the maritime front became more active and, as it moved ahead of the fast-moving polar continental front sweeping across the Great Plains, was reported as a squall line by the time it crossed the Mississippi River early on the morning of the 20th of February. During the later stages of the storm system, the polar maritime cold front-squall line was located in the developing warm sector of the polar front wave. The entire ensemble of cold front, polar front wave and squall line then moved rapidly to the east coast by the morning of the 21st, thus completing the sequence.

Charts of N_0 were prepared from Weather Bureau surface observations taken at twelve-hour intervals from 0130 EST, February 18th until 0130 EST, February 21st, 1952, or, in other words, the period of

time that it took the polar front wave to develop and move across the country. The synoptic sequence is seen in figures 23 through 29 where contours of N_o are derived for various stages of the storm and compared to the superimposed Weather Bureau frontal analysis. The same procedure of comparing derived contours with the existing frontal pattern was followed throughout the example. Observations from sixty-two weather stations were used in preparing the surface weather maps. Figure 23 indicates that the cold front extending from Utah southward displays weak N_o changes across the frontal interface. In the early stages of the sequence (figures 23 and 24) this lack of air mass contrast is evidenced in another way by the slight change of the position of the $N_o = 290$ contour encircling west Texas and New Mexico as the frontal system moves through that area.

By comparison, the cold front sweeping down across the Great Plains (figures 24 to 26) has a rather marked N_o gradient across the front, due in large measure to the northward flow of warm, moist air that forms a definite warm sector by 1330 EST on the 19th. It is perhaps significant that the N_o contours indicate that the various frontal systems are transition zones rather than the sharply defined discontinuities of textbook examples, a point that has been enlarged upon by Palmer [1957].

Figures 26 to 29 trace the course of this vigorous push of cold air across the Gulf Coastal Plain and the southeastern states. The most spectacular gradients on this map series are in the eastern half of Texas where the marked contrast of cold, dry polar air of low N_o and warm moist Gulf air of very high N_o occurs. A prominent feature of meteorological significance in figures 24 to 27 is the northward advection of tropical maritime air in the warm sector ahead of the cold front. The advection is evidenced by the northward bulge of high N_o over the Mississippi Valley on these charts. Figure 29 shows the synoptic situation as the front moves off the Atlantic Coast and refractivity gradients across

the continent gradually weaken.

The variation of N_o due to the passage of the frontal system can be seen in figures 30 to 34, where the 24-hour changes of N_o are shown. The 24-hour change, designated ΔN_o , is obtained by subtracting the value of N_o observed 24 hours ago from the current value. The change is determined on a 24-hour basis in order to remove effects of the diurnal cycle of N_o . The ΔN_o charts show a general rise of N_o in the warm sector and a drop in N_o behind the front, amounting, in the warm sector, to 35 to 40 N units by 1330 EST on the 20th of February (figure 33) accompanied by a 40 to 50 N unit drop behind the front.

The relative sensitivity of N_o to humidity changes is emphasized by the ΔN_o charts. The N drop behind the cold front occurs in a region of increasing pressure and decreasing temperature -- a combination that increases the dry term and depresses the wet term of the refractive index (see equation 2). The decrease in the wet term from the rapidly dropping dewpoint more than compensates for the increased dry term. As an example, in the 24-hour period ending 0130 EST on the 19th the station pressure at Oklahoma City increased 13 millibars. The dry term increased 12 N units while the wet term dropped 42 N units, giving a net change of minus 30 N units. This N_o rise in the warm sector and drop behind the cold front is consistent throughout the development of this polar front wave. The present system had about a 35 N unit rise and a 40 N unit drop. This general pattern might be expected to occur in all fast-moving cold fronts, with varying intensity depending upon the individual synoptic pattern. In any case, it appears that the N_o pattern is a sufficiently stable and conservative property of the atmosphere so that it should be possible to develop forecasting rules for N_o but not, of course, without the analysis of many more N patterns.

6. Constant Pressure Chart Analysis

The same frontal system (February 18-21, 1952) was analyzed for selected constant pressure levels. The 850 millibar (mb) charts (about 5,000 feet above mean sea level) and the 700 mb charts (about 10,000 feet above mean sea level) were prepared for the times of radiosonde ascent (10 A.M. and 10 P.M. EST) throughout the synoptic sequence from the radiosonde reports of 43 U.S. sounding stations. It is not necessary to reduce the 850 mb or 700 mb level data since they are referenced by definition to the indicated constant pressure level. Contours for the charts aloft are shown in figures 35 to 40 while their respective 24-hour changes, N_{850} and N_{700} , are given in figures 41 to 44.

The N_{850} charts show that the northerly flow of warm humid air within the warm sector that was so prominent on the N_0 maps is also clearly in evidence at the 850 mb level. Further, a change pattern similar to that on the N_0 maps is also observed at the 850 mb level, particularly in figure 43. That is, a rise in N_{850} values in the warm sector and a decrease behind the cold front is apparent. Surprisingly enough, by the time the frontal system was well developed, at 1000 EST on the 20th, the N_{850} values were nearly as large as those on the surface.

The N_{700} charts are more difficult to interpret than those of N_0 or N_{850} . It appears that at this altitude the wet term is usually negligible and N will normally vary inversely as temperature since the pressure is constant at the 700 mb level. By 1000 EST on the 19th (figure 38) an intrusion of low N values is observed in the 700 mb warm sector due to the advection of warm, low-density air northward. The chart for 24 hours later (figure 40) displays two prominent highs in which $N_{700} \doteq 225$. One of these highs lies between the squall line and the cold front and the other just south of the apex of the 700 mb wave. Interestingly enough, these two highs are due to quite different causes. The high centered

over Atlanta appears to have arisen from the unusually high transport of moisture to the 10,000 foot level, since the 700 mb wet term at Atlanta increases from 4.5 to 25 N units in the 24-hour period ending with 1000 EST on the 20th of February. The second high, centered over Omaha, appears to be due to an intense dome of cold air as indicated by the drop of the 700 mb temperature from -7.3°C to -21.4°C in the twelve hours preceding map time. When temperatures are below 0°C the wet term contribution to N is quite small and density changes become significant in producing changes in N. Falling temperatures produce higher density air and, consequently, a region of high N values around Omaha as depicted on the N_{700} chart of figure 40 and ΔN_{700} chart of figure 44, which shows this change more clearly.

7. Vertical Distribution of the Refractive Index Using A Units

The synoptic study of the vertical distribution of the radio refractive index extends the foregoing constant-level analyses by considering the problem of whether the air mass properties associated with this typical wintertime outbreak of polar air are reflected in the vertical refractive index structure. Charts showing the structure of the storm have been prepared using radiosonde measurements from stations located along a line normal to the frontal zone between Glasgow, Montana, and Lake Charles, Louisiana (figure 45). Plots of N versus height along this cross-section line were obtained at 12-hour intervals during a four-day period and converted to A units.

Figure 46 is a sample cross-section along the Glasgow-Lake Charles line analyzed in terms of unmodified N as in the idealized cases of figures 15 and 16. Compare figure 46 with the A unit analysis of figure 52 for the highlighting of air mass differences in refractive index. Examples of the distribution of the N components, temperature and humidity,

around the front are shown in figures 47 and 48. Various stages in the advance of this intense storm system across the continent are shown in figures 49 to 54 in terms of modified N (A units). At the outset of the period of observation (figure 49) the polar front was located over the northern Great Plains between Rapid City, South Dakota, and North Platte, Nebraska. At this time the entire cross section is characterized by weak to moderate gradients of refractivity. In figure 50, twelve hours later, this front had moved some 300 km southward. The contrast of the southward push of polar air and the northerly advection of tropical maritime air from the Gulf of Mexico into the developing warm sector of the polar front wave is evidenced by the relatively large gradients in the neighborhood of Dodge City. The core of tropical maritime air has evidently not progressed far enough northward to displace the warm but dry air that had been over the Great Plains prior to the outbreak, with the result that a region of low A values is found between the front and the tropical maritime air. In figure 51 the effects of the Pacific front are apparent in the build-up of a secondary region of high N some 400 km ahead of the polar front, located at this time over Dodge City. Twelve hours later (figure 52) the core of tropical maritime air has become more extensive and now reaches to a height of 3 km. The second (Pacific) front is picked up now on the cross section and the area of low A values is confined between the two fronts. By 0300 Z on the 20th (figure 53) the polar front is approaching Lake Charles and the Pacific front is reported on the daily weather map as a squall line. Finally, by the morning of February 20th (figure 54) both fronts have passed to the south of Lake Charles and the polar air just behind the front is characterized by relatively low A values.

The use of space cross-sections does not always yield measurements at the most desirable points along a frontal zone. Another method of arriving at the probable refractive index structure about the frontal

interface is to plot radiosonde observations for a single station arranged according to observation times as on figures 55 to 61.

The time cross-section for Glasgow, Montana (figure 55), which is in the cold air behind the polar front for the entire period of observation of the storm, displays gradients of A values that are generally weak. An exception occurs on the evening of the 19th (20/0300Z), apparently as a result of subsidence effects. Rapid City, South Dakota (figure 56), also shows generally weak gradients throughout the cold air behind the front. North Platte, Nebraska (figure 57), exhibits moderate gradients with increasing A-values in the post-frontal higher-density polar air. The wet-term contribution to N at North Platte is insignificant because of the low temperature at this season. Dodge City, Kansas (figure 58), has a warm, dry low ahead of the polar front and increasing A values in the cold air just behind the front. Oklahoma City, Oklahoma (figure 59), represents a classic synoptic situation in which advection of tropical maritime air from the Gulf of Mexico produces a strong high ahead of the front and a low within the cool, dry polar continental air. Again in the region around Little Rock, Arkansas (figure 60), there is warm moist air of extremely high refractivity ahead of the front being replaced by polar continental air of characteristically low A value. The time cross-section for Lake Charles, Louisiana (figure 61), is complex but represents again the same general features: high A values ahead of the front and low values behind.

The time cross-section presentation is referred to as an epoch chart when the observations are normalized with respect to the frontal passage. Thus, as a frontal system advances and passes over a station, one obtains yet another perspective of the space cross-section. Such a

presentation is given in figures 62 to 68. Figure 63 represents a typical continental station located in the polar continental air mass throughout the occurrence of the storm. The essential feature here, as in figure 56, is the absence of detail of A structure due to the presence of a uniform air mass over this station. Compare this figure with the epoch chart for Oklahoma City (figure 66), where the structure of the idealized model is clearly reflected by the prefrontal A-unit high, strong gradient across the frontal zone, and the A-unit low behind the front. This rather fortuitous agreement is felt to be due to the strategic location of Oklahoma City with respect to the motion of contrasting air masses about the polar front. That is, this epoch chart represents a point of confluence of virtually unmodified polar continental and tropical maritime air.

The exponential correction to the refractive index height distribution used in this storm series allows air mass properties to be clearly seen. By use of such an exponential correction one may construct an idealized refractive index field about a frontal transition zone that shows the temperature and humidity contrasts of the different air masses. Further, when this technique is applied to the analysis of a synoptic tropospheric disturbance, it does indeed highlight air mass differences.

8. Summary

With presently-available techniques, field meteorological measurements can be converted to a synoptic refractive index analysis in a few hours. The accuracy of refractive index forecasts depends largely on the adequacy of current synoptic forecasting techniques in predicting the distribution of the common meteorological parameters of pressure, temperature, and relative humidity, since these three variables determine uniquely the N patterns that will exist. It is well known that meteorological forecasting skill drops off quite rapidly with

increasing interval of prognosis. This implies, then, that in certain clear-cut situations over short time periods N patterns and profiles may be predicted with reasonable accuracy. At the outset the use of such a relatively untested device is limited to obvious synoptic situations. Gradual perfection of N forecasting techniques may, at some future date, result in a considerably wider application of N patterns, perhaps even on a regular synoptic basis.

Because of the extent and complexity of the problem, discussion of the relationship between N structure and radio propagation phenomena such as fadeouts, radio ducts and holes, and enhancement of beyond-the-horizon radio fields has been omitted. There is in the literature, however, a large body of evidence supporting a strong correlation between large gradients of N and enhancement of radio fields. The indicated direction of future work is toward the understanding of the interrelation of atmospheric structure and electromagnetic propagation.

Among the plausible avenues for continued research in the field of synoptic radio meteorology is that suggested by the Moler-Holden study on atmospheric circulation. These writers clearly demonstrate a relation between a synoptic situation (a small-scale area of horizontal mass divergence and local downward-directed vertical motion) and enhancement of field strength on a beyond-the-horizon radio link operating over a path through the synoptic feature (evidenced by a high pressure area at the surface). The subsidence mechanism produces an elevated layer that acts to reflect radio energy and consequently enhance the received fields. The Moler-Holden study relates atmospheric structure and electromagnetic fields in a fundamental way and represents a definite step toward a more sophisticated picture of physical processes that change the character of the atmosphere as a propagation medium.

References

- Arvola, W. A., Refractive index profiles and associated synoptic patterns, Bull. Am. Meteor. Soc. 38, No. 4, 212-220 (April, 1957).
- Bean, B. R., Some meteorological effects on scattered radio waves, IRE Trans. PGCS-4, No. 1, 32 (March, 1956).
- Bean, B. R., and E. J. Dutton, On the calculation of the departures of radio wave bending from normal, J. Research NBS, 64D, (Radio Prop.) No. 3, 259-263 (May, 1960).
- Bean, B. R., and J. D. Horn, Radio-refractive-index climate near the ground, J. Research of NBS, 63D, (Radio Prop.) 259-271 (November-December, 1959).
- Bean, B. R., J. D. Horn, and A. M. Ozanich, Jr., Climatic charts and data of the radio refractive index for the United States and the world, NBS Monograph No. 22 (November, 1960).
- Bean, B. R., J. D. Horn, and L. P. Riggs, Refraction of radio waves at low angles within various air masses, J. Geophys. Research 65, 1183 (April, 1960).
- Bean, B. R., and L. P. Riggs, Synoptic variation of the radio refractive index, J. Research NBS, 63D, (Radio Prop.) No. 1, 91-97 (1959).
- Bean, B. R., L. P. Riggs, and J. D. Horn, Synoptic study of the vertical distribution of the radio refractive index, J. Research NBS, 63D, (Radio Prop.) No. 2, 249-258 (September-October, 1959).
- Bean, B. R., and G. D. Thayer, On models of the atmospheric radio refractive index, Proc. IRE, 47, No. 5, 740-755 (May, 1959a).
- Bean, B. R., and G. D. Thayer, CRPL exponential reference atmosphere, NBS Monograph No. 4, (U. S. Government Printing Office, Washington 25, D. C., (October, 1959b).
- Berry, F. A., E. Bollay, and Norman F. Beers, Handbook of Meteorology, page 638 (McGraw-Hill Book Company, Inc., New York, 1945).

- Booker, H. G., and W. E. Gordon, A theory of radio scattering in the troposphere, Proc. IRE, 38, 401-412 (April, 1950).
- Byers, H. B., General Meteorology, page 327 (McGraw-Hill Book Company Inc., New York, 1944).
- England, C. R., A. B. Crawford, and W. W. Mumford, Ultra-short-wave radio transmission through the non-homogeneous troposphere, Bull. Am. Meteor. Soc., 19, (1938).
- Fannin, B. M., and K. H. Jehn, A study of radio elevation angle error due to atmospheric refraction, Trans. IRE, AP-2, No. 1, 71-77 (1957).
- Flavell, R. G., and J. A. Lane, The application of potential refractive index in tropospheric wave propagation, J. of Atmospheric and Terres. Phys., 24, 47-56 (1962).
- Gerson, N. C., Variations in the index of refraction of the atmosphere, Geofisica Pura E Applicata 13, 88 (1948).
- Godske, C. C., T. Bergeron, J. Bjerknes, and R. C. Bundgaard, Dynamic Meteorology and Weather Forecasting, page 526 (American Meteorological Society and Carnegie Institute of Washington, D. C., 1957).
- Gray, R. E., The refractive index of the atmosphere as a factor in tropospheric propagation far beyond the horizon, IRE National Convention Record, Part 1, page 3 (1957).
- Gray, R. E., Tropospheric scatter propagation and meteorological conditions in the Caribbean, IRE Transactions on Antennas and Propagation, AP-9, No. 5, 492-496 (September, 1961).
- Hay, D. R., Air-mass refractivity in central Canada, Can. J. Phys., 36, 1678-1683 (1958).
- Hull, R. A., Air-mass conditions and the bending of ultra-high-frequency waves, QST 19, 13-18 (1935).
- Hull, R. A., Air-wave bending of ultra-high-frequency waves, QST, 21, 16-18 (1937).

- Jehn, K. H., The use of potential refractive index in synoptic-scale radio meteorology, *J. Meteorology*, 17, 264 (June, 1960a).
- Jehn, K. H., Microwave refractive index distributions associated with the Texas-Gulf cyclone, *AMS Bulletin*, 41, 304-312 (June, 1960b).
- Jehn, K. H., Microwave refractive-index distributions associated with the central United States cold outbreak, *AMS Bulletin*, 42, 77-84 (February, 1961).
- Katz, I., Gradient of refractive modulus in homogeneous air, potential modulus, pages 198-199 in *Propagation of Short Radio Waves*, by D. E. Kerr, (McGraw-Hill Book Co., New York, 1951).
- Lukes, G. D., Radio meteorological forecasting by means of the thermodynamics of the modified refractive index, Third Conference on Propagation, November 16-17, 1944, Washington, D. C., Committee on Propagation, NDRC, Pages 107-113 (1944).
- Megaw, E.C.S., Scattering of electromagnetic waves by atmospheric turbulence, *Nature*, 166, 1100-1104 (December, 1950).
- Misme, P., Influence of abrupt air mass changes upon tropospheric propagation, *Annales des Telecommunications* (Paris, May, 1957).
- Misme, P., Comments on "Models of the atmospheric radio refractive index", *Proc. IRE*, 48, 1498-1501 (August, 1960).
- Moler, W. F., and W. A. Arvola, Vertical motion in the atmosphere and its effect on VHF radio signal strength, *Trans. Am. Geophys. U.*, 37, (August, 1956).
- Moler, W. F., and D. B. Holden, Tropospheric scatter propagation and atmospheric circulations, *J. Research NBS*, 64D, (Radio Prop.) No. 1, 81-93 (January-February, 1960).
- Norton, K. A., Point-to-point radio relaying via the scatter mode of tropospheric propagation, *IRE Trans.*, PGCS-4, 39 (1956).
- Onoe, M., M. Hirai, S. Niwa, Results of experiment of long-distance overland propagation of ultra-short waves, *J. Radio Research Labs.*, Japan 5, 79 (October, 1958).

- Palmer, C. E., Some kinematic aspects of frontal zones, *J. Meteor.*, 14, No. 5, 403-409 (October, 1957).
- Perlat, Andree, Meteorology and radioelectricity, *L'Onde Elec.*, 28, 44 (1948).
- Pickard, G. W., and H. T. Stetson, Comparison of tropospheric reception, *J. Atmospheric and Terrest. Phys.* 1, 32 (1950a).
- Pickard, G. W., and H. T. Stetson, Comparison of tropospheric reception at 44.1 Mc with 92.1 Mc over the 167-mile path of Alpine, New Jersey, to Needham, Massachusetts, *Proc. IRE*, 38, 1450 (1950b).
- Randall, D. L., A study of the meteorological effects on radio propagation at 96.3 Mc between Richmond, Virginia, and Washington, D. C., *Bull. Amer. Met. Soc.*, 35, 56-59 (February, 1954).
- Saxton, J. A., G. W. Luscombe, and G. H. Bazzard, The propagation of metre radio waves beyond the normal horizon, *Proc. IEE III*, 98, No. 55, 370-378 (September, 1951).
- Saxton, J. A., Propagation of metre radio waves beyond the normal horizon, *Proc. IEE*, 98, 360-369 (September, 1951).
- Schulkin, M., Average radio-ray refraction in the lower atmosphere, *Proc. IRE*, 40, No. 5, 554-561 (1952).
- Sheppard, P. A., The structure and refractive index of the atmosphere, Report on a Conference on Meteorological Factors in Radio Wave Propagation (1946).
- Smith, E. K., Jr., and S. Weintraub, The constants in the equation for atmospheric refractive index at radio frequencies, *Proc. IRE*, 41, 1035-1037 (August, 1953).
- Smyth, J. B., and L. G. Trolese, Propagation of radio waves in the troposphere, *Proc. IRE*, 35, 1198 (1947).
- Ugai, S., Y. Kaneda, and T. Amekura, Microwave propagation test in mirage district, *Rev. of Electrical Communication Lab.*, 9, Nos. 11-12, 687-717 (November-December, 1961), Nippon Telegraph and Telephone Public Corporation, Tokyo, Japan.

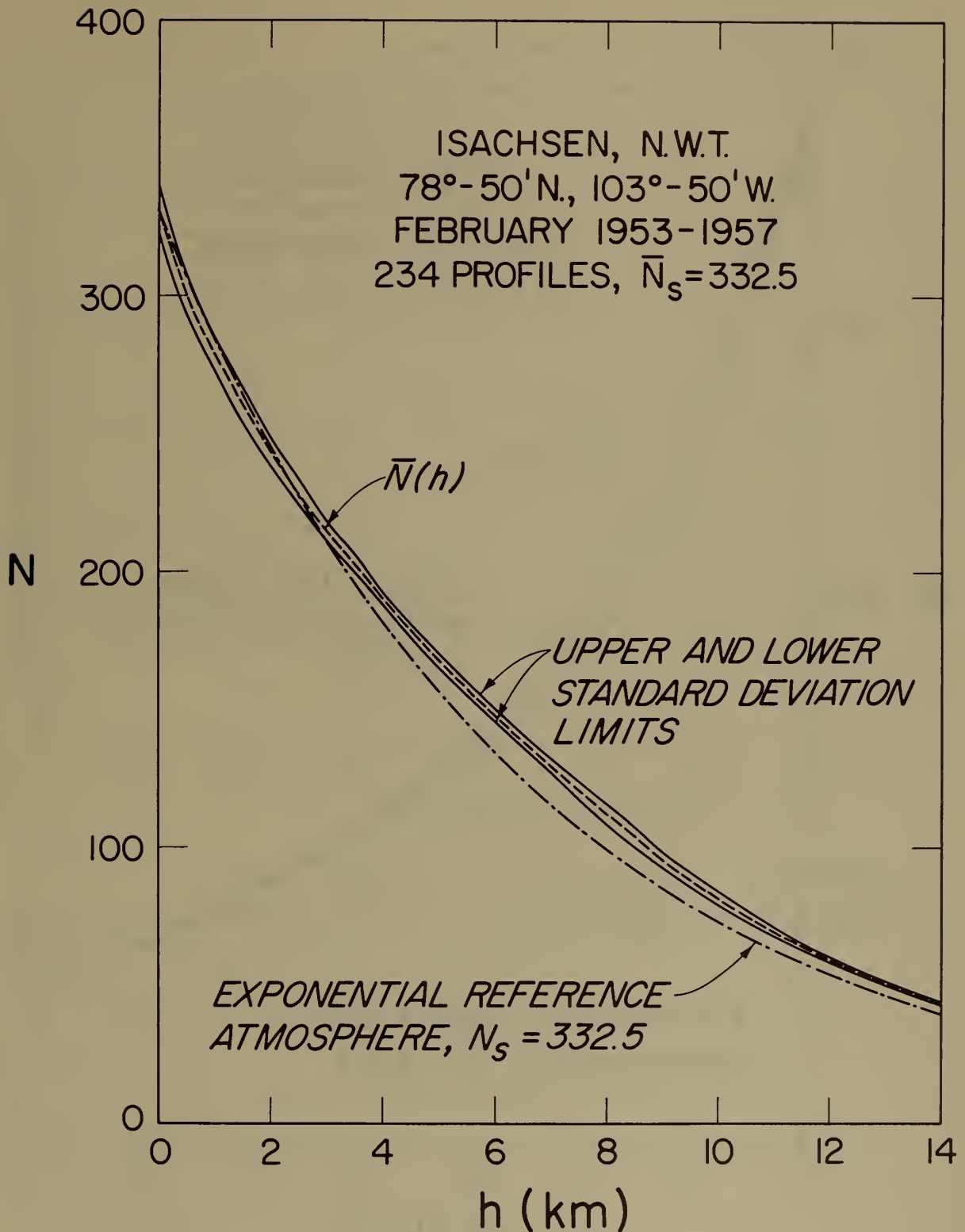


Figure 1. Mean N Distribution for Isachsen, N. W. T., Canada

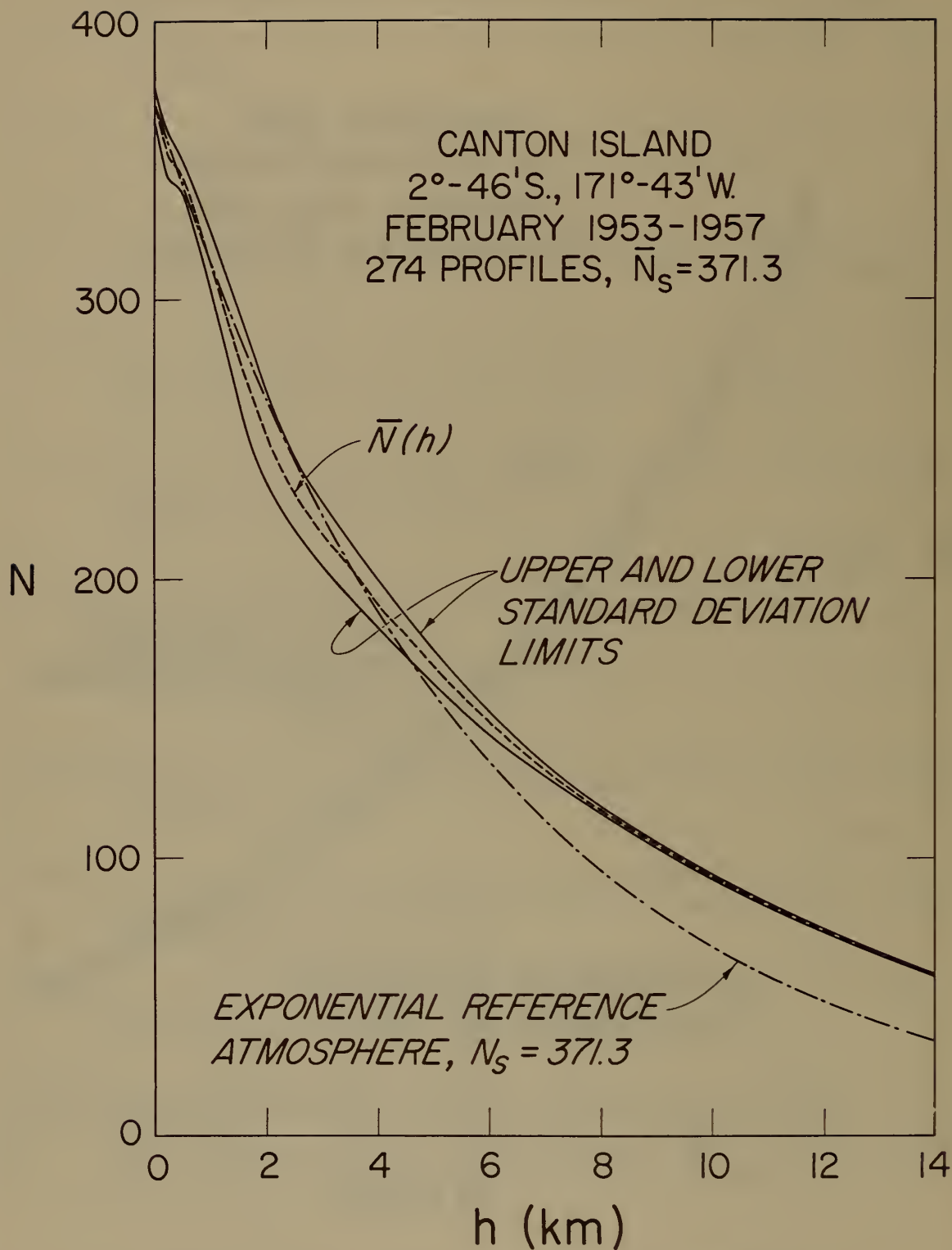
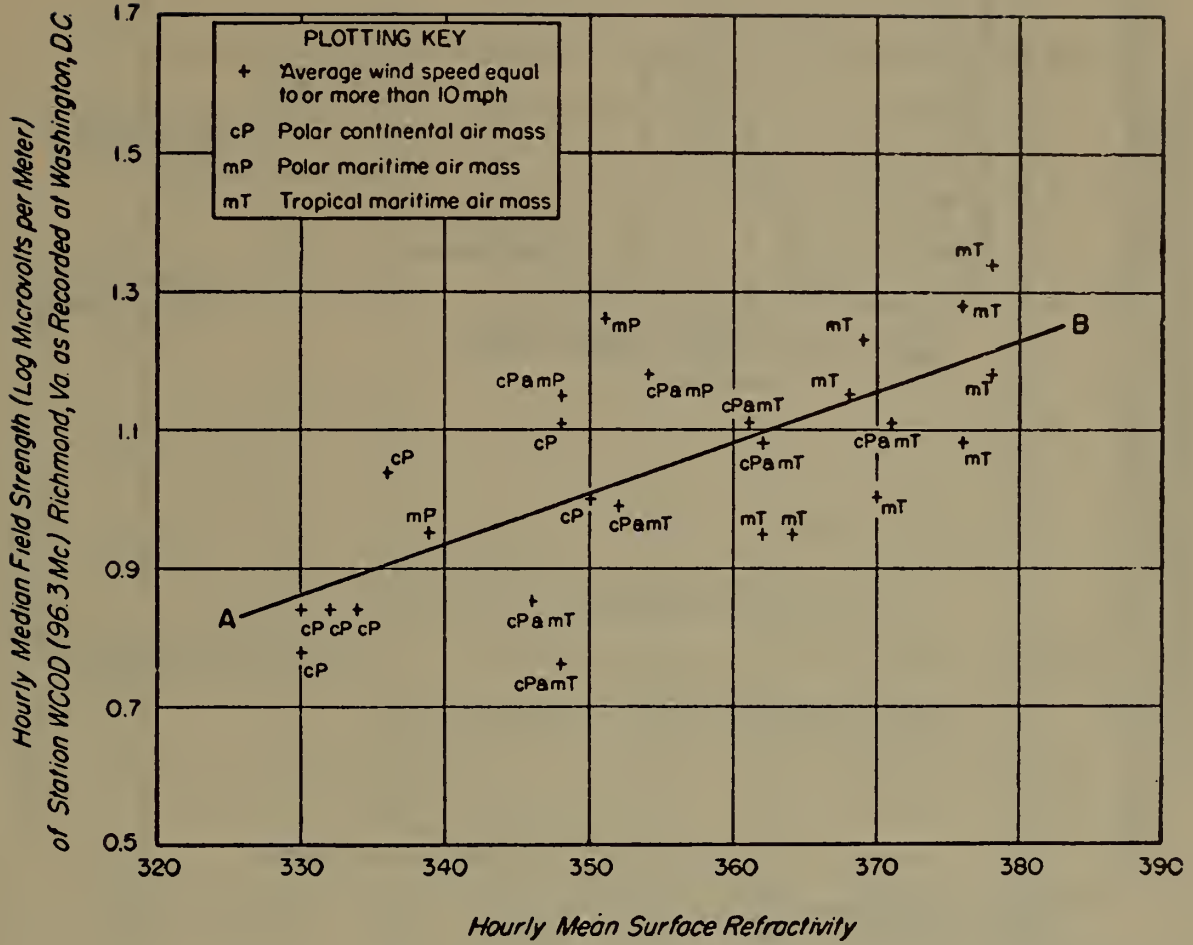
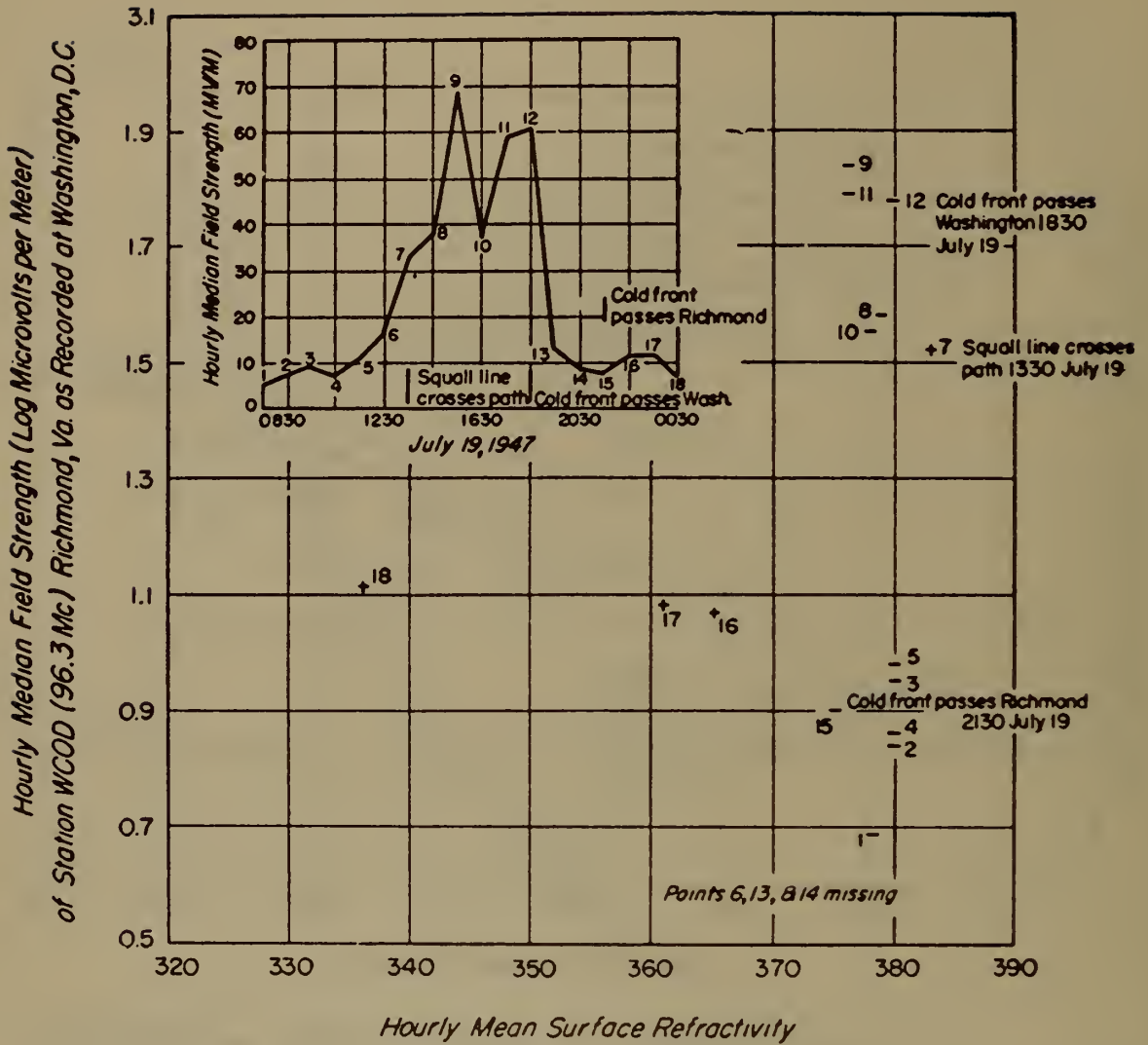


Figure 2. Mean N Distribution for Canton Island, Pacific Ocean



Scatter diagram of select hourly median field strength vs. hourly mean refractivity July 17 to August 8, 1947.

Figure 3. Field Strength versus Refractivity



Scatter diagram showing passage of a cold front system over the Washington-Richmond path and graph indicating the fluctuation of hourly median field strength with time.

Figure 4. Field Strength and N Changes During Frontal Passage

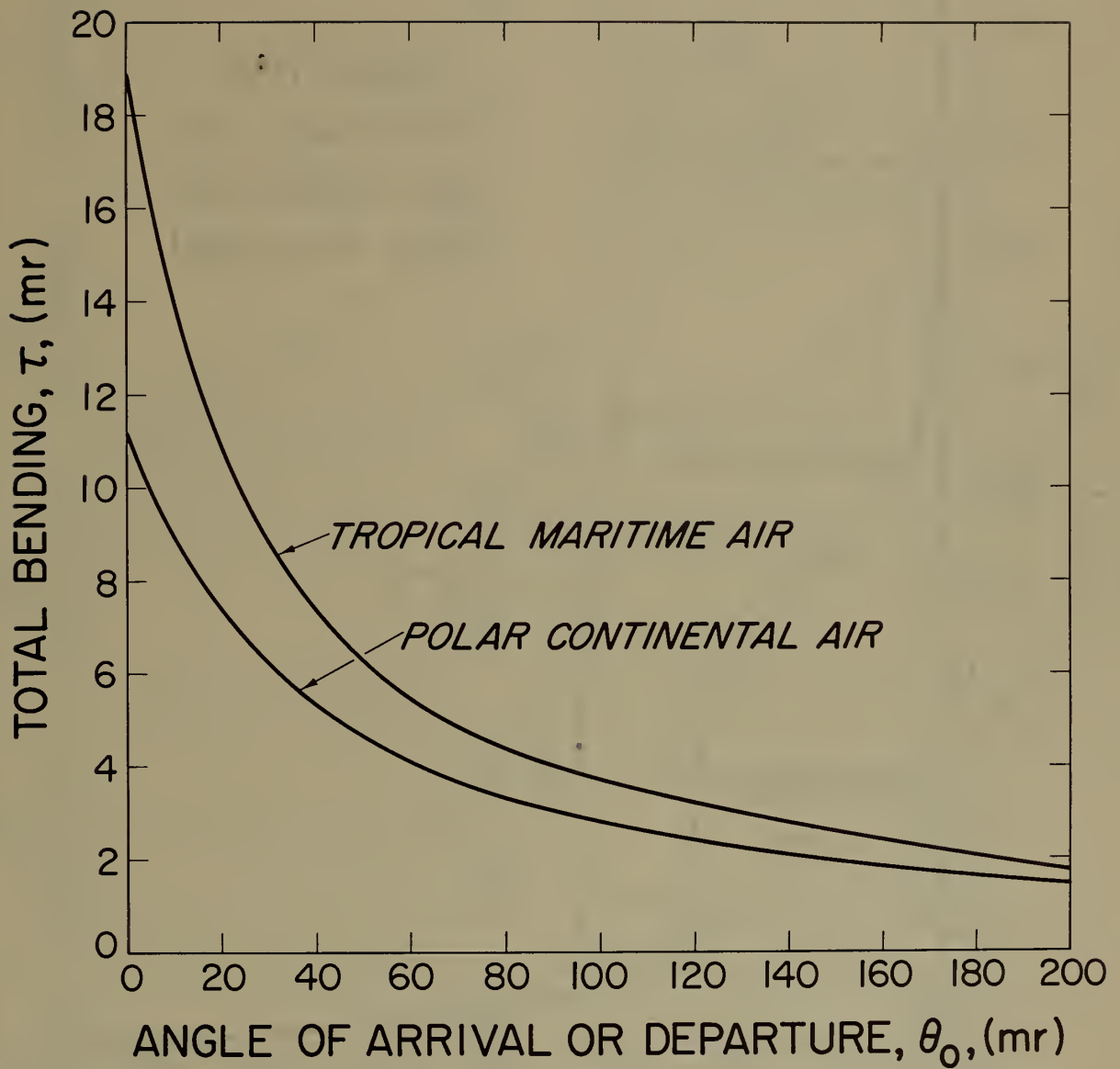


Figure 5. Mean Angular Bending for Two Air Masses

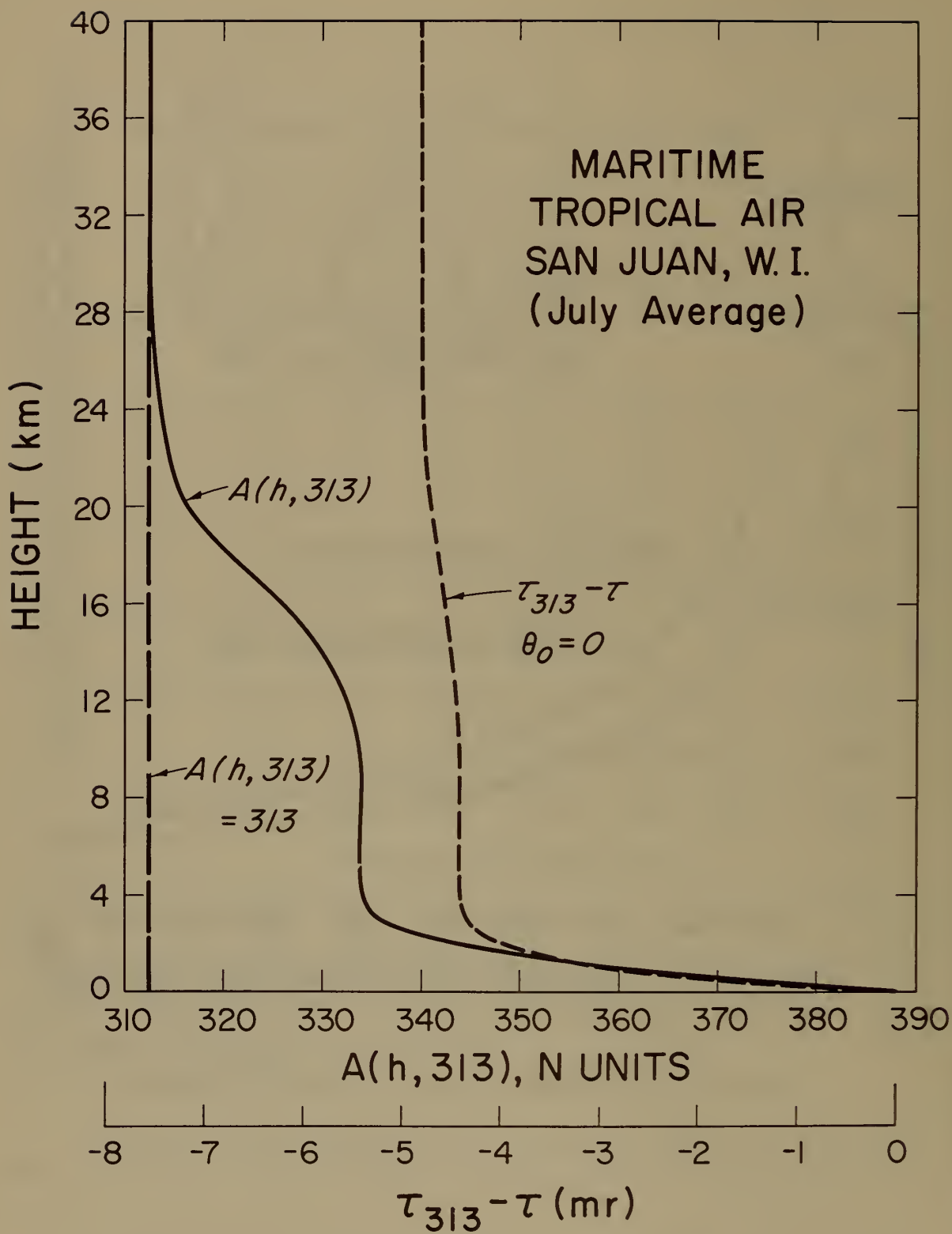
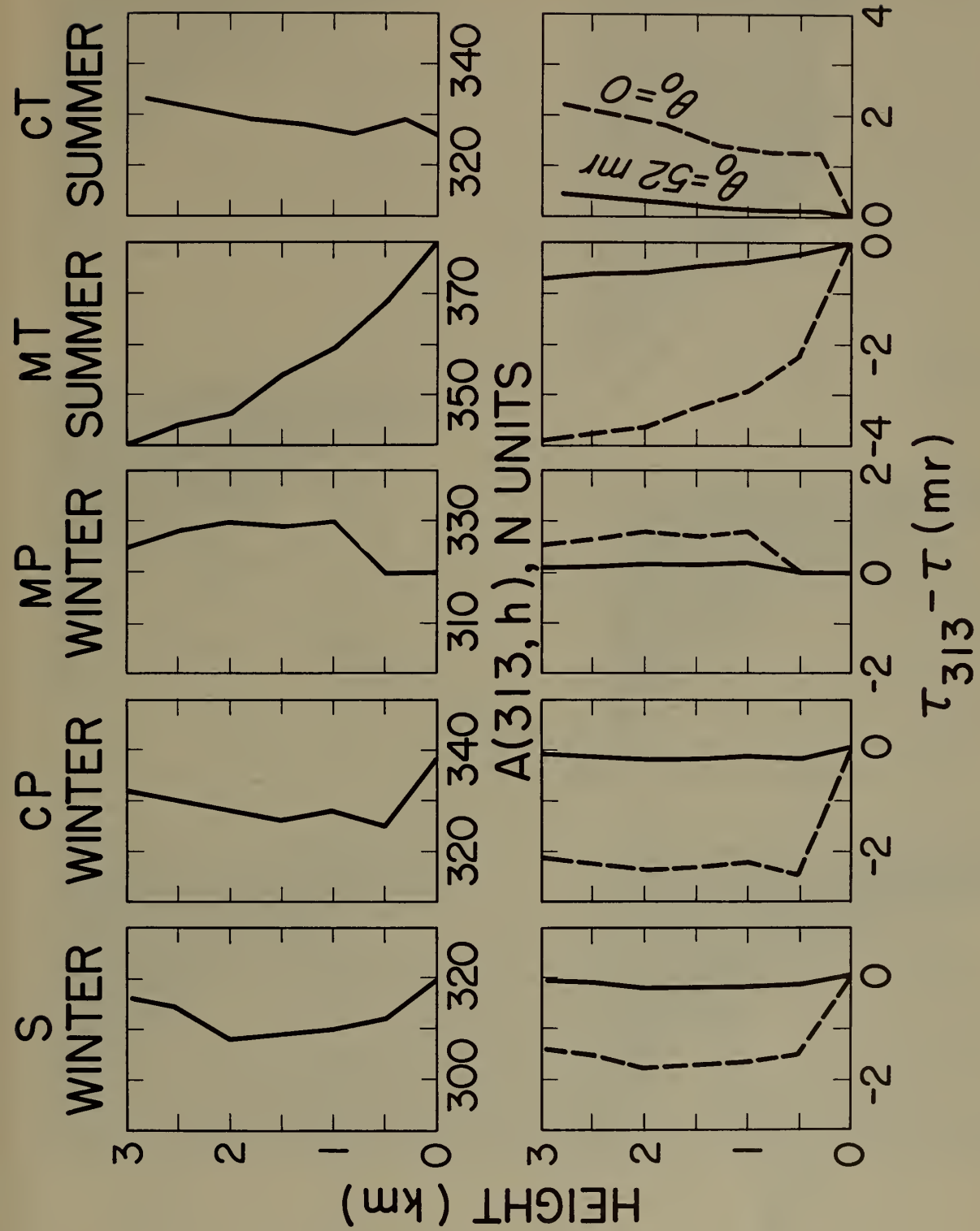


Figure 6. Departures of τ and N from Normal for Maritime Tropical Air

Figure 7. Departures of τ and N for Various Air Masses

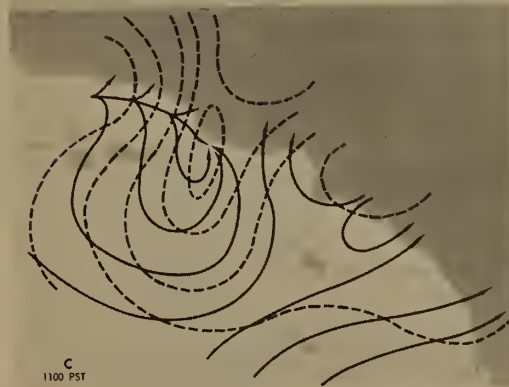
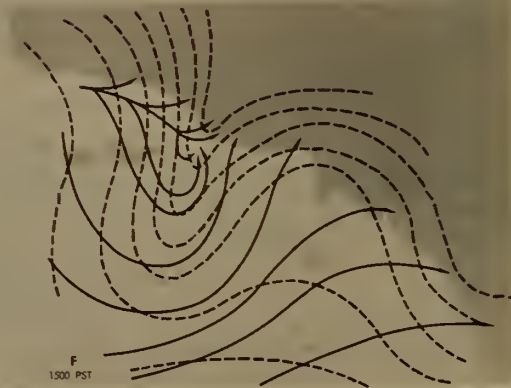
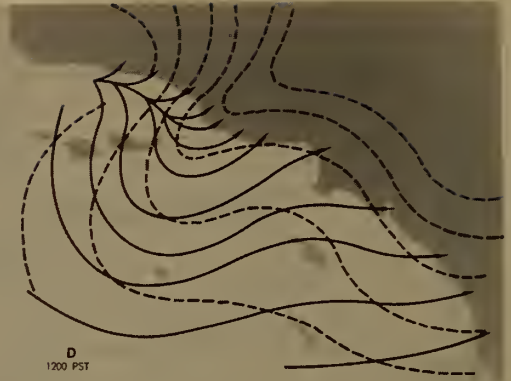


Figure 8. Isobaric and Streamline Maps

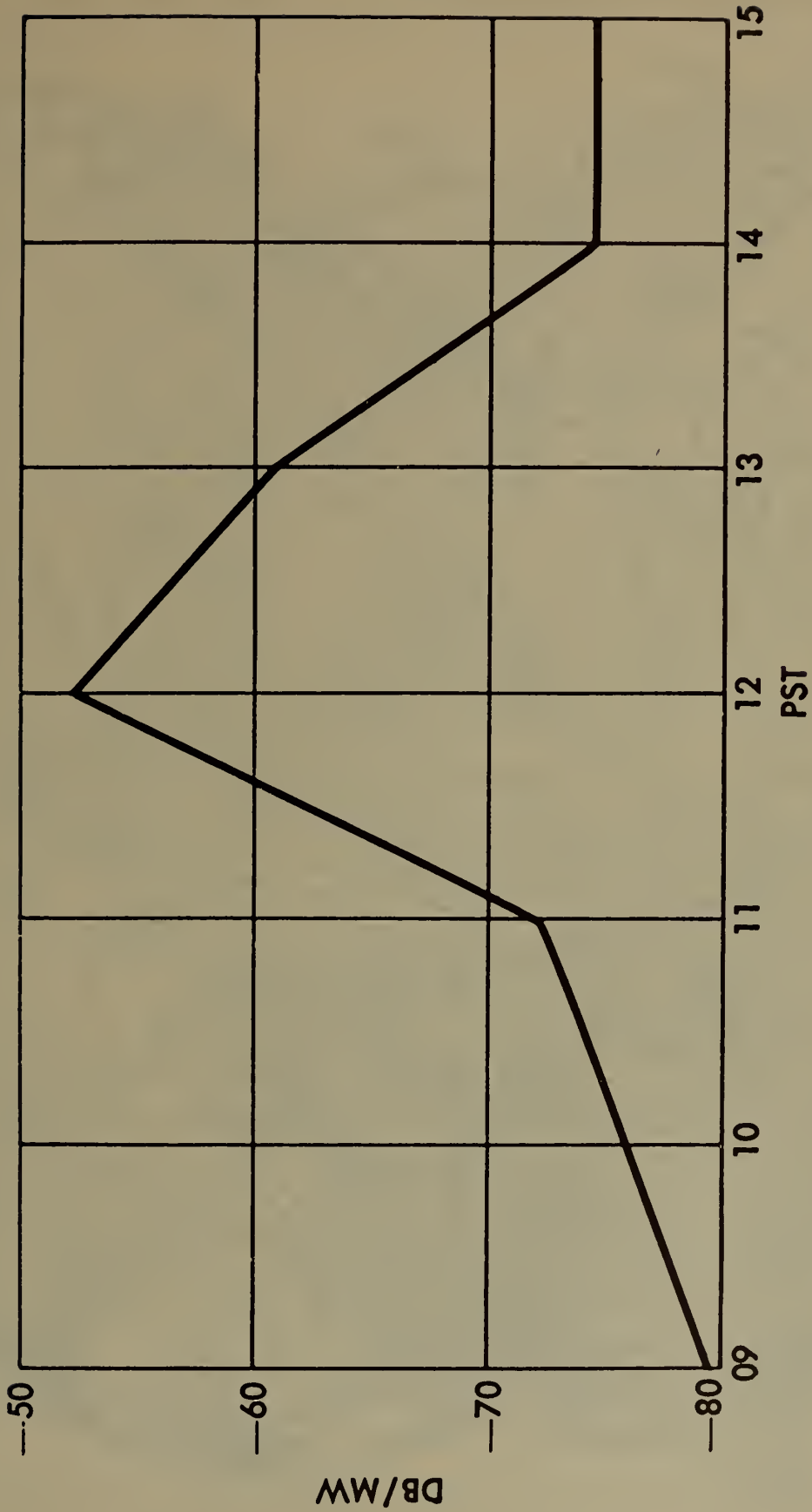
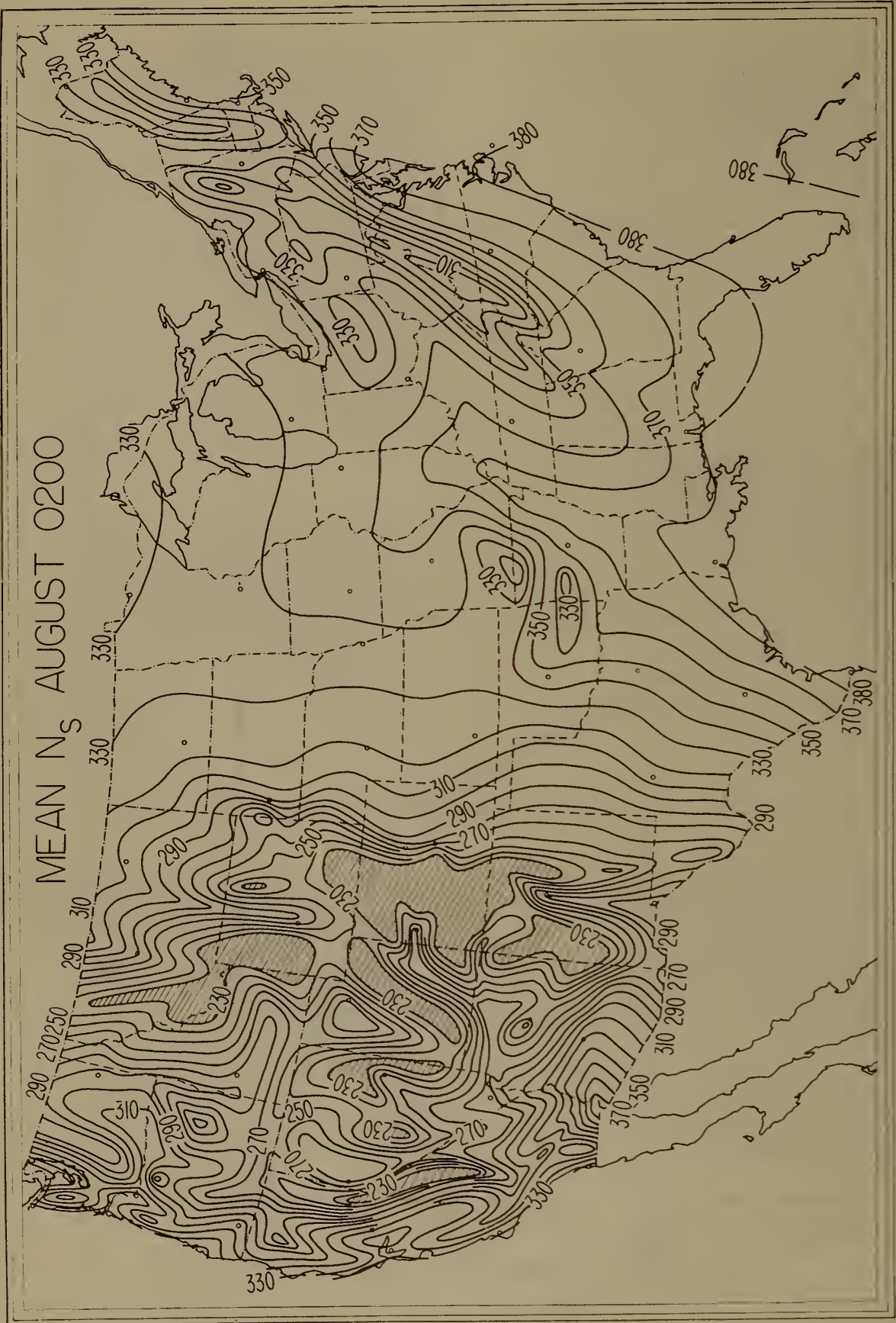


Figure 9. X-Band Signal Level versus Time

Figure 10. Mean N_s , August 0200

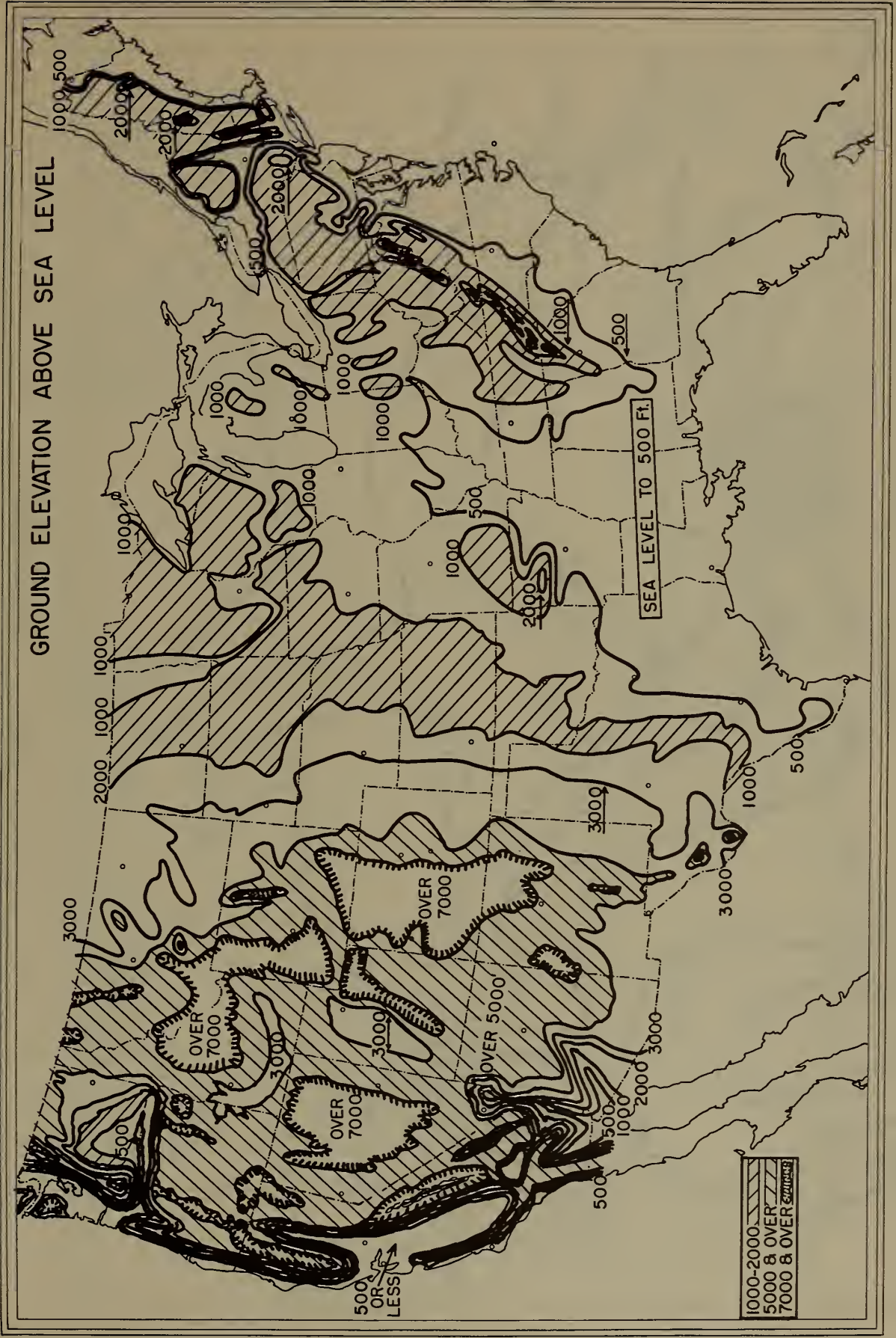


Figure 11. Ground Elevation Above Sea Level

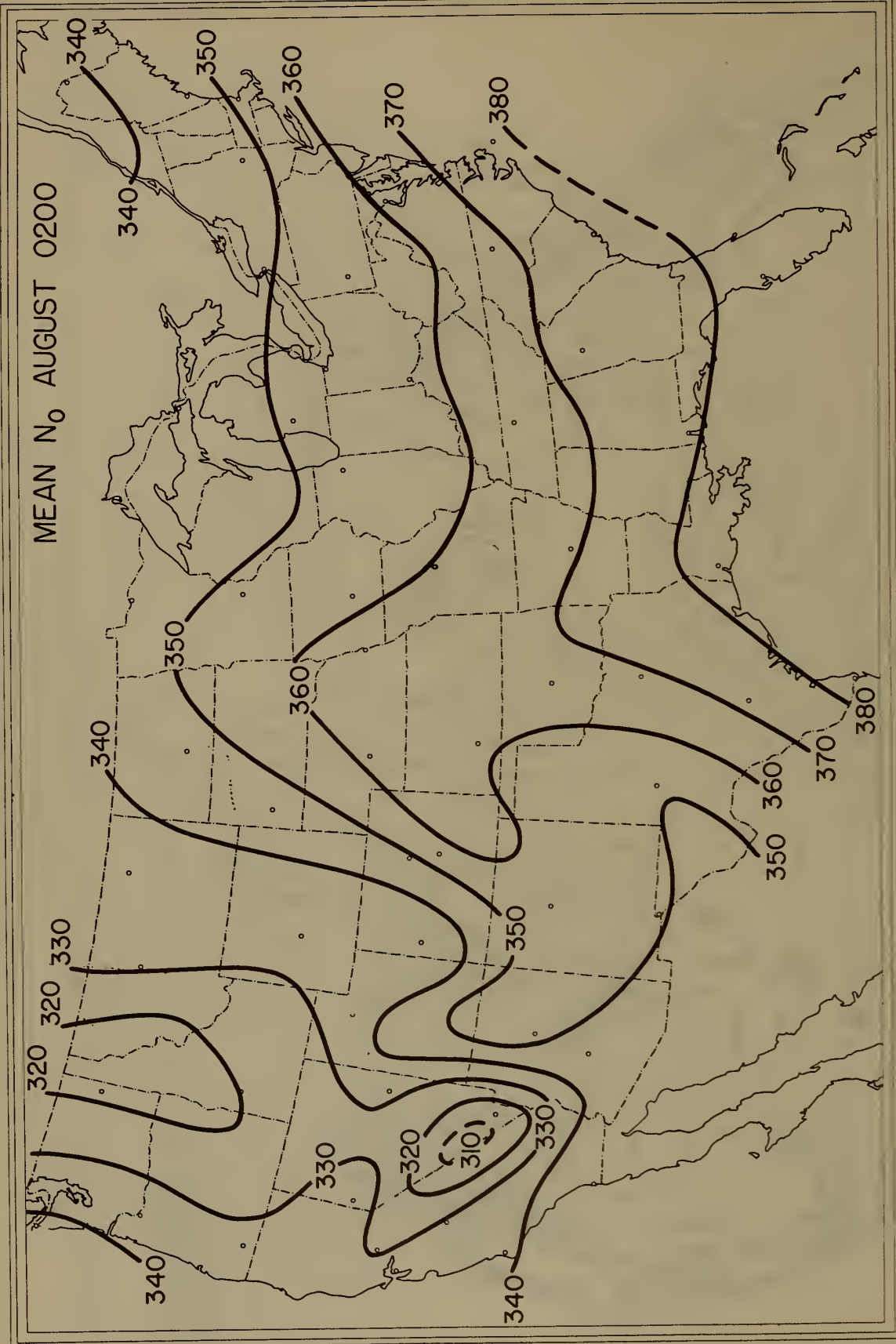


Figure 12. Mean N_0 , August 0200

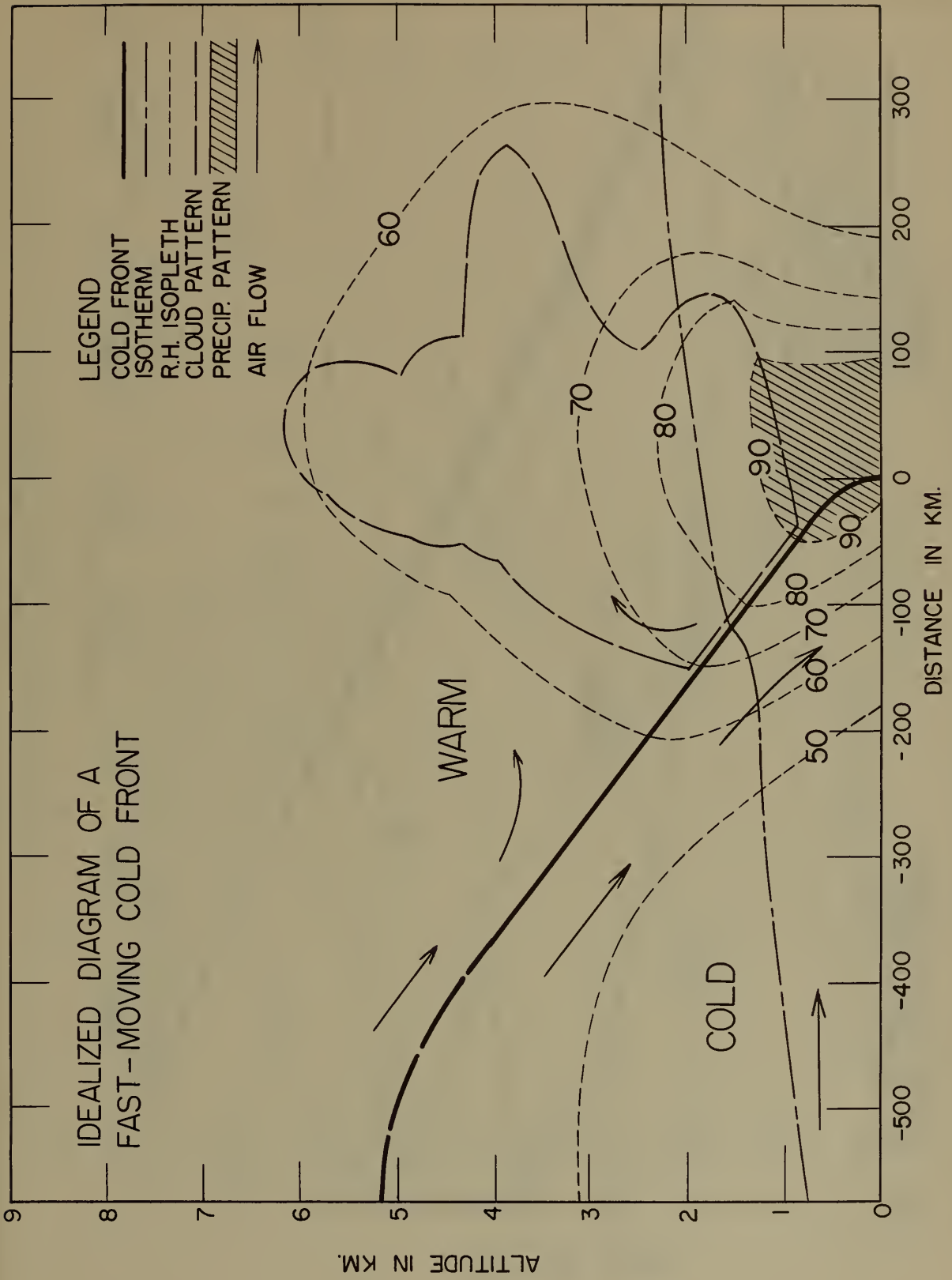


Figure 13. Idealized Cold Front

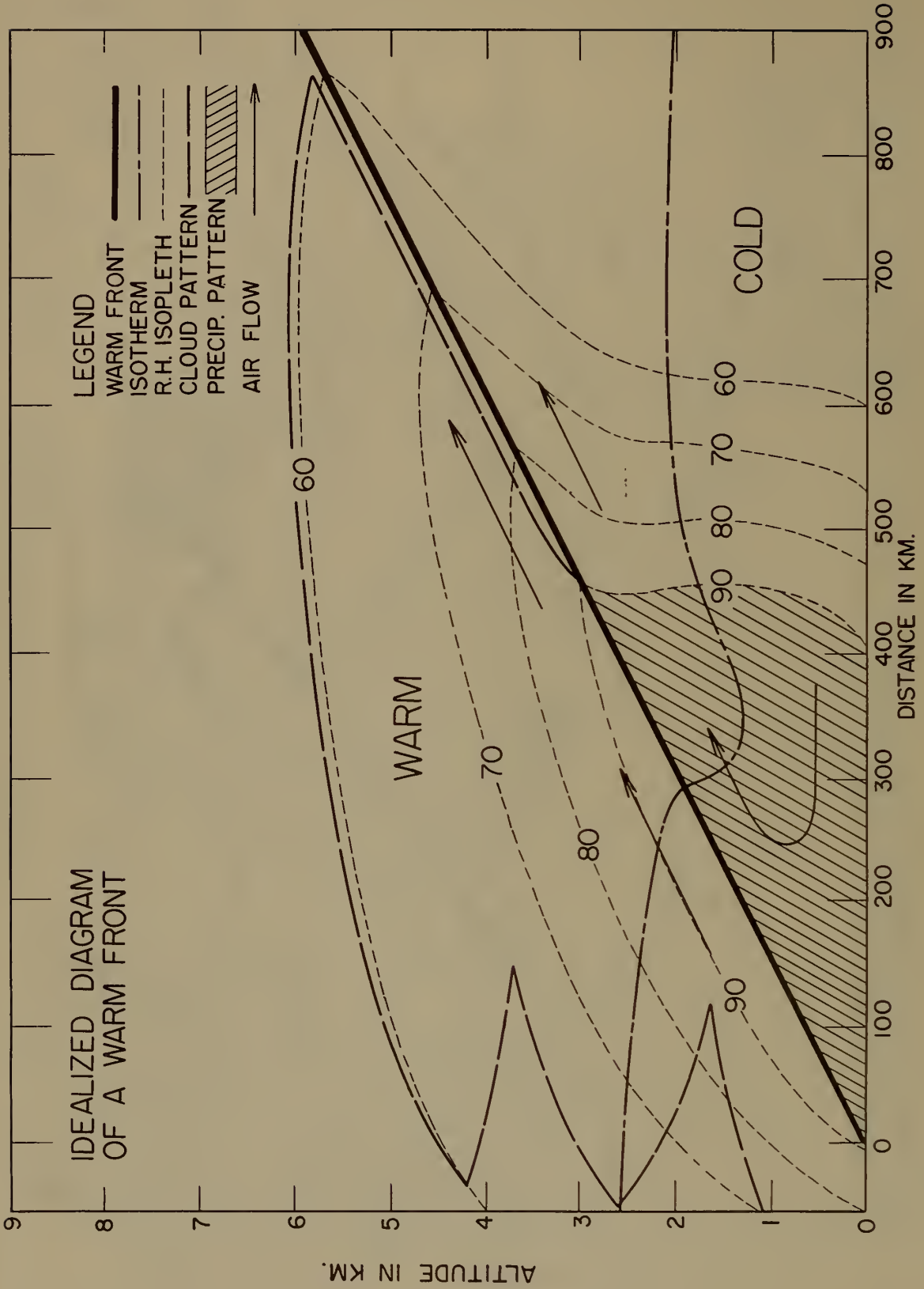


Figure 14. Idealized Warm Front

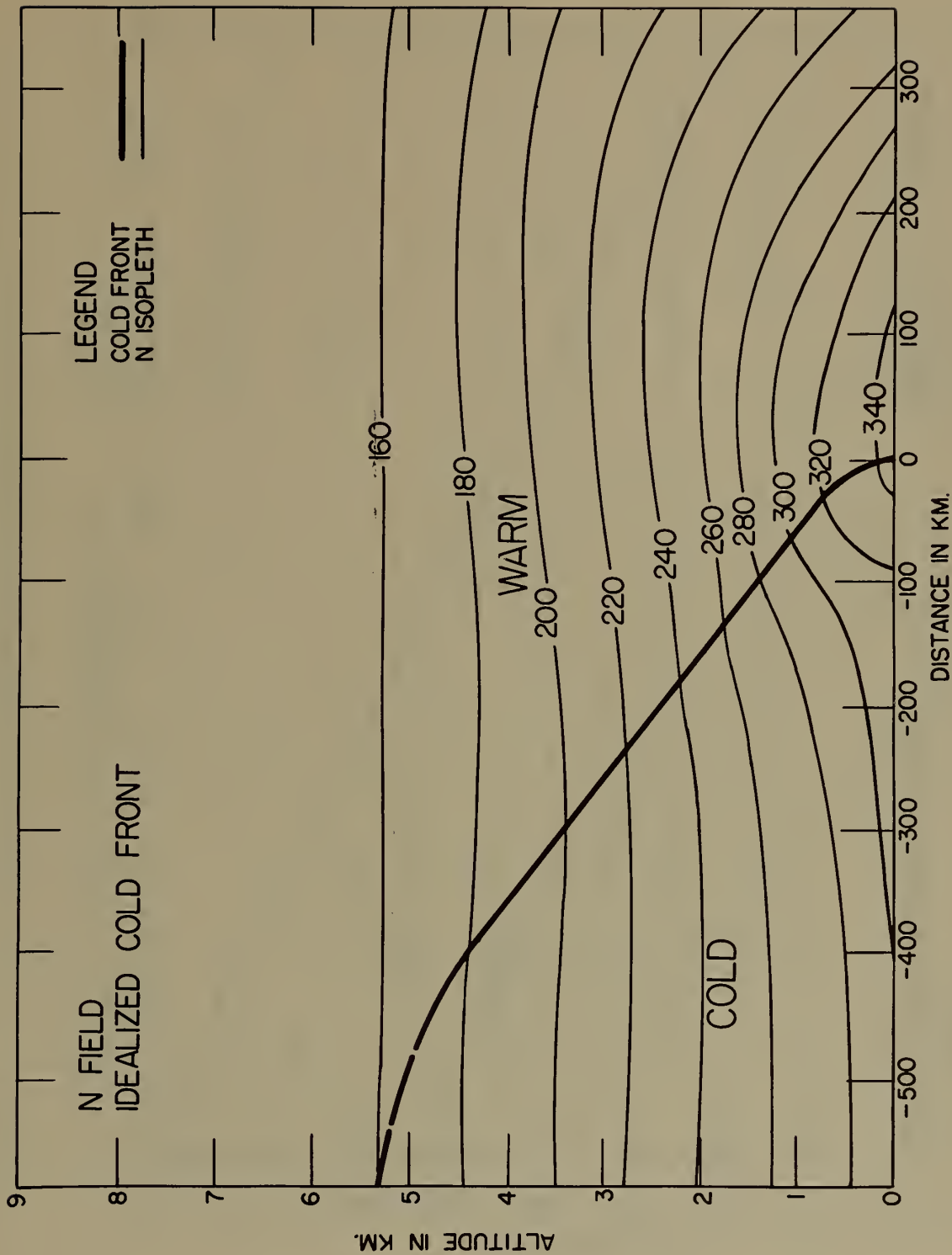


Figure 15. Idealized Cold Front in N Units

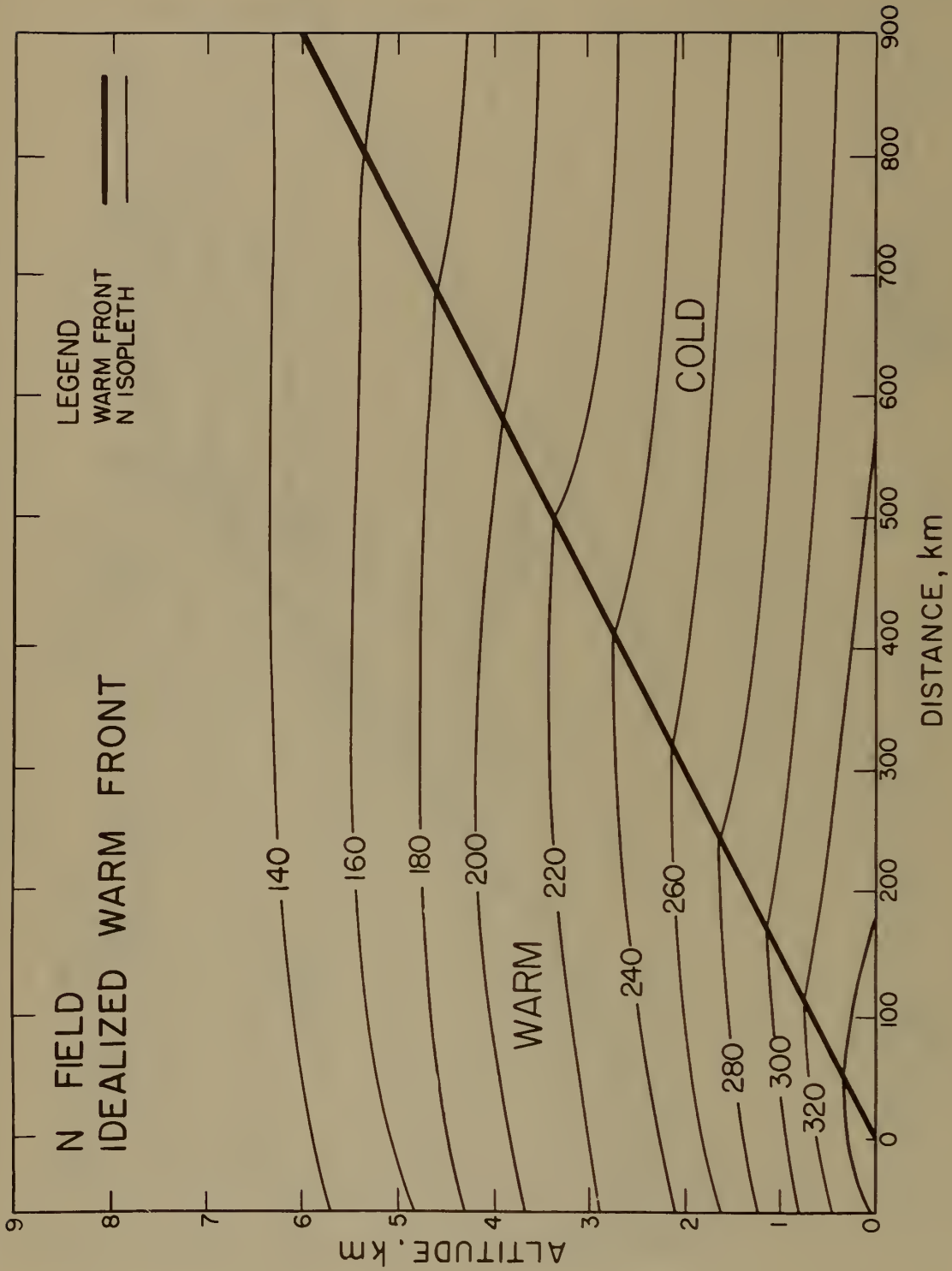


Figure 16. Idealized Warm Front in N Units

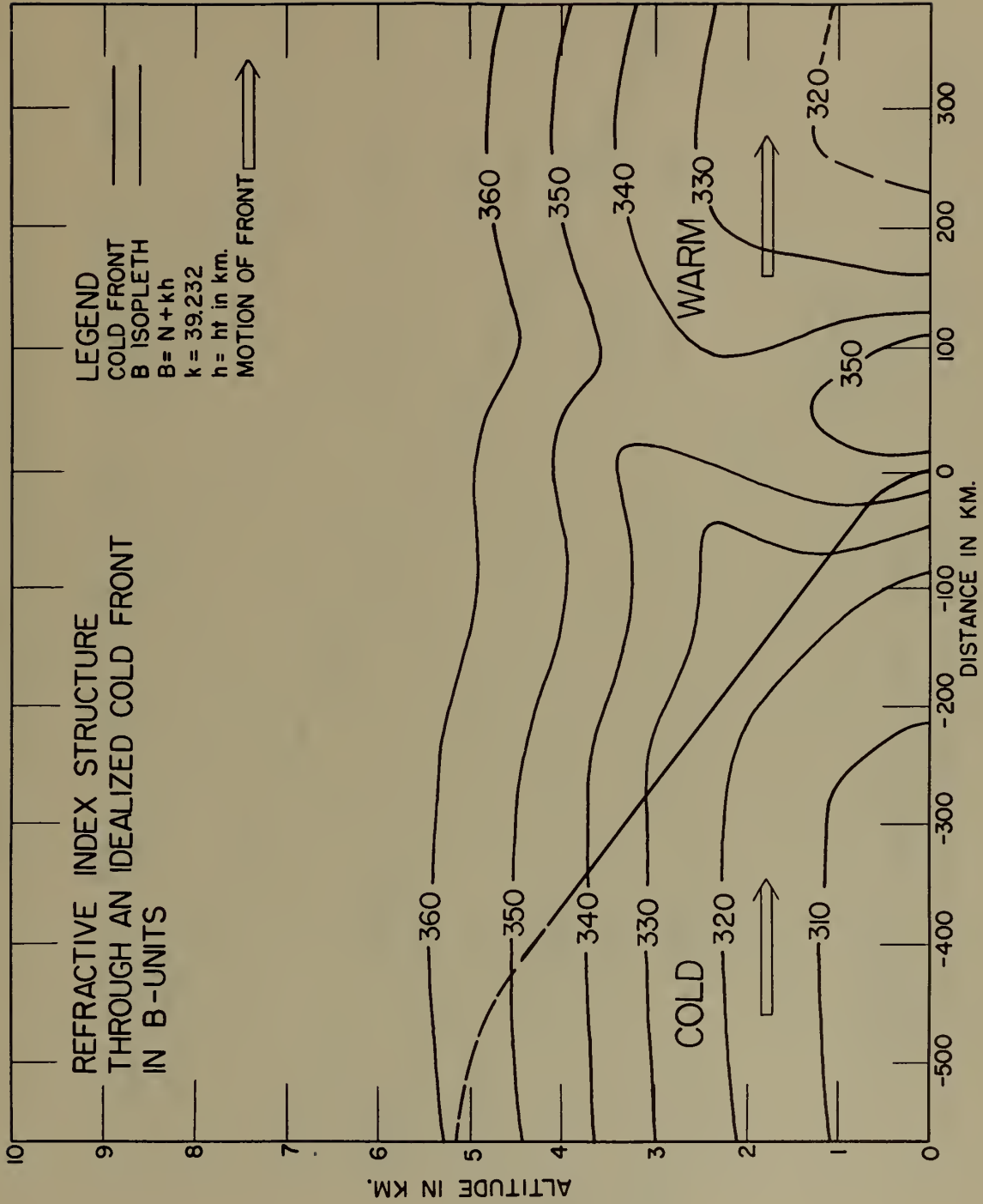


Figure 17. Idealized Cold Front in B Units

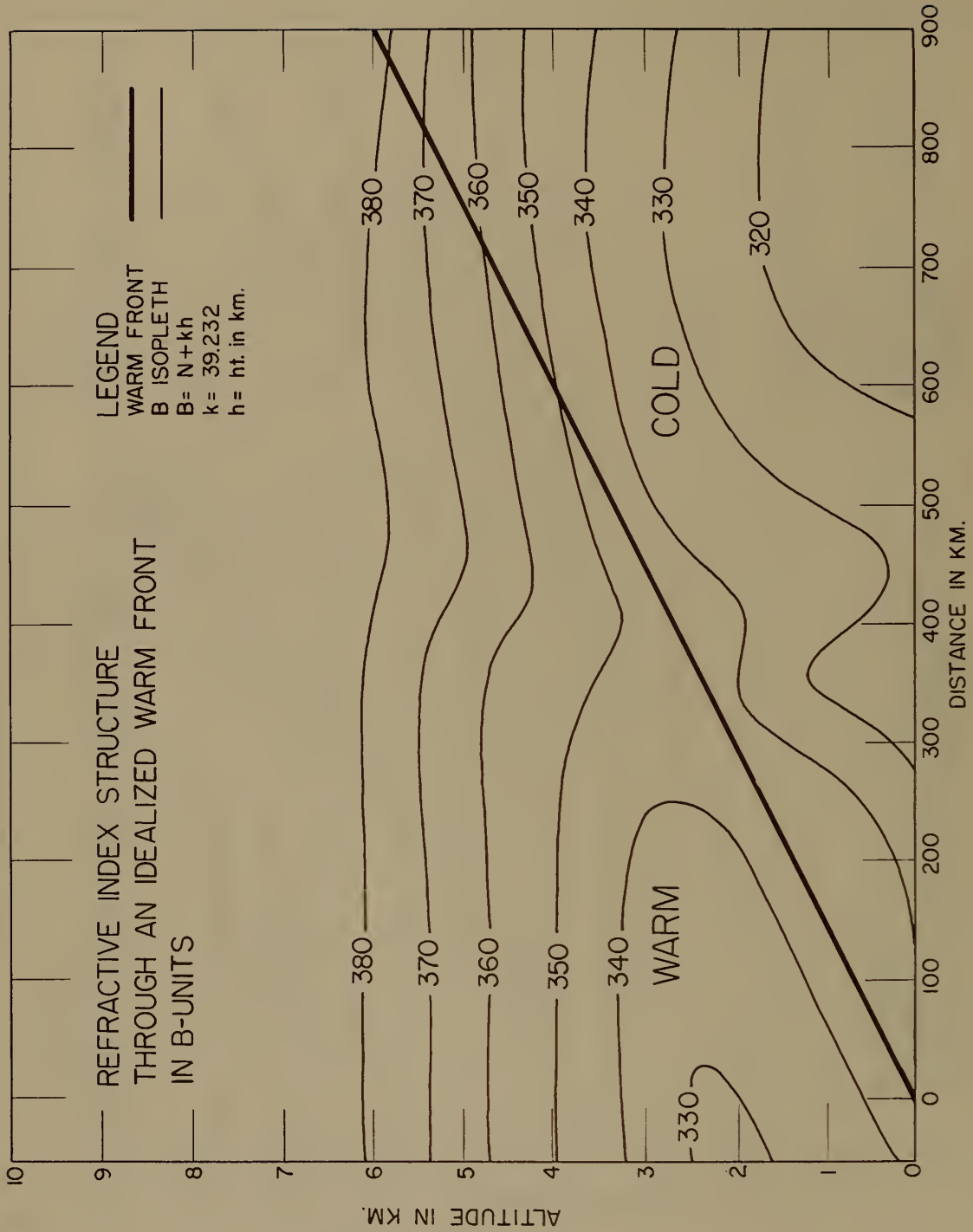


Figure 18. Idealized Warm Front in B Units

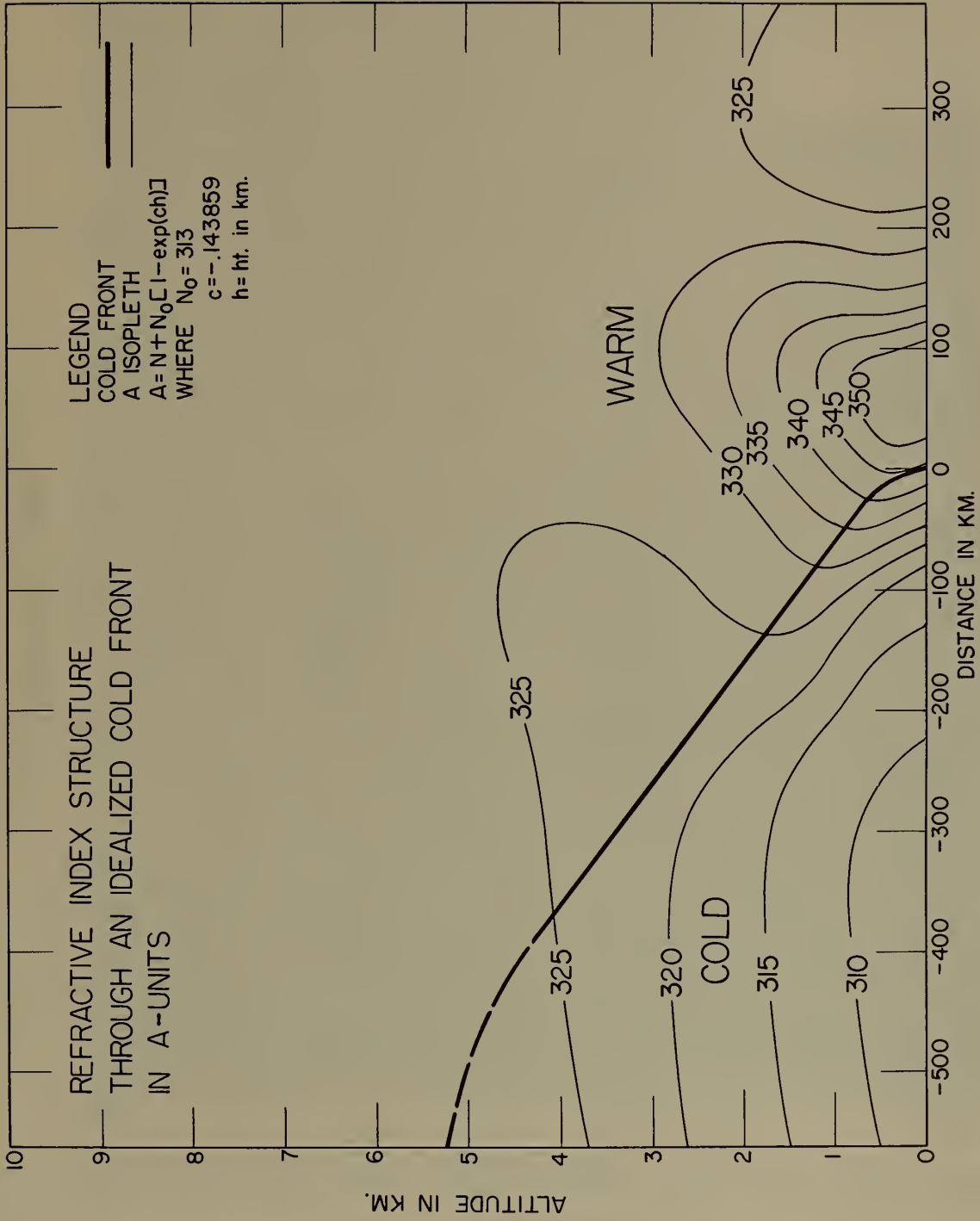


Figure 19. Idealized Cold Front in A Units

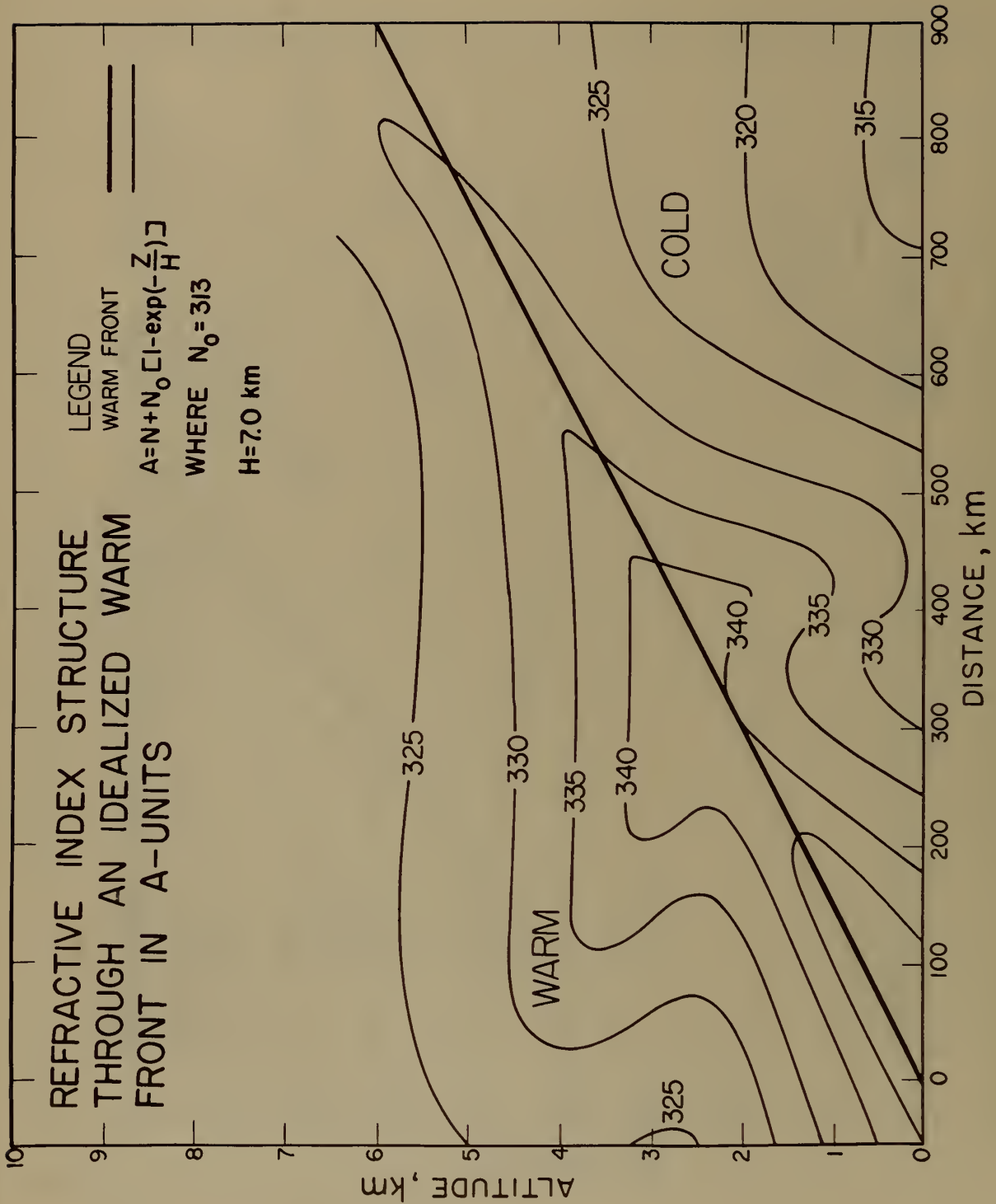


Figure 20. Idealized Warm Front in A Units

POTENTIAL REFRACTIVITY

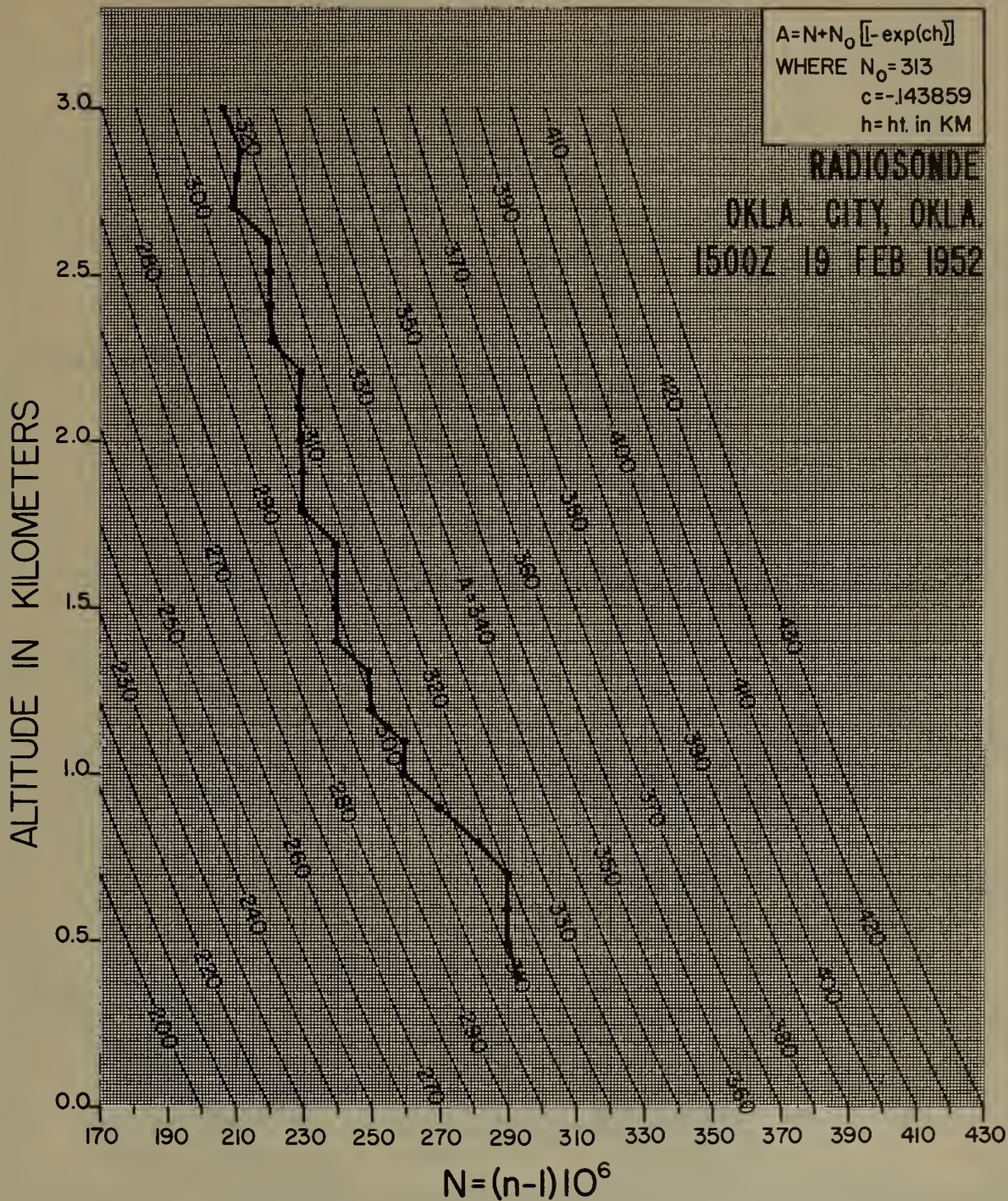


Figure 21. Potential Refractivity Chart

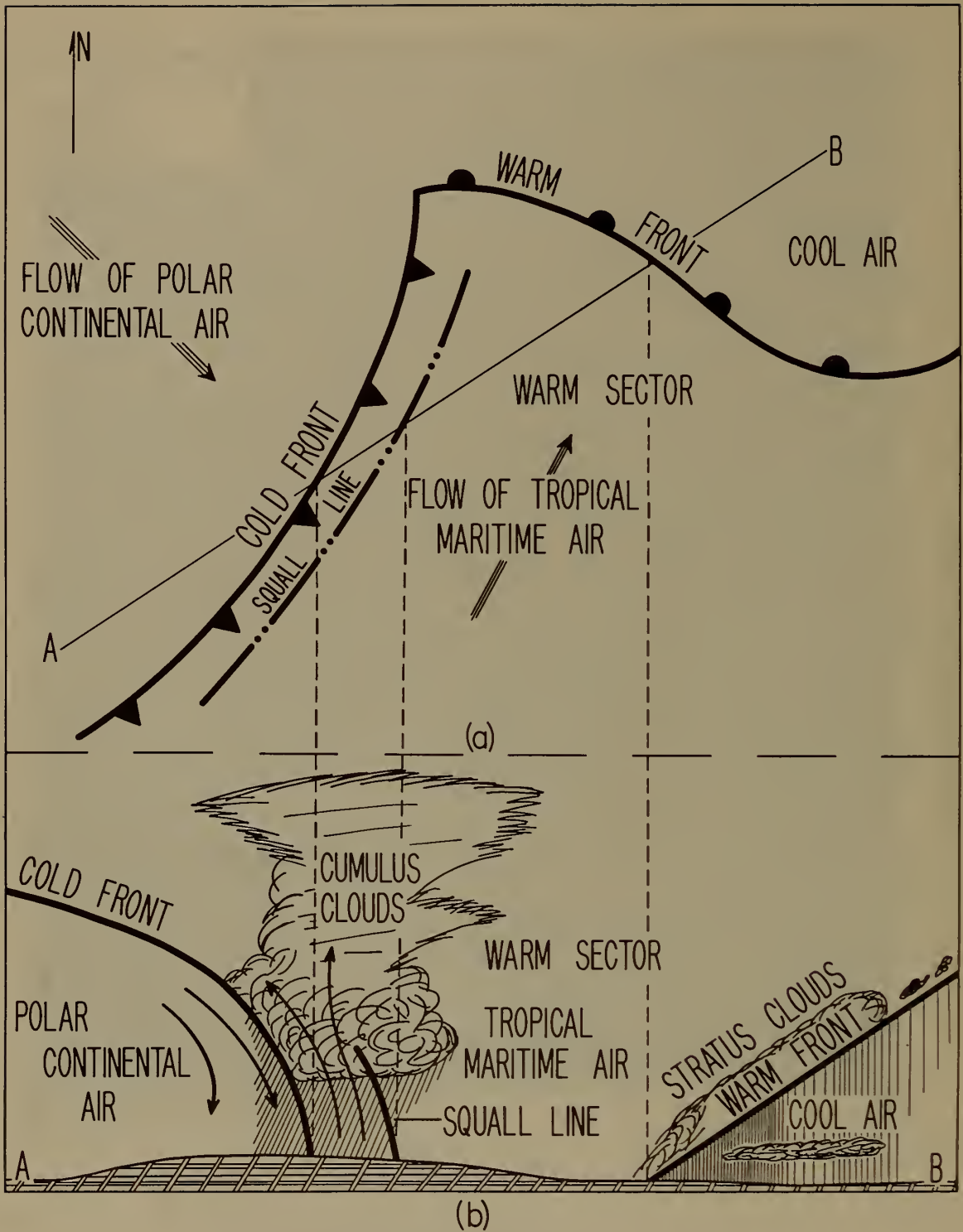


Figure 22. The Polar Front Wave

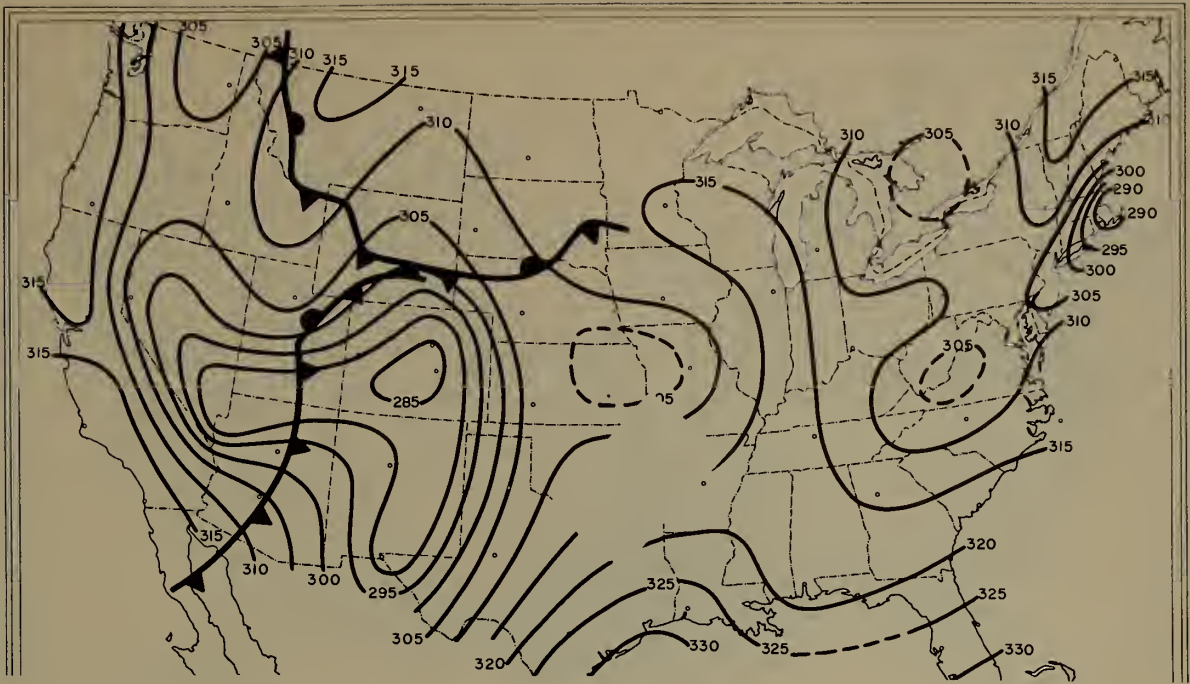


Figure 23. N_O Chart for Storm System 0103E 18 February, 1952

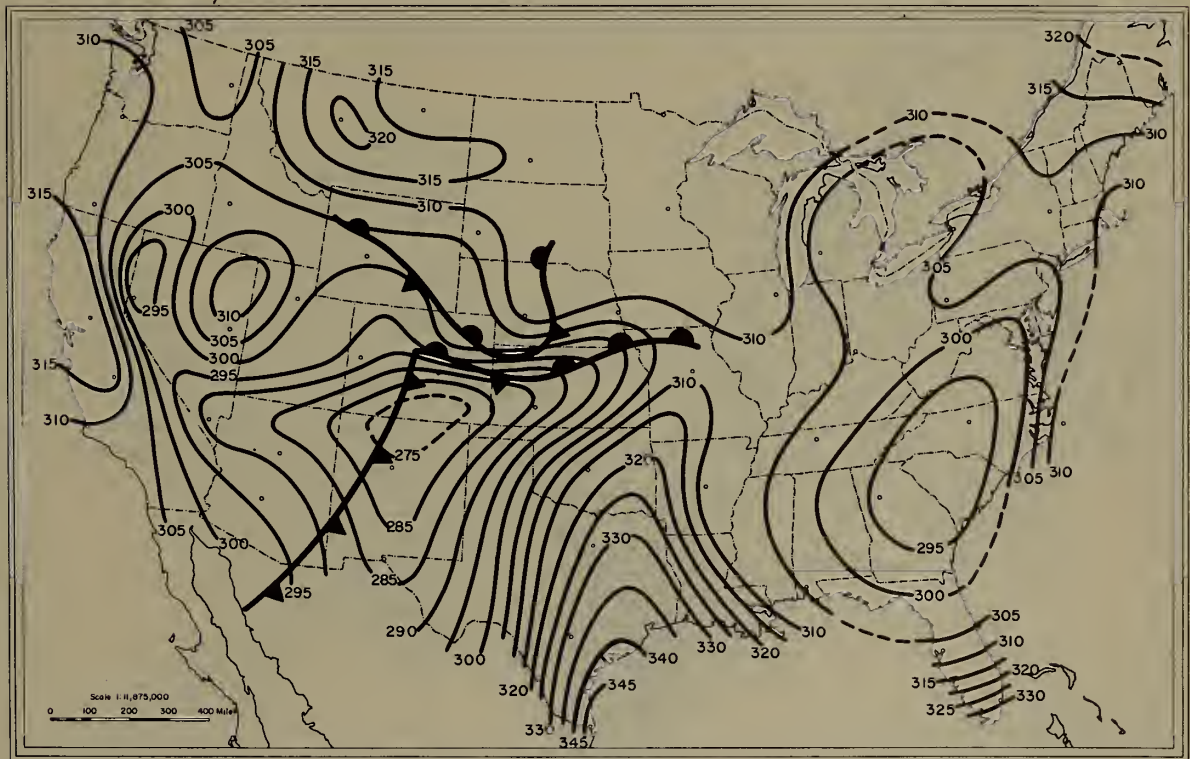


Figure 24. N_O Chart for Storm System 1330E 18 February, 1952

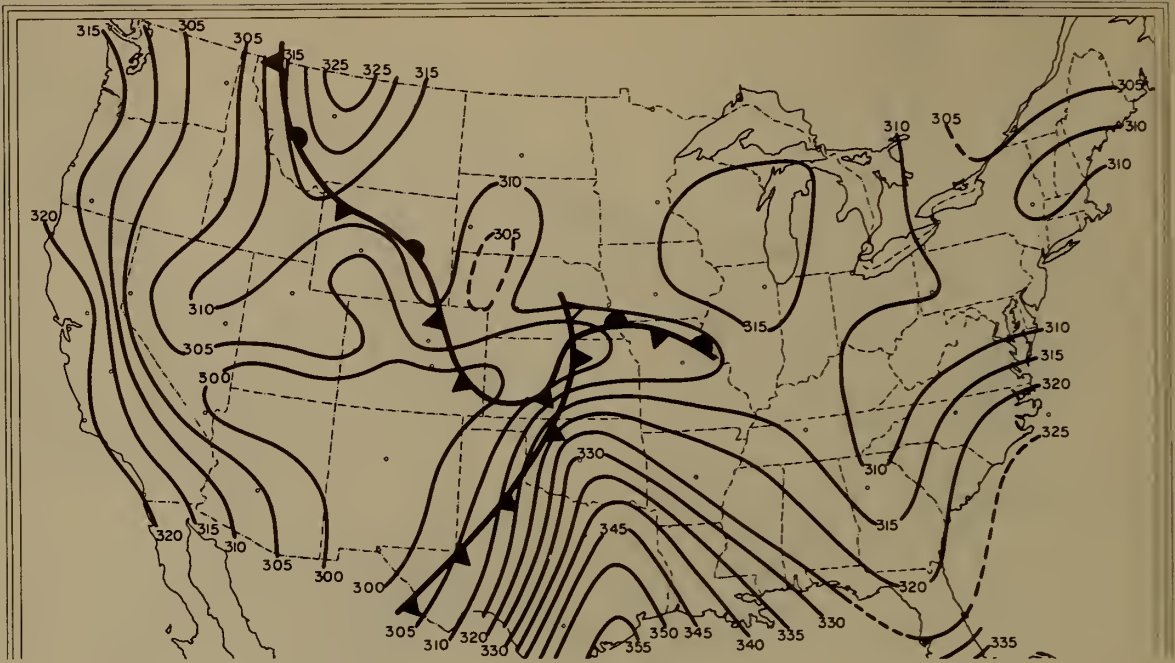


Figure 25. N_0 Chart for Storm System 0130E 19 February, 1952

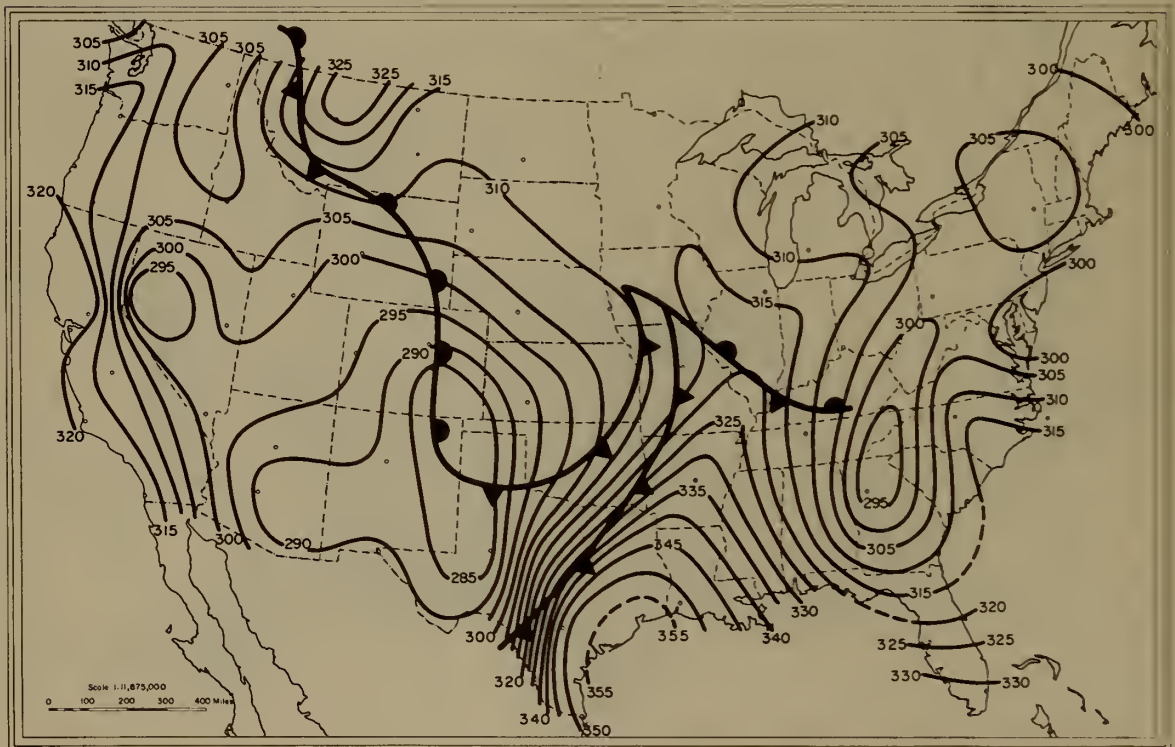


Figure 26. N Chart for Storm System 1330E 19 February, 1952

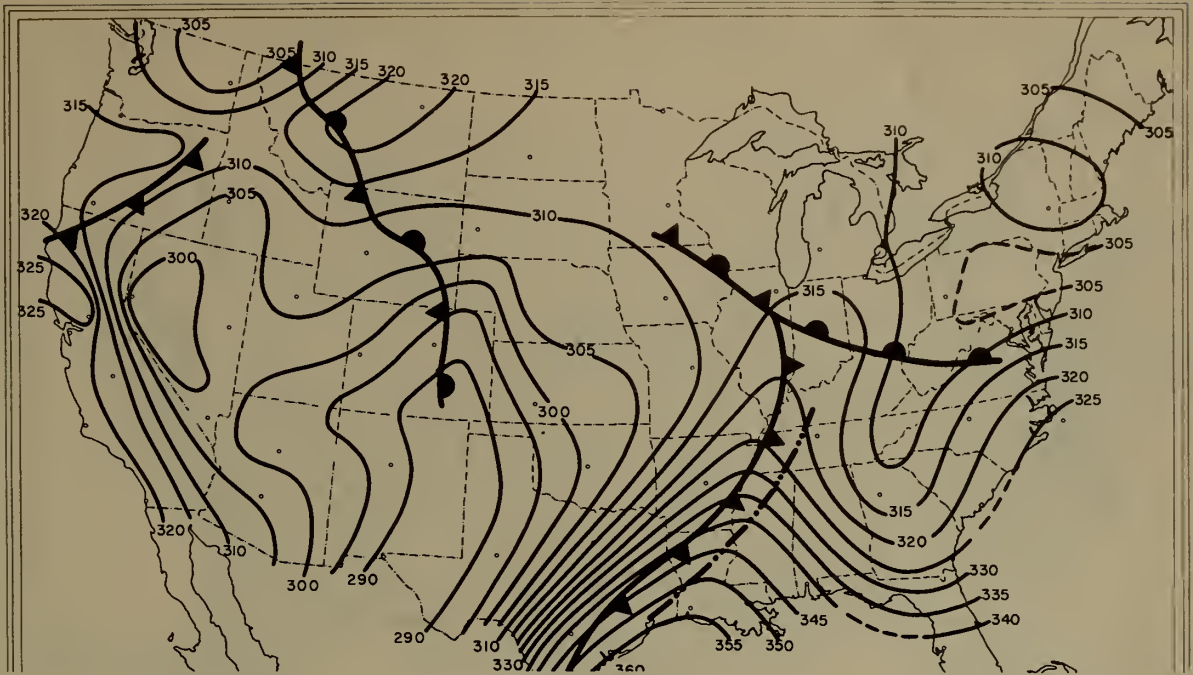


Figure 27. N_o Chart for Storm System 0130E 20 February, 1952

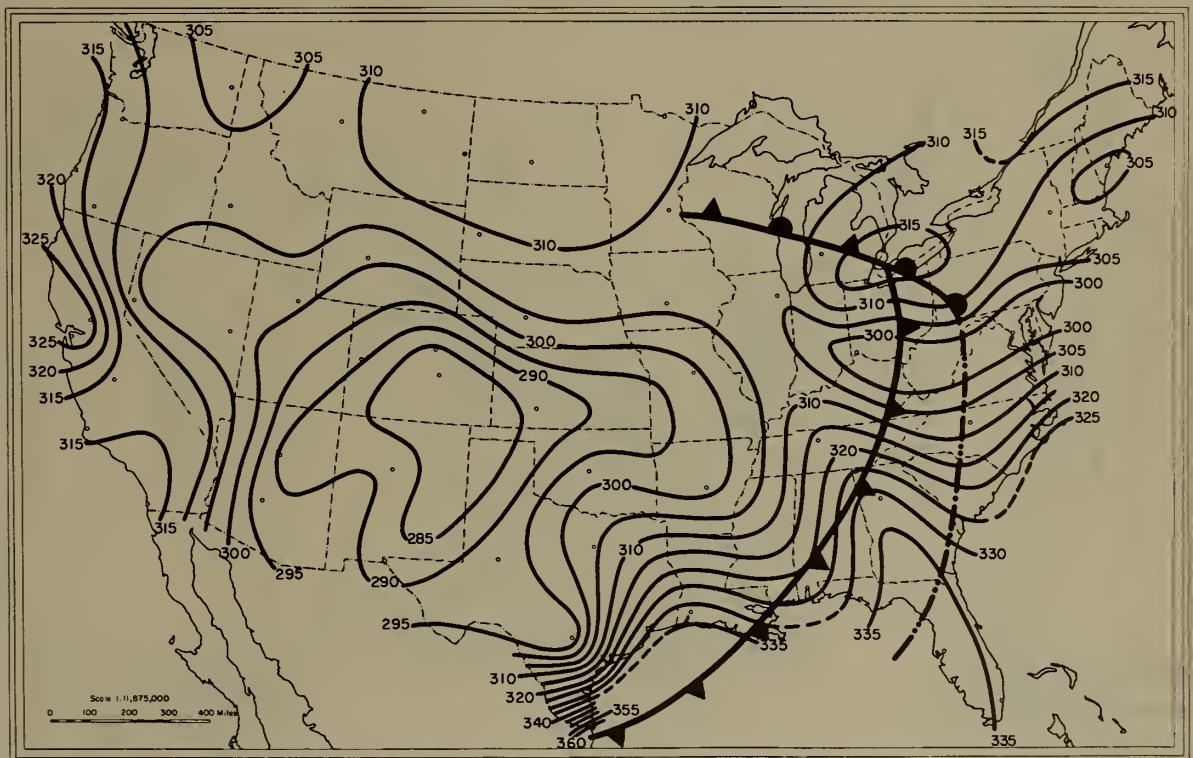


Figure 28. N_o Chart for Storm System 1330E 20 February, 1952

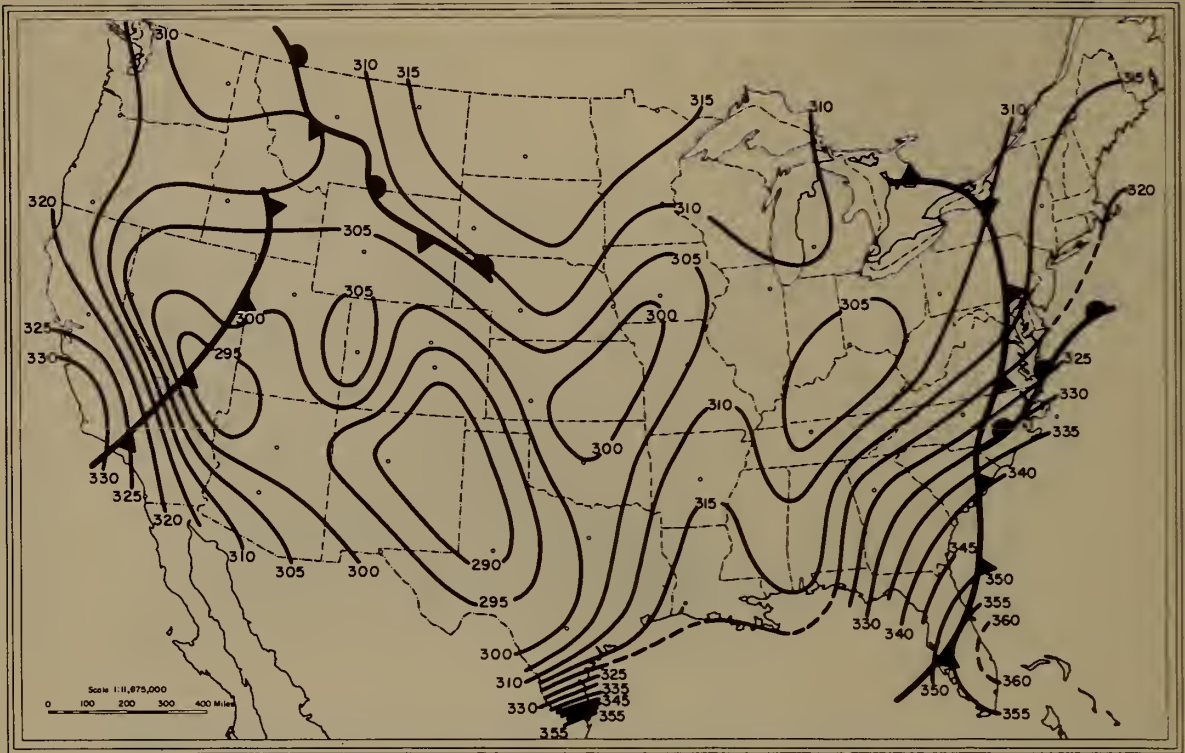


Figure 29. N_0 Chart for Storm Systems 0130E 21 February, 1952

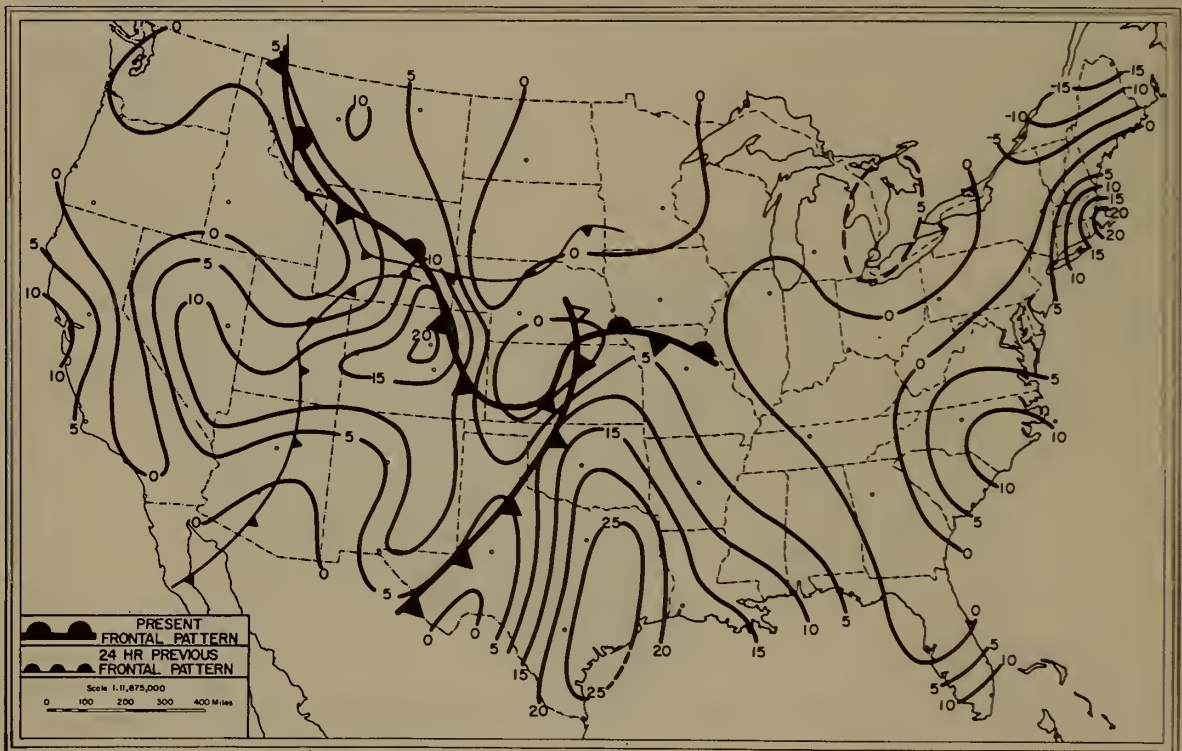


Figure 30. 24-Hour ΔN_0 Chart, 0130E 19 February, 1952

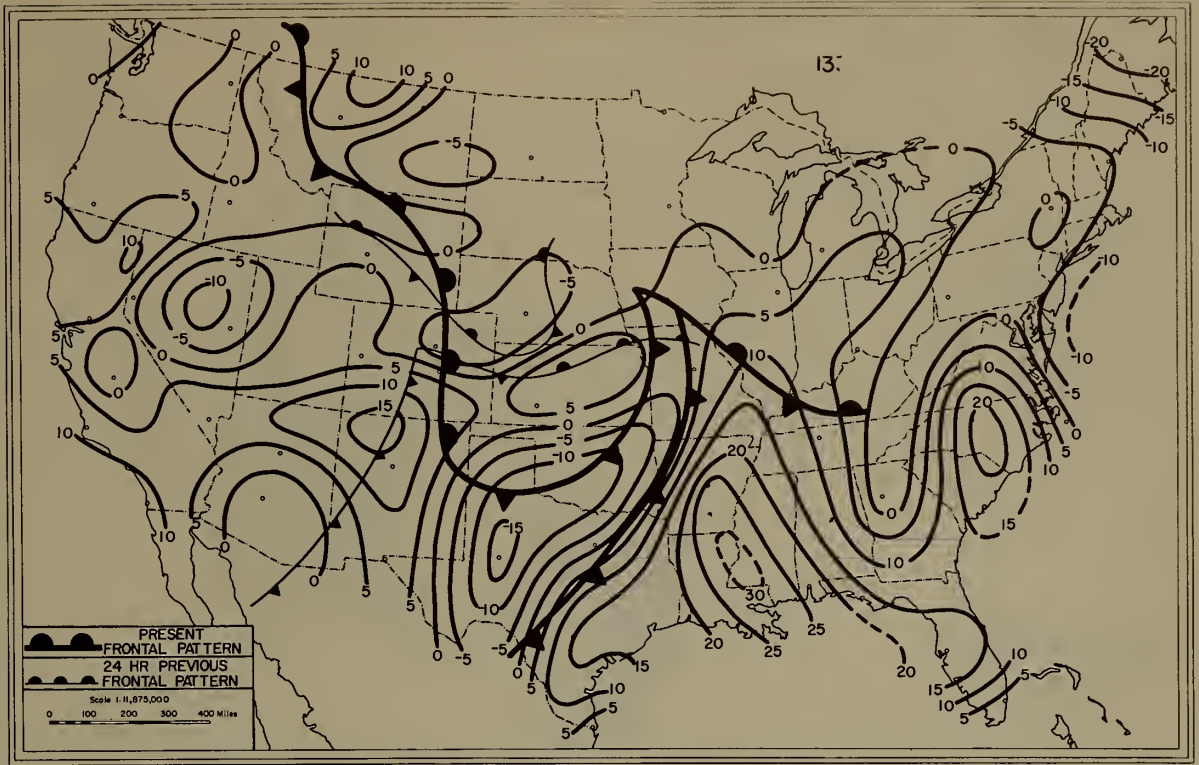


Figure 31. 24-Hour ΔN_0 Chart, 1330E 19 February, 1952

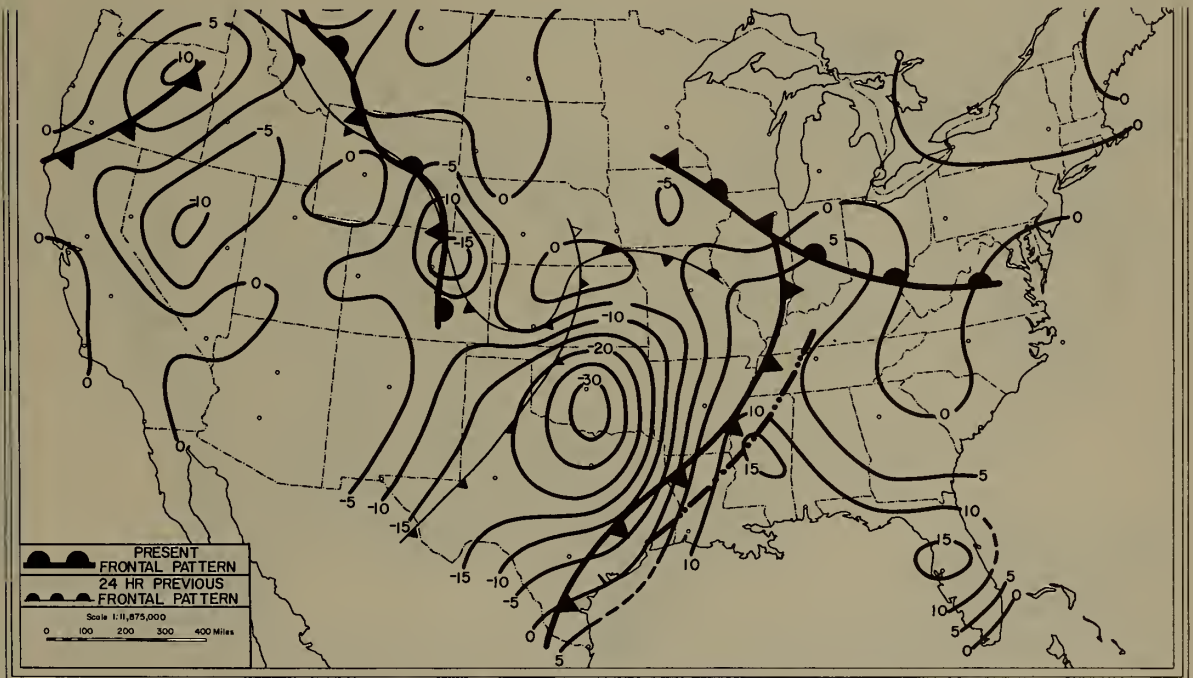


Figure 32. 24-Hour ΔN_0 Chart, 0130E 20 February, 1952

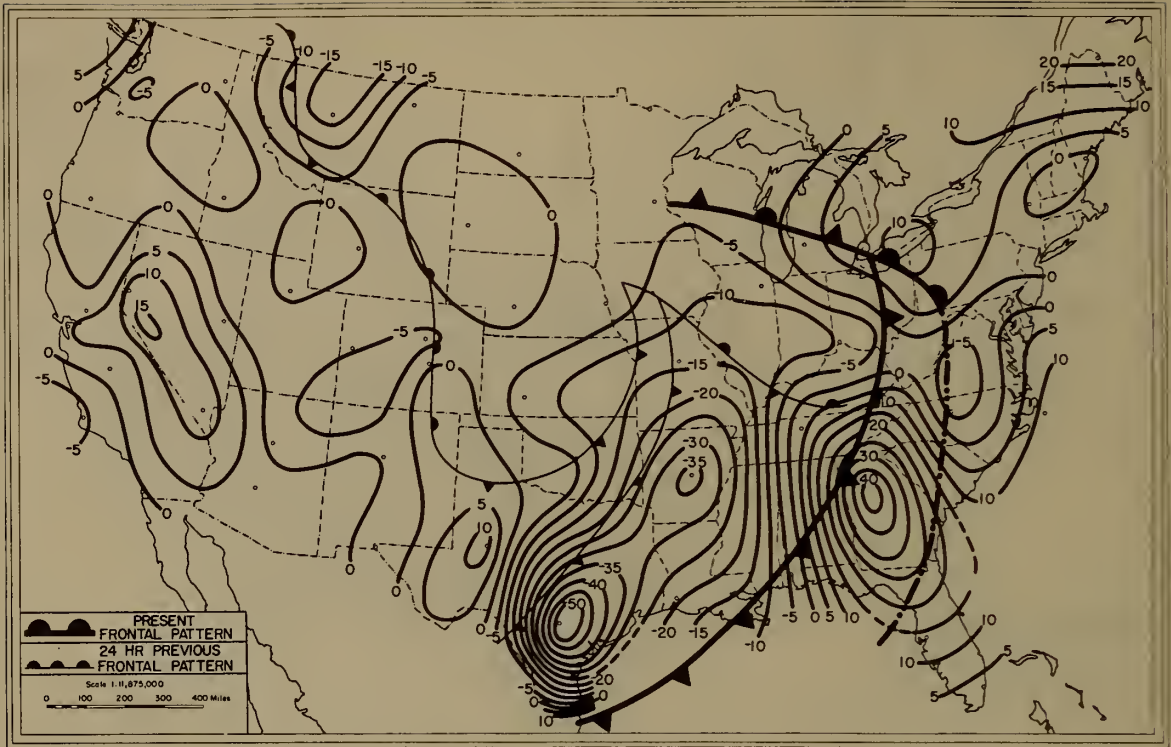


Figure 33. 24-Hour ΔN_o Chart, 1330E 20 February, 1952

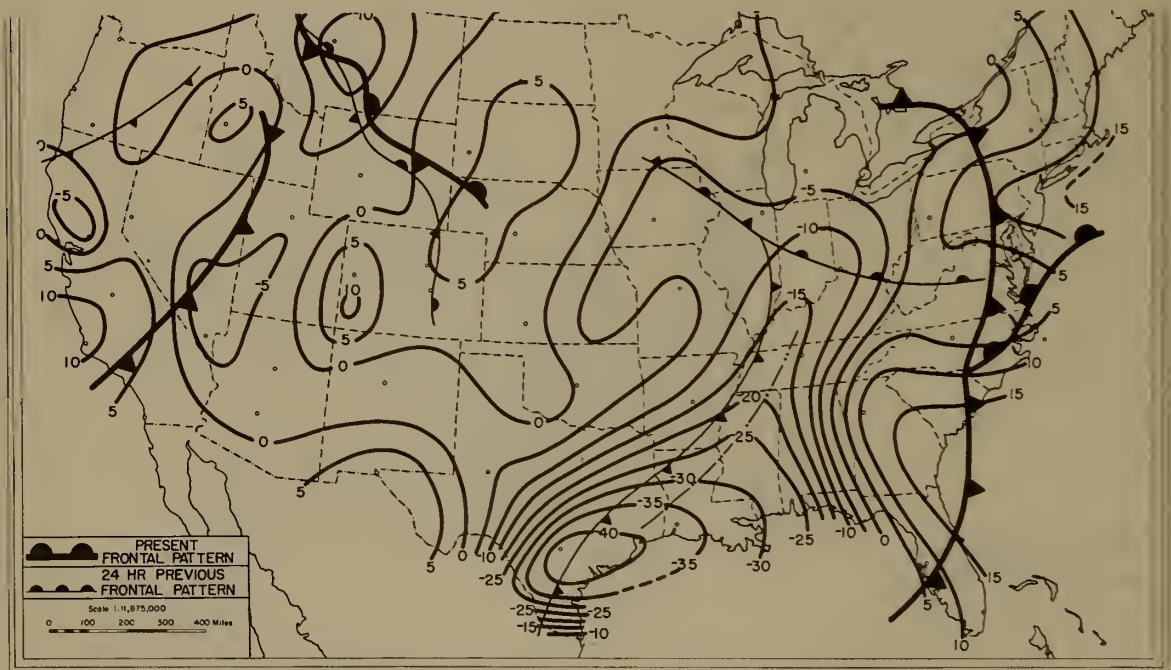


Figure 34. 24-Hour ΔN_o Chart, 0130E 21 February, 1952

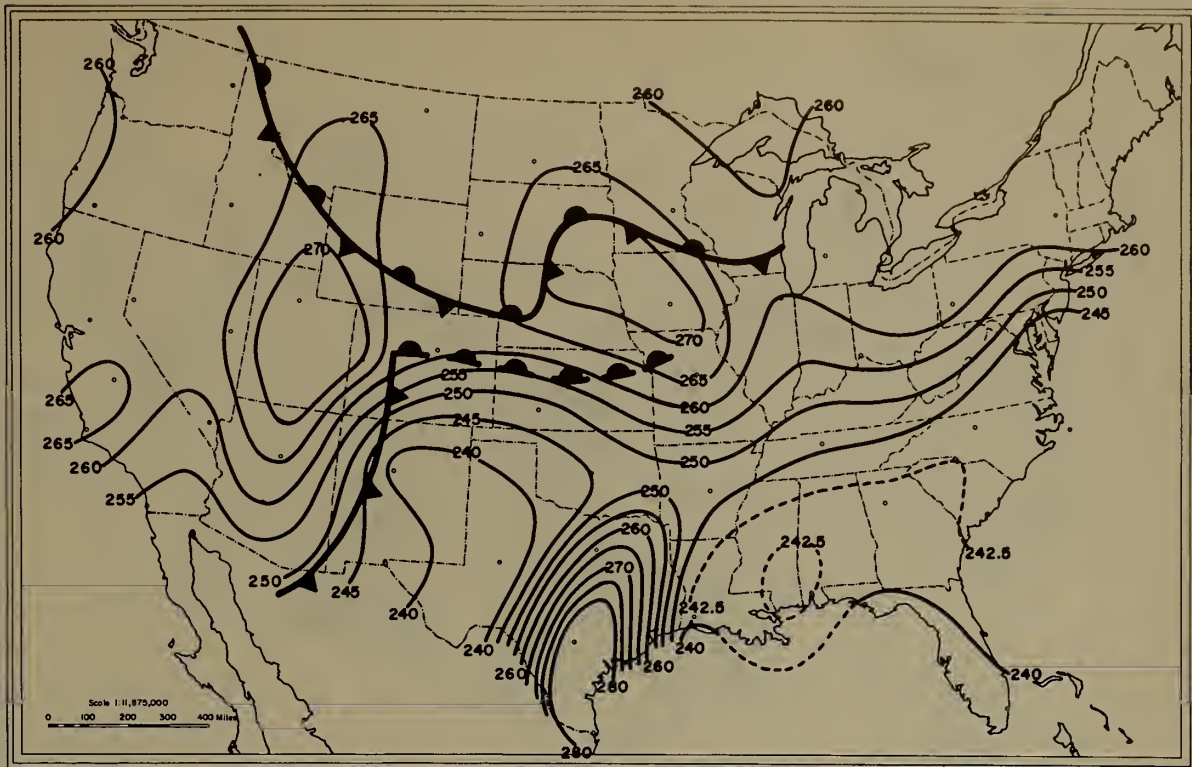


Figure 35. N_{850} Chart, 1000E 18 February, 1952

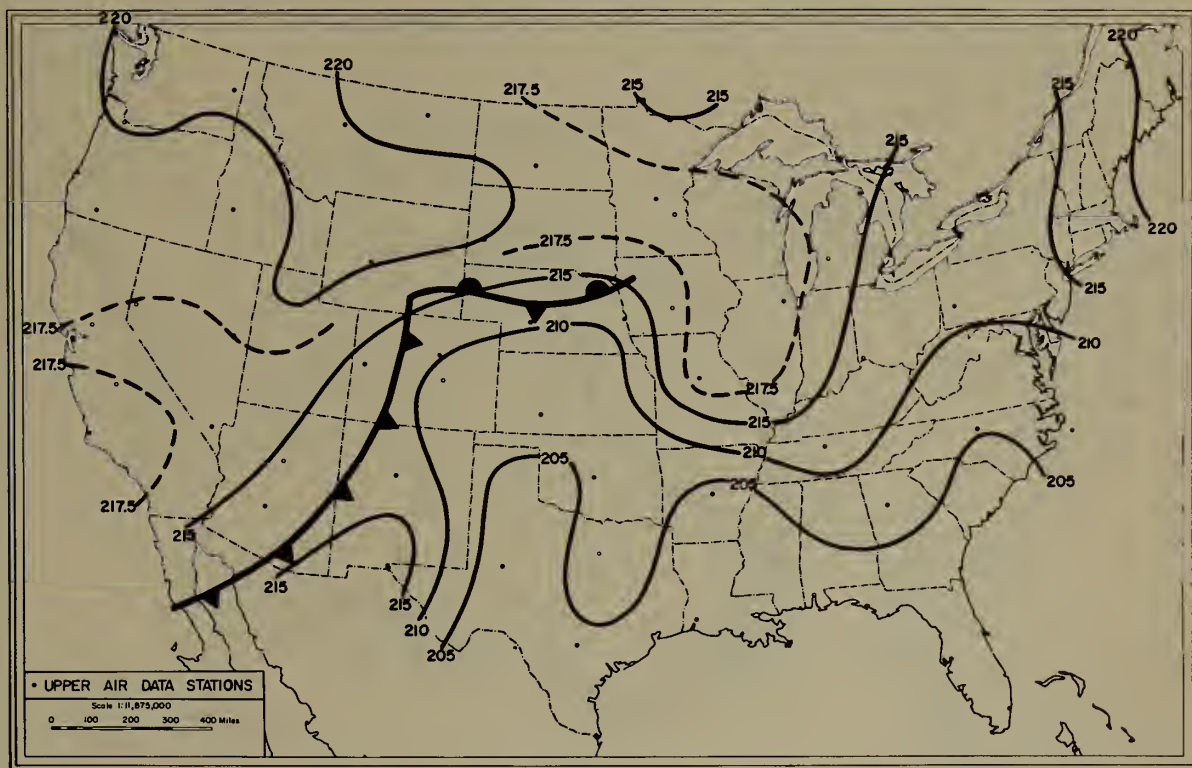


Figure 36. N_{700} Chart, 1000E 18 February, 1952

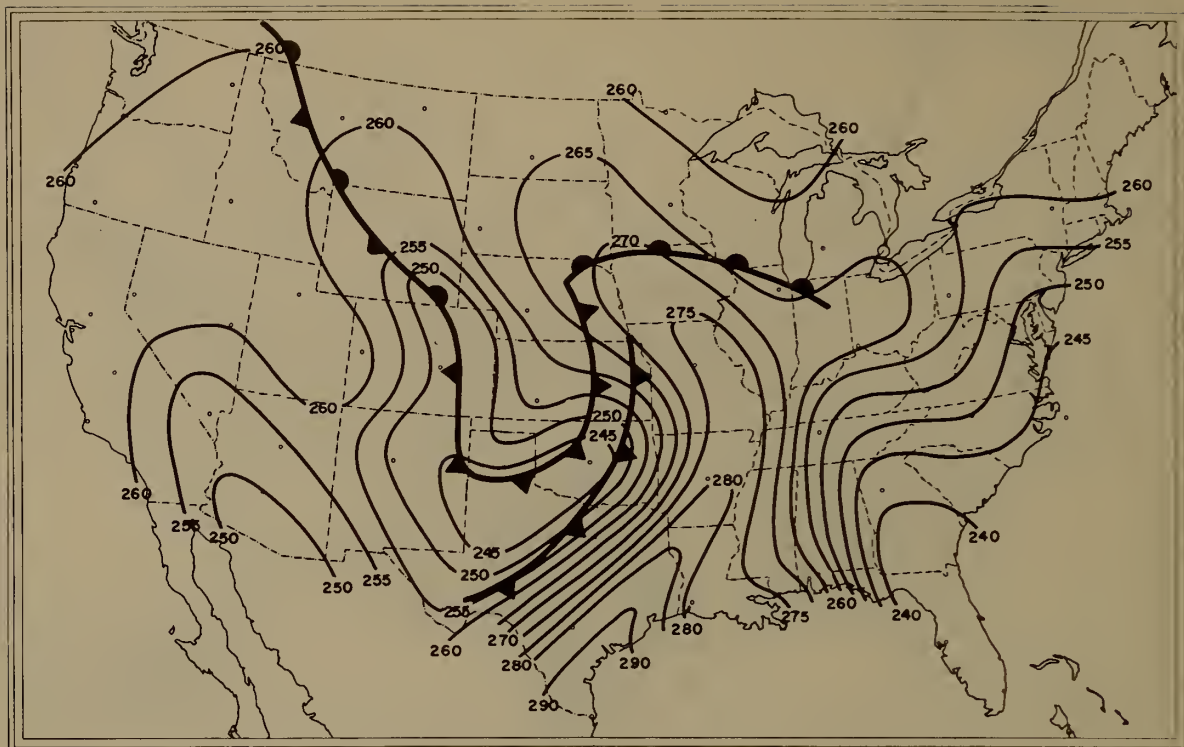


Figure 37. N₈₅₀ Chart, 1000E 19 February, 1952

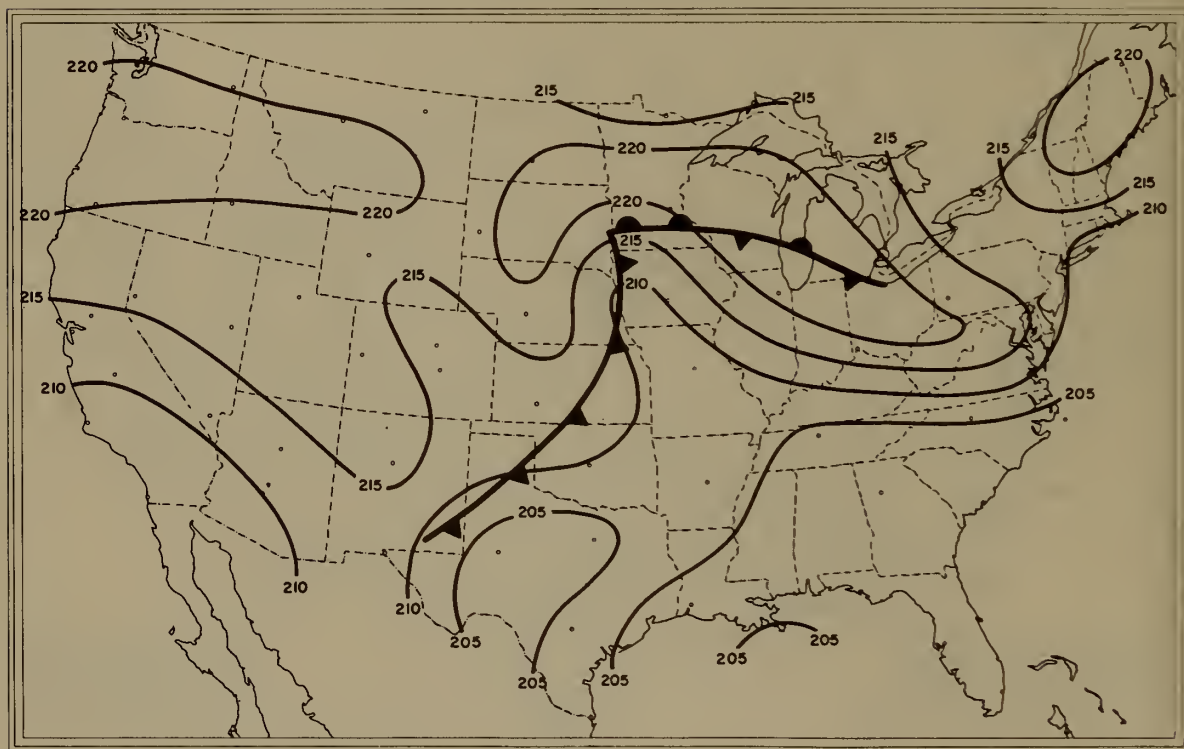


Figure 38. N₇₀₀ Chart, 1000E 19 February, 1952

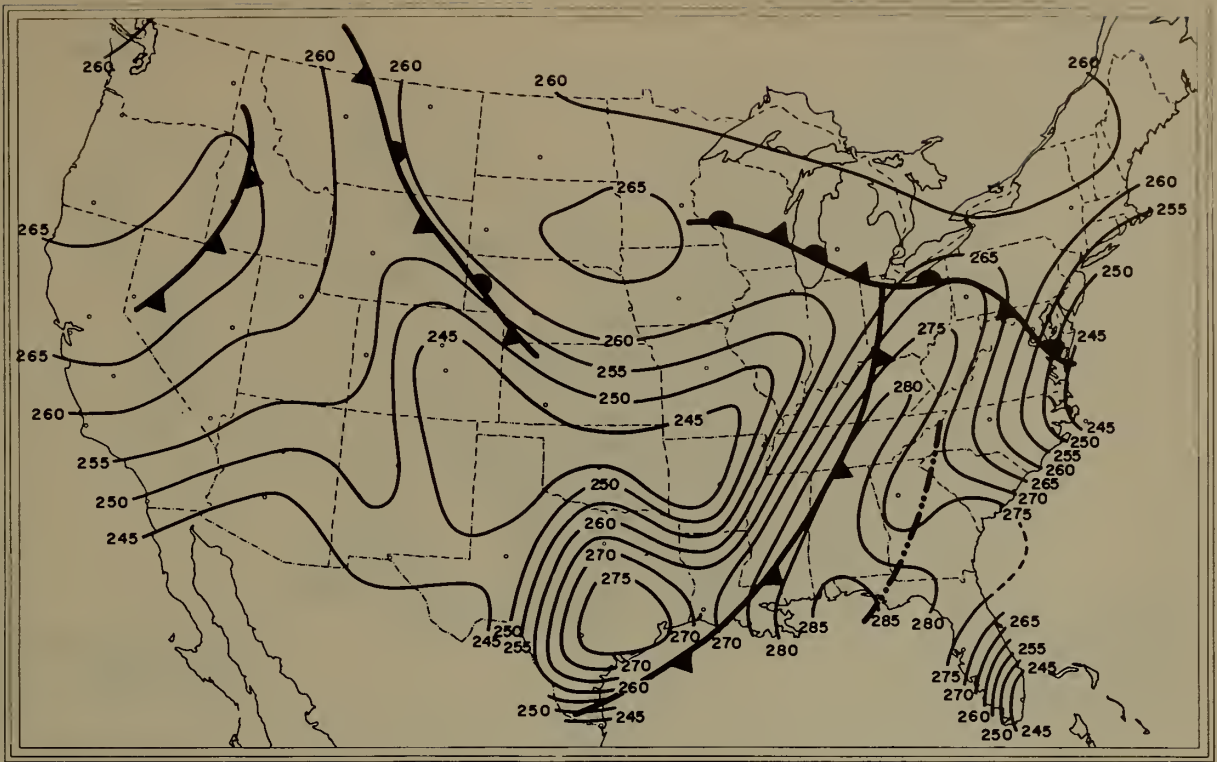


Figure 39. N₈₅₀ Chart, 1000E 20 February, 1952

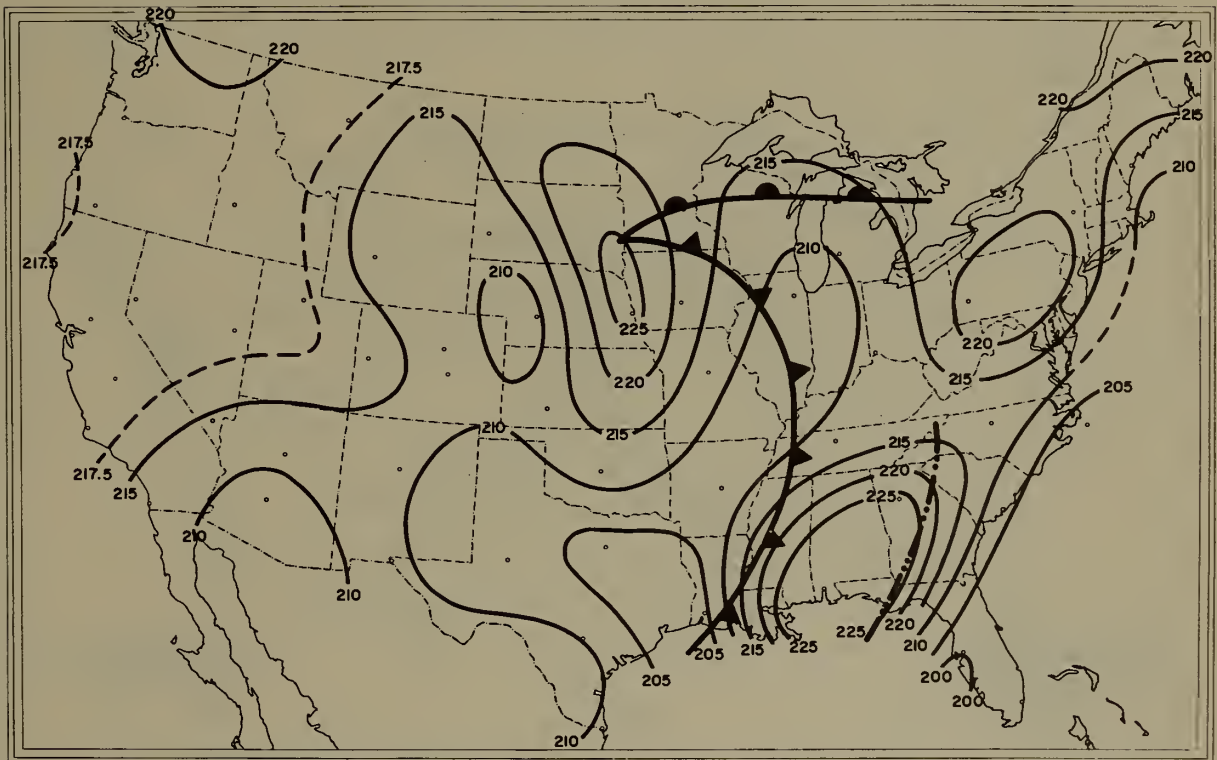


Figure 40. N₇₀₀ Chart, 1000E 20 February, 1952

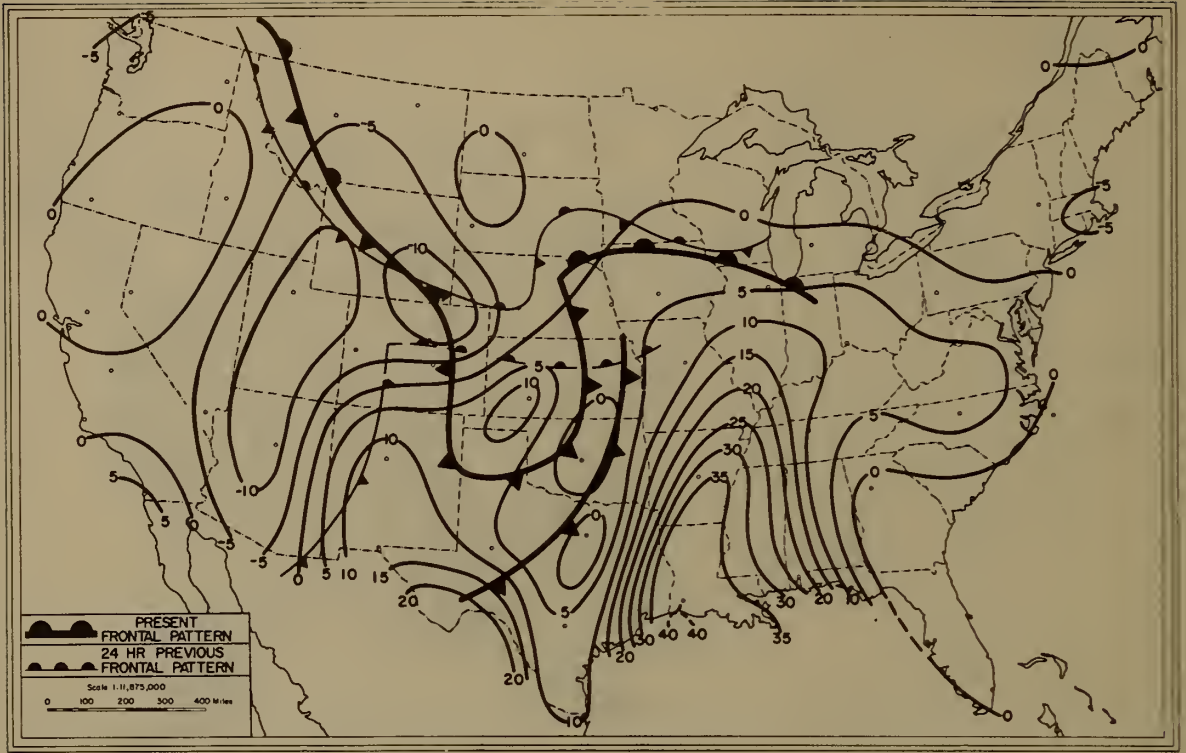


Figure 41. 24-Hour ΔN_{850} Chart, 1000E 19 February, 1952

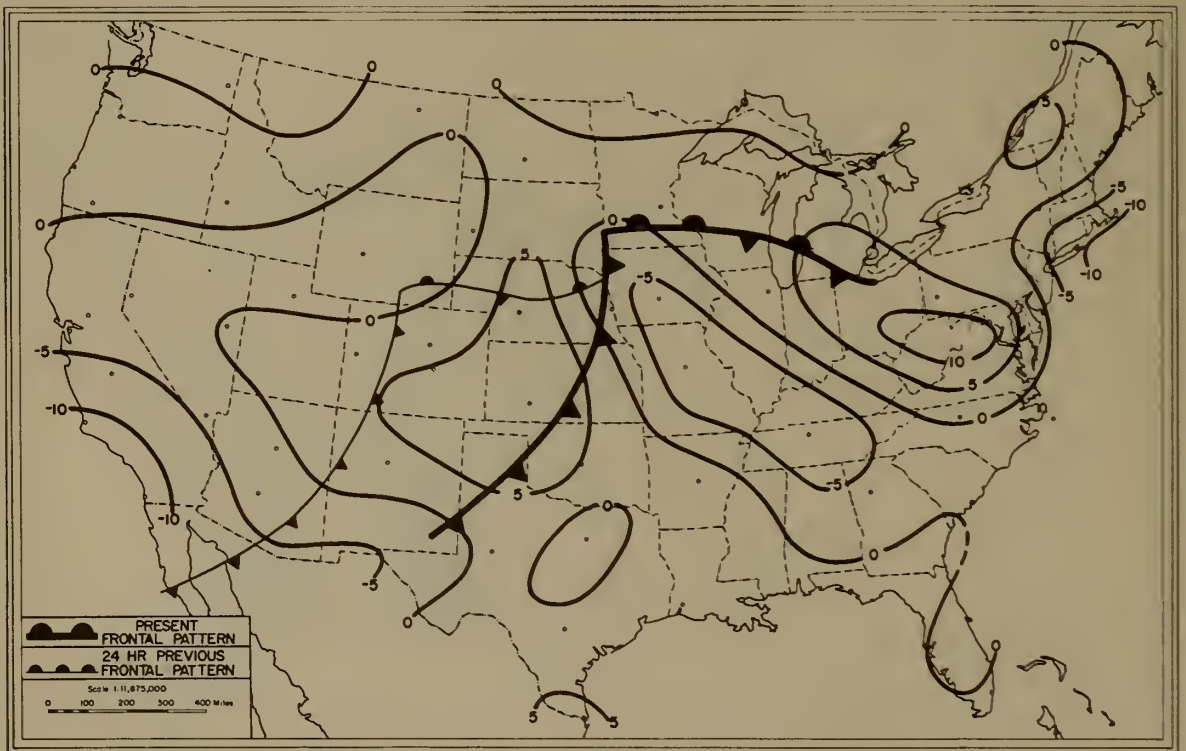


Figure 42. 24-Hour ΔN_{700} Chart, 1000E 19 February, 1952

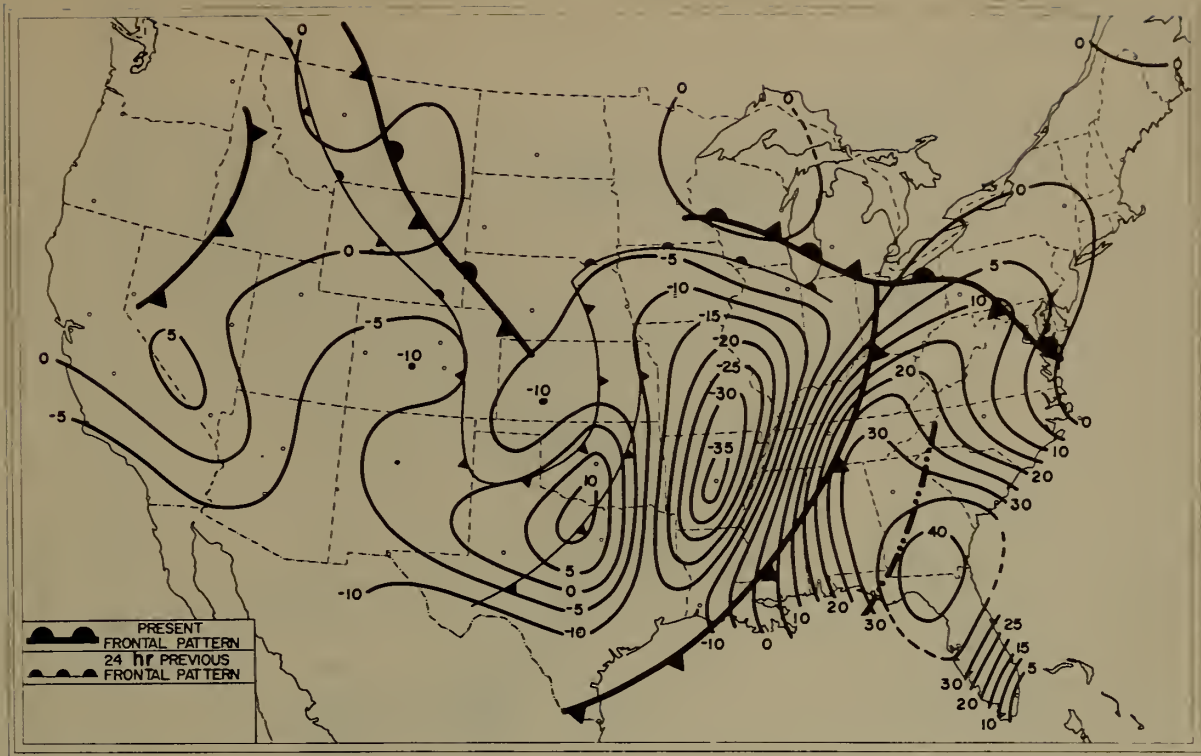


Figure 43. 24-Hour ΔN_{850} Chart, 1000E 20 February, 1952

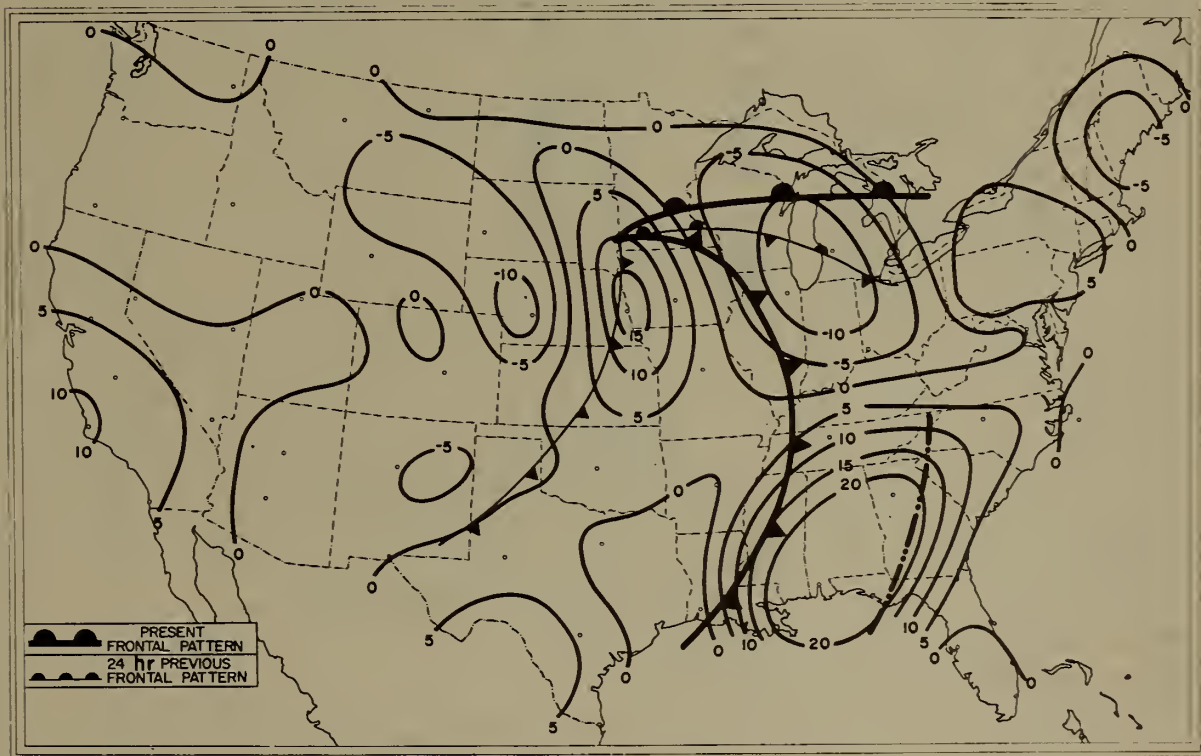


Figure 44. 24-Hour ΔN_{700} Chart, 1000E 20 February, 1952

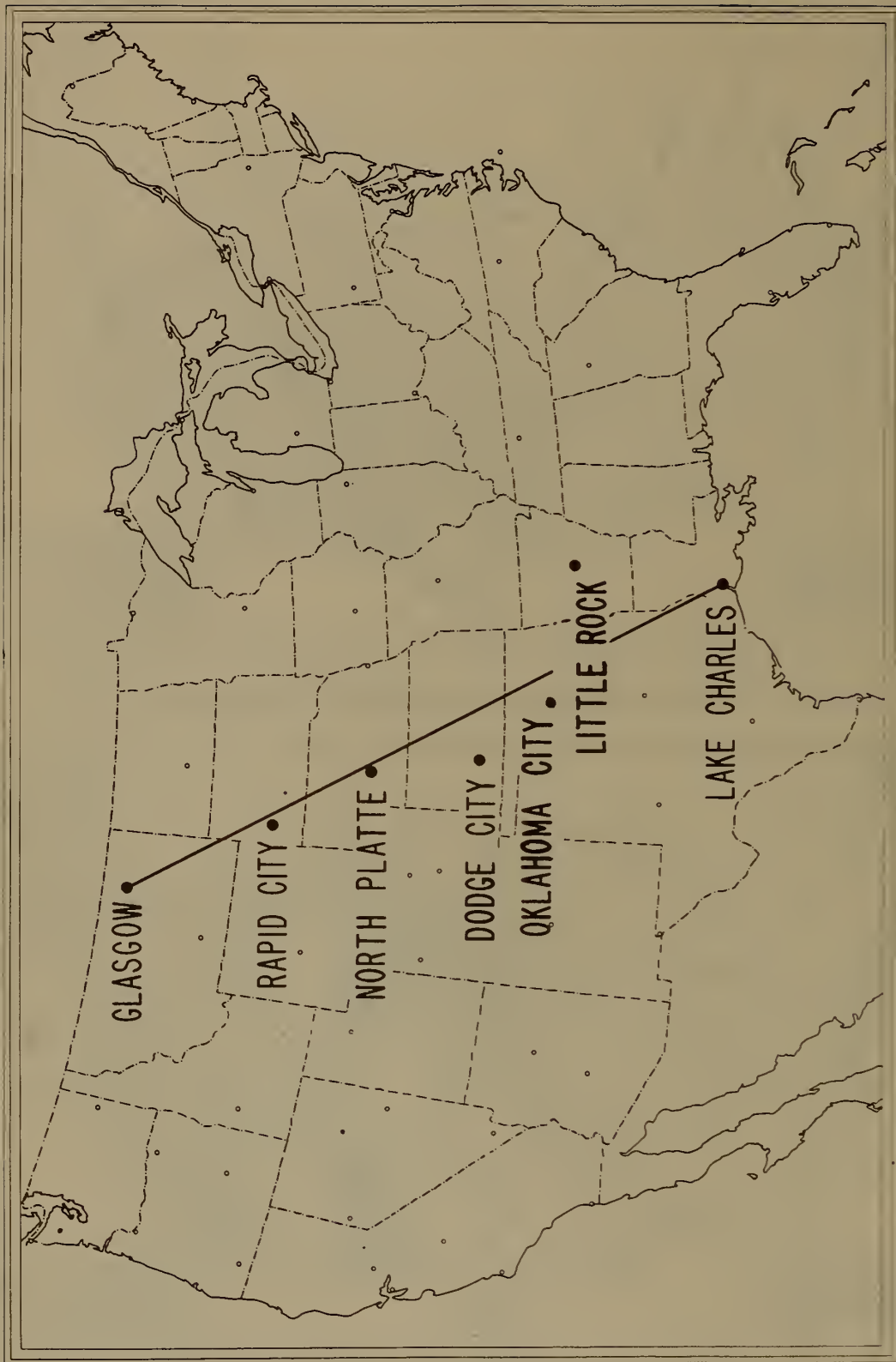


Figure 45. Station Identification Chart

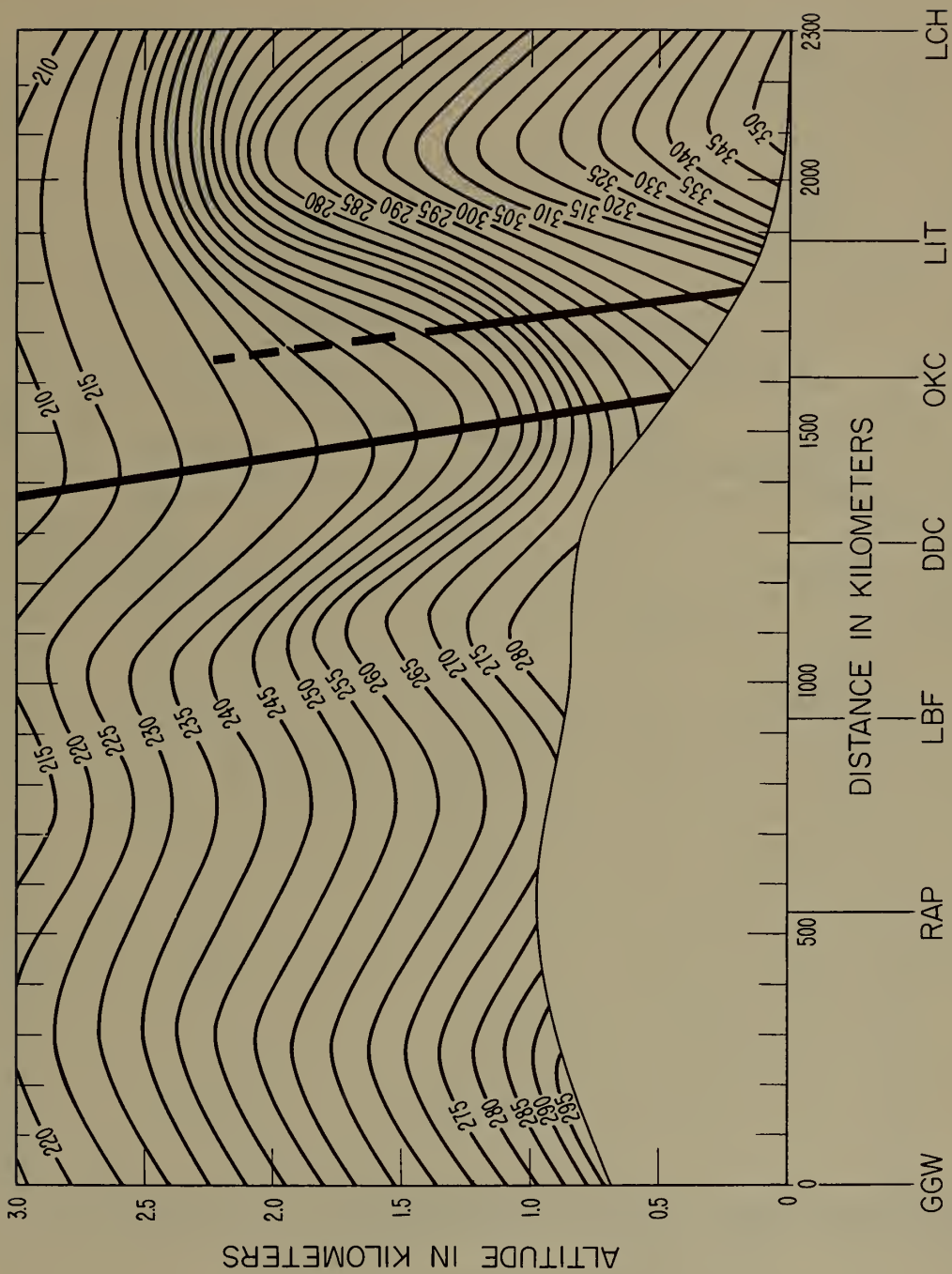


Figure 46. Space Cross-Section in N Units, 1500Z, 19 February, 1952

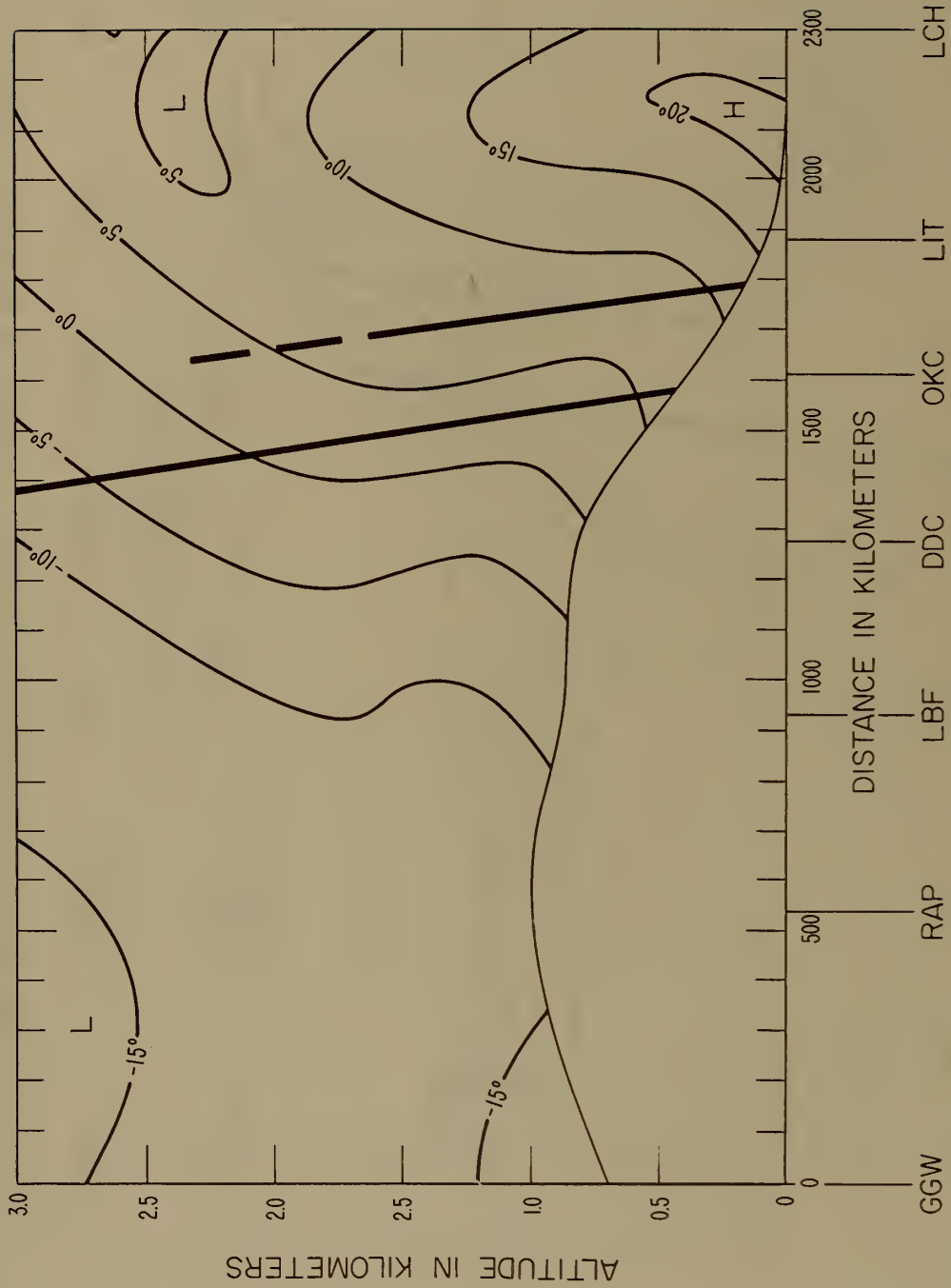


Figure 47. Temperature Cross-Section in °C, 1500Z, 19 February, 1952

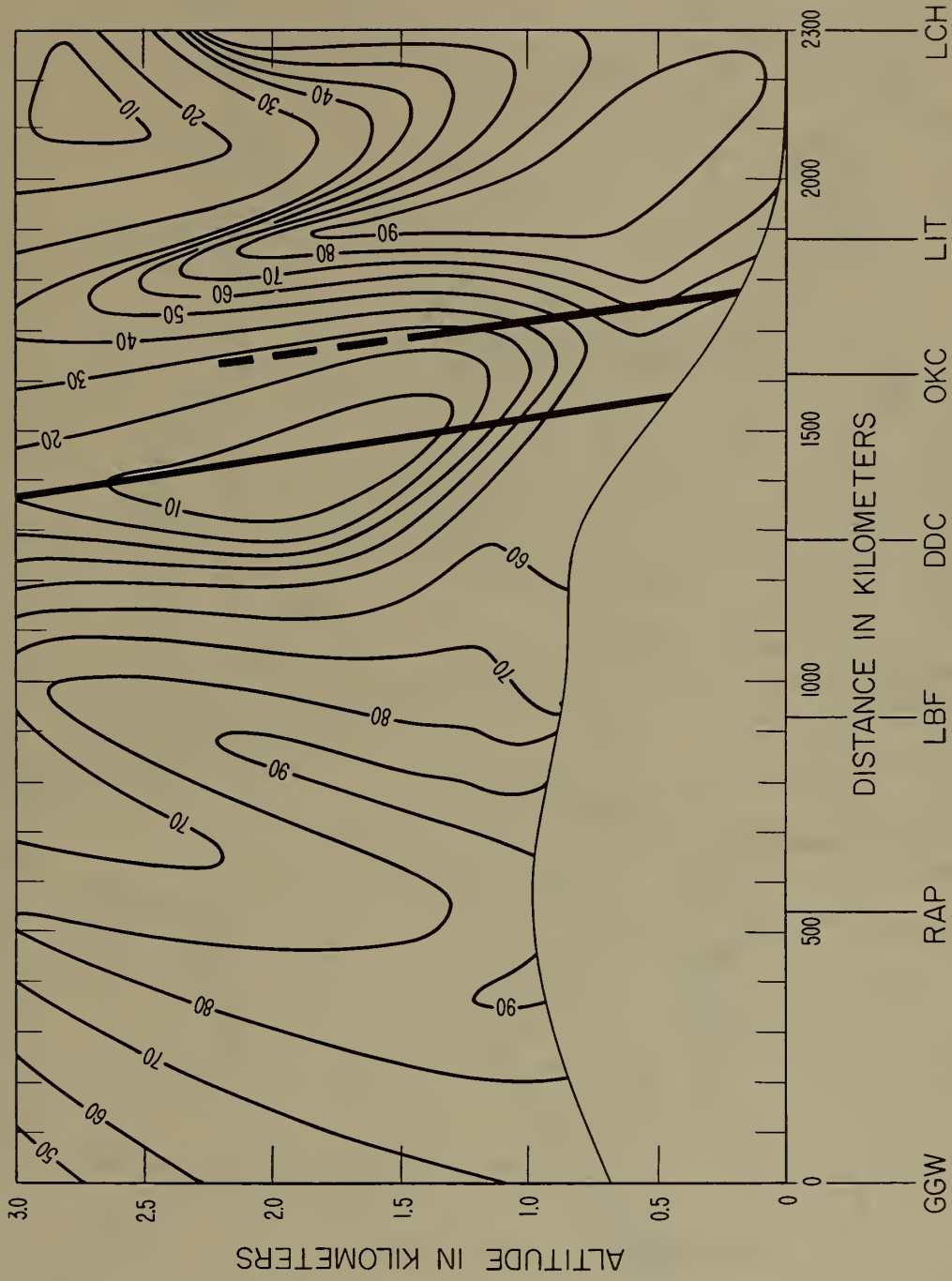


Figure 48. Relative Humidity Cross-Section (%), 1500Z, 19 February, 1952

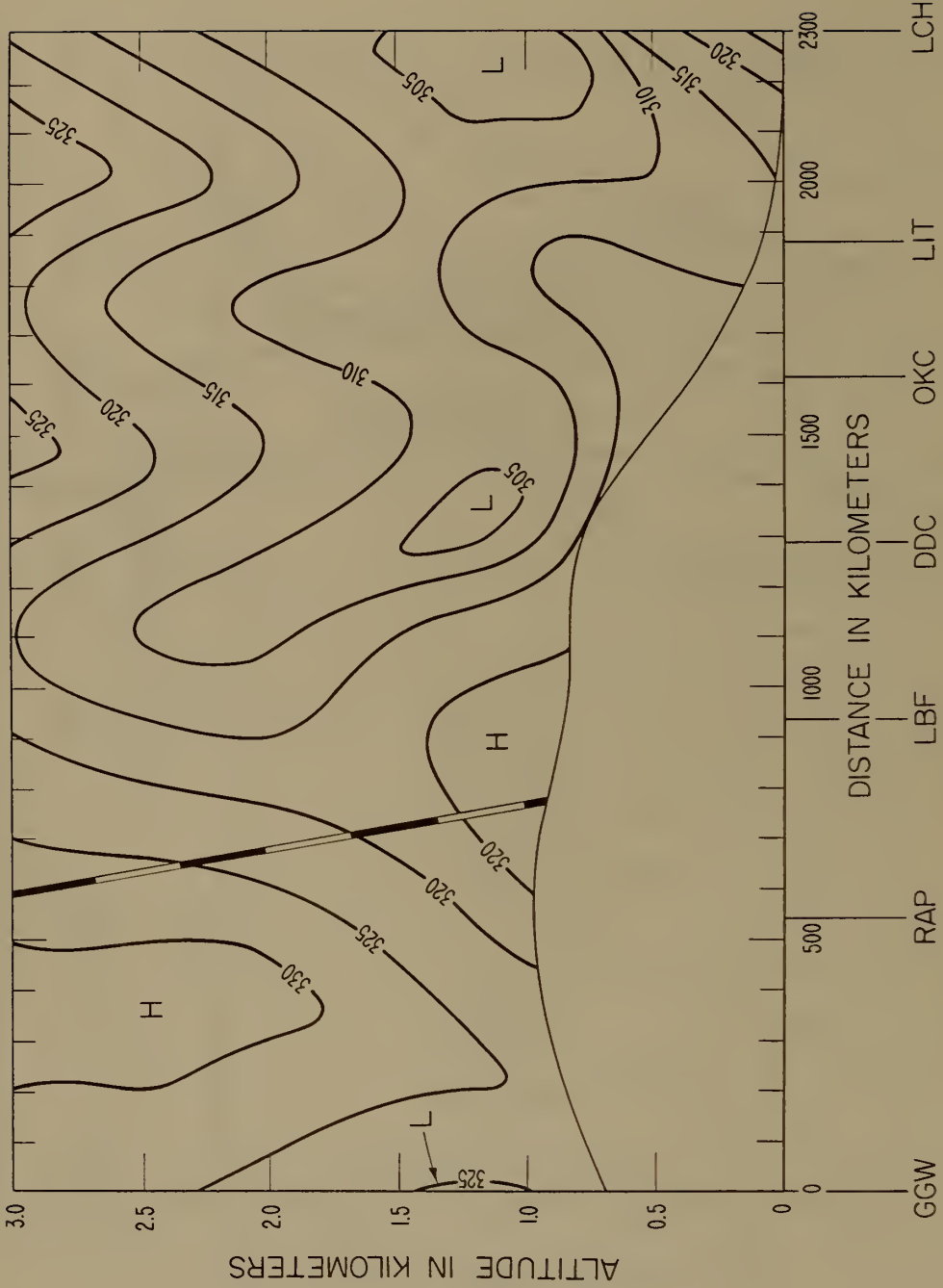


Figure 49. Space Cross-Section in A Units, 0300Z, 18 February, 1952

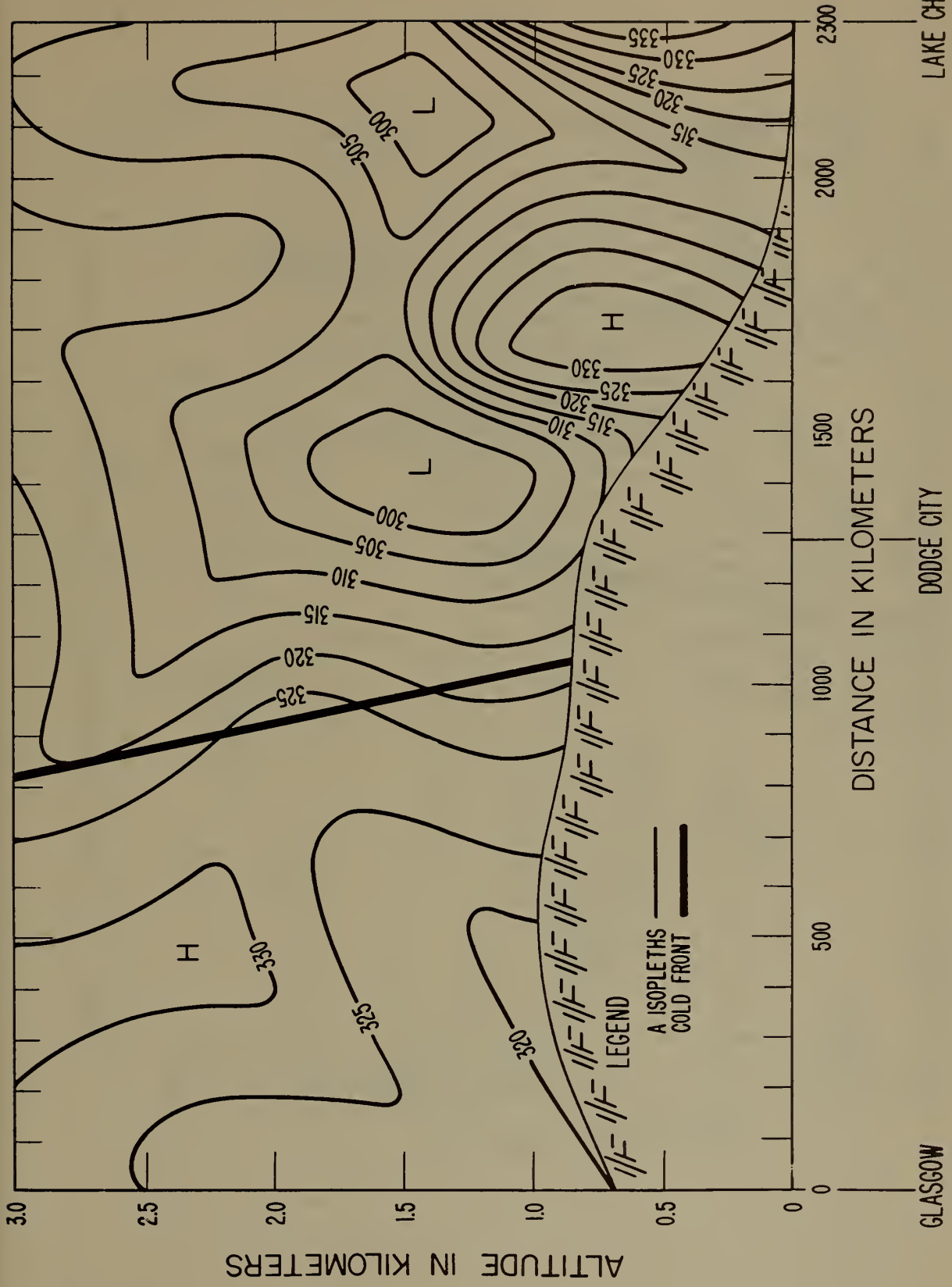


Figure 50. Space Cross-Section in A Units, 1500Z, 18 February, 1952

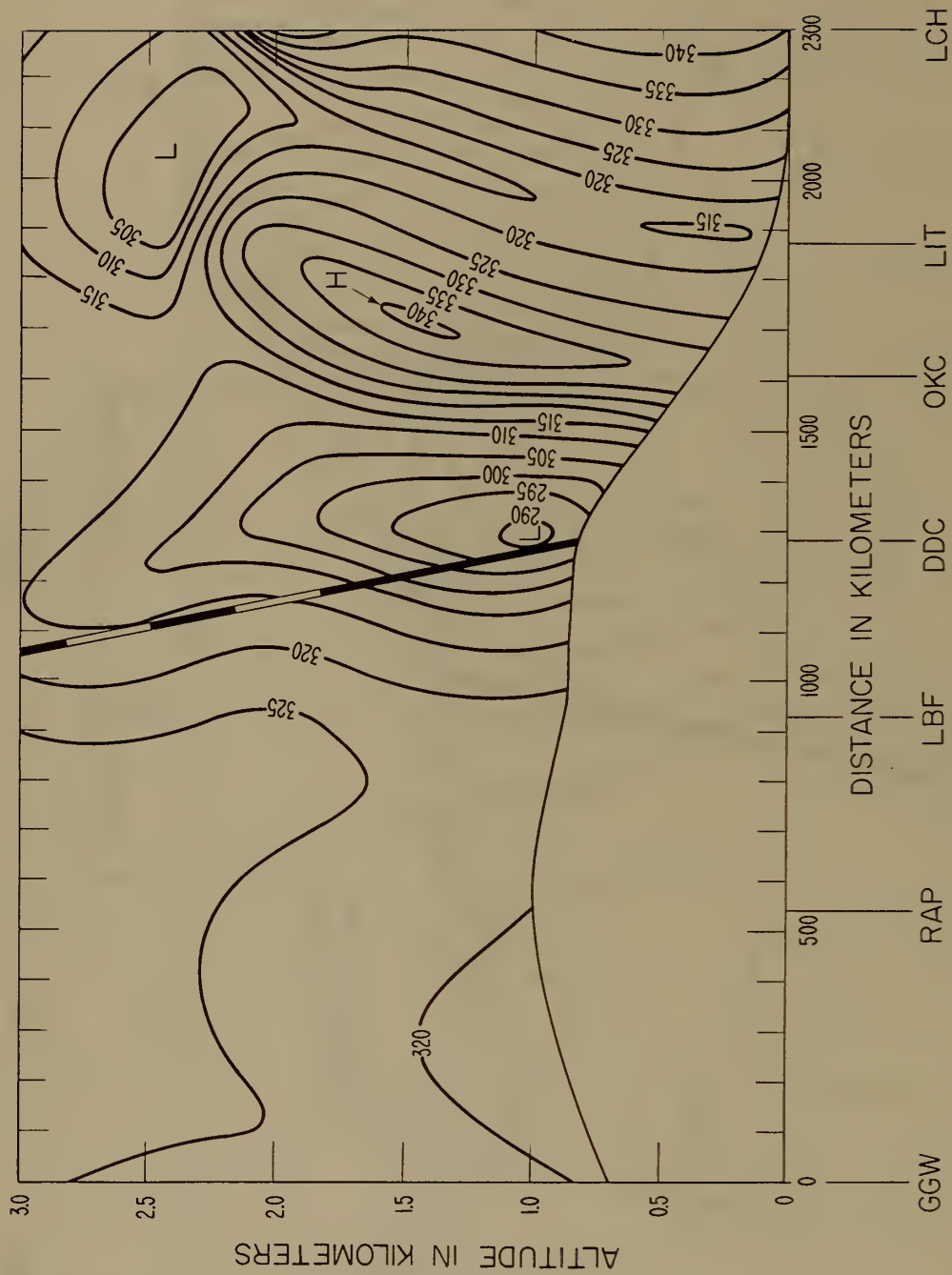


Figure 51. Space Cross-Section in A Units, 0300Z, 19 February, 1952

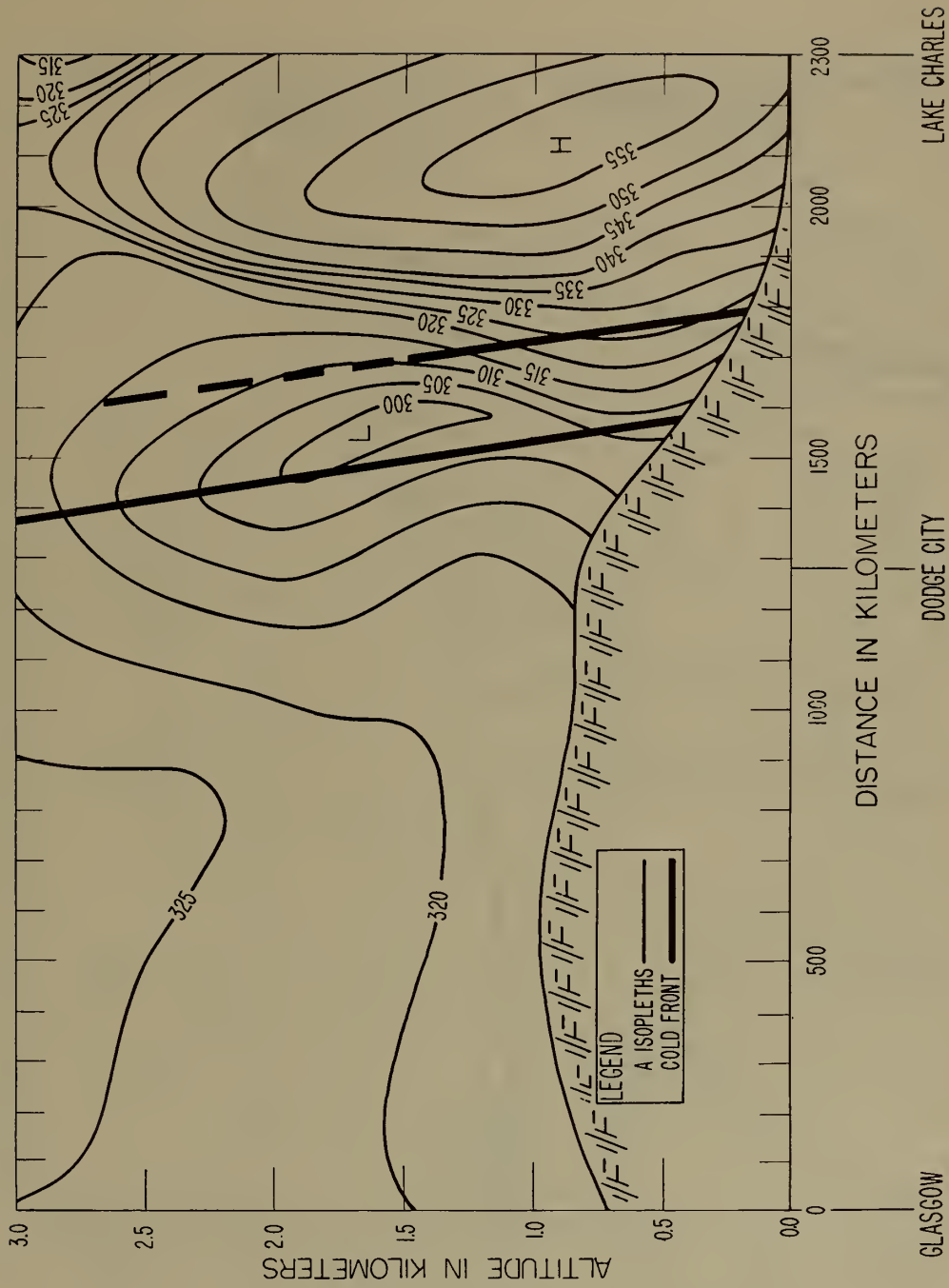


Figure 52. Space Cross-Section in A Units, 1500Z, 19 February, 1952

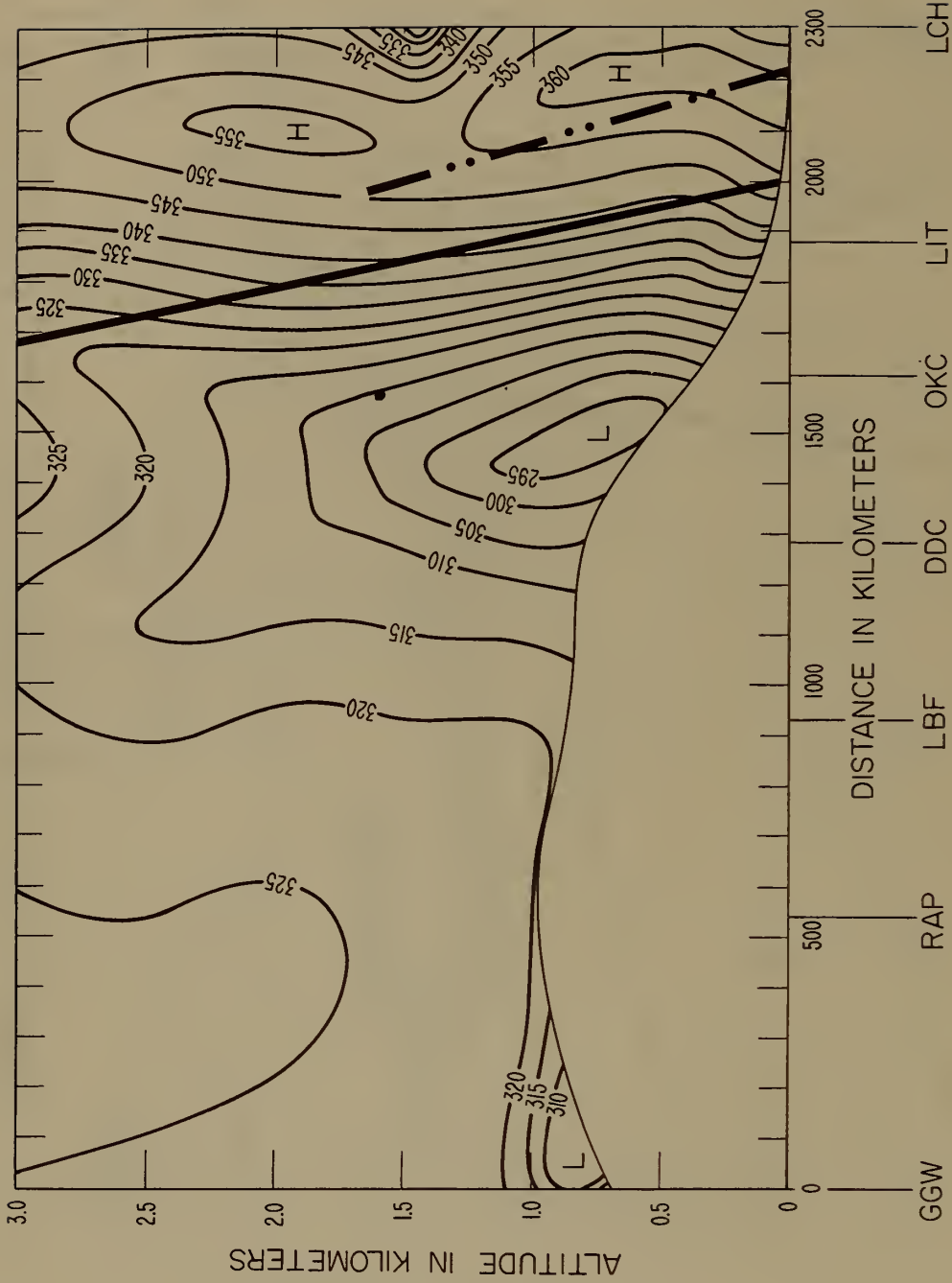


Figure 53. Space Cross-Section in A Units, 0300Z, 20 February, 1952

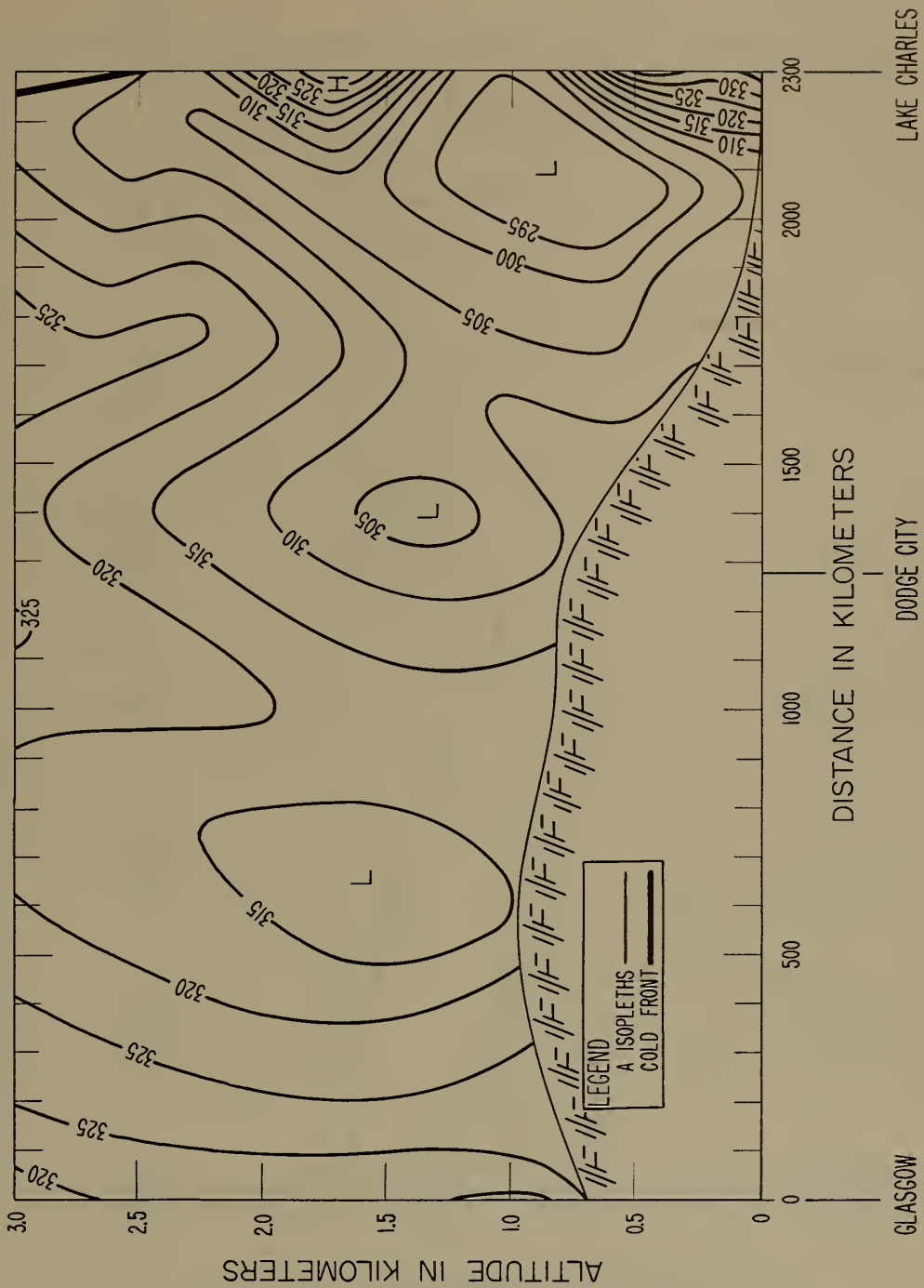


Figure 54. Space Cross-Section in A Units, 1500Z, 20 February, 1952

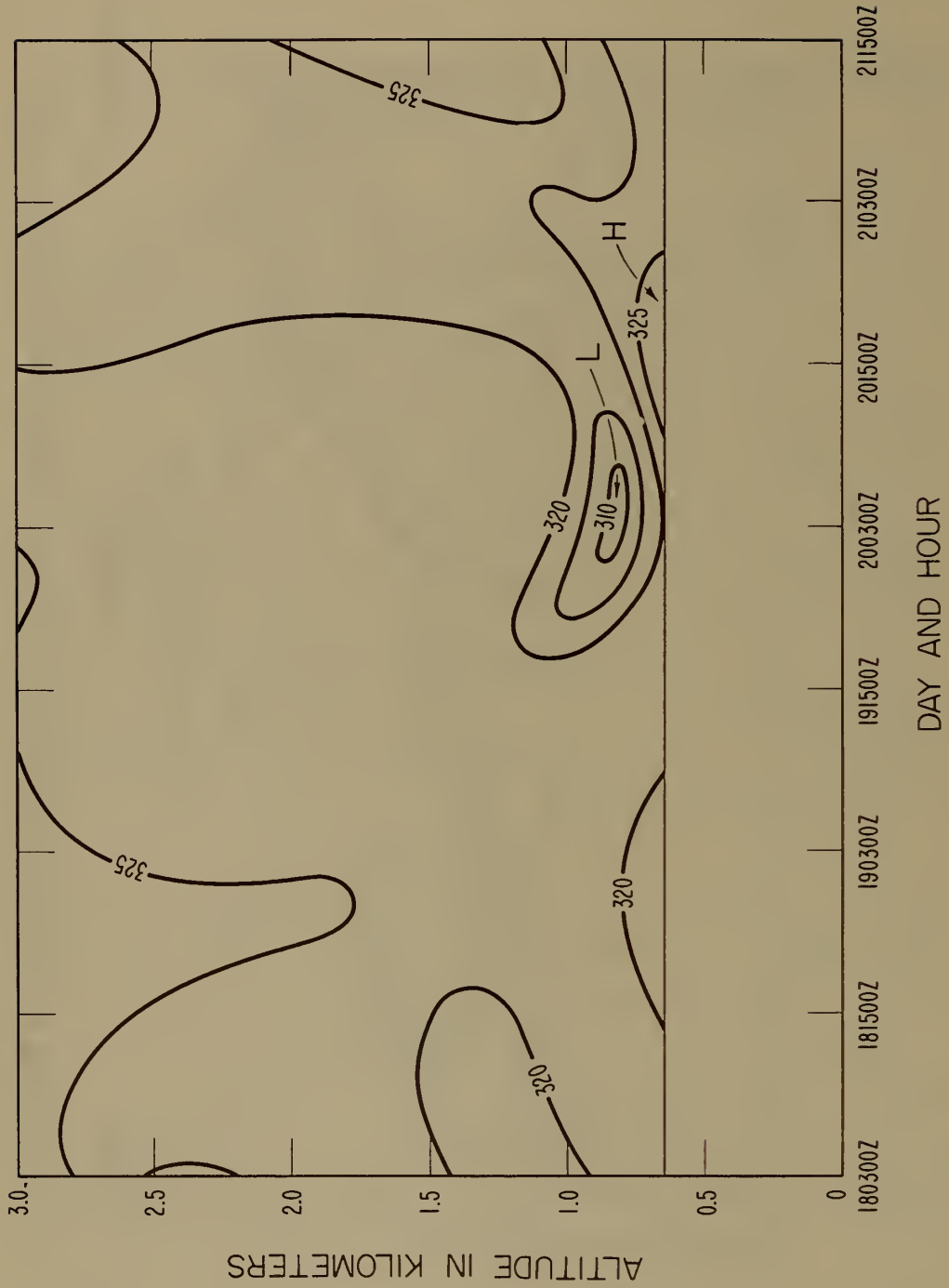


Figure 55. Time Cross-Section, Glasgow, Montana, in A Units

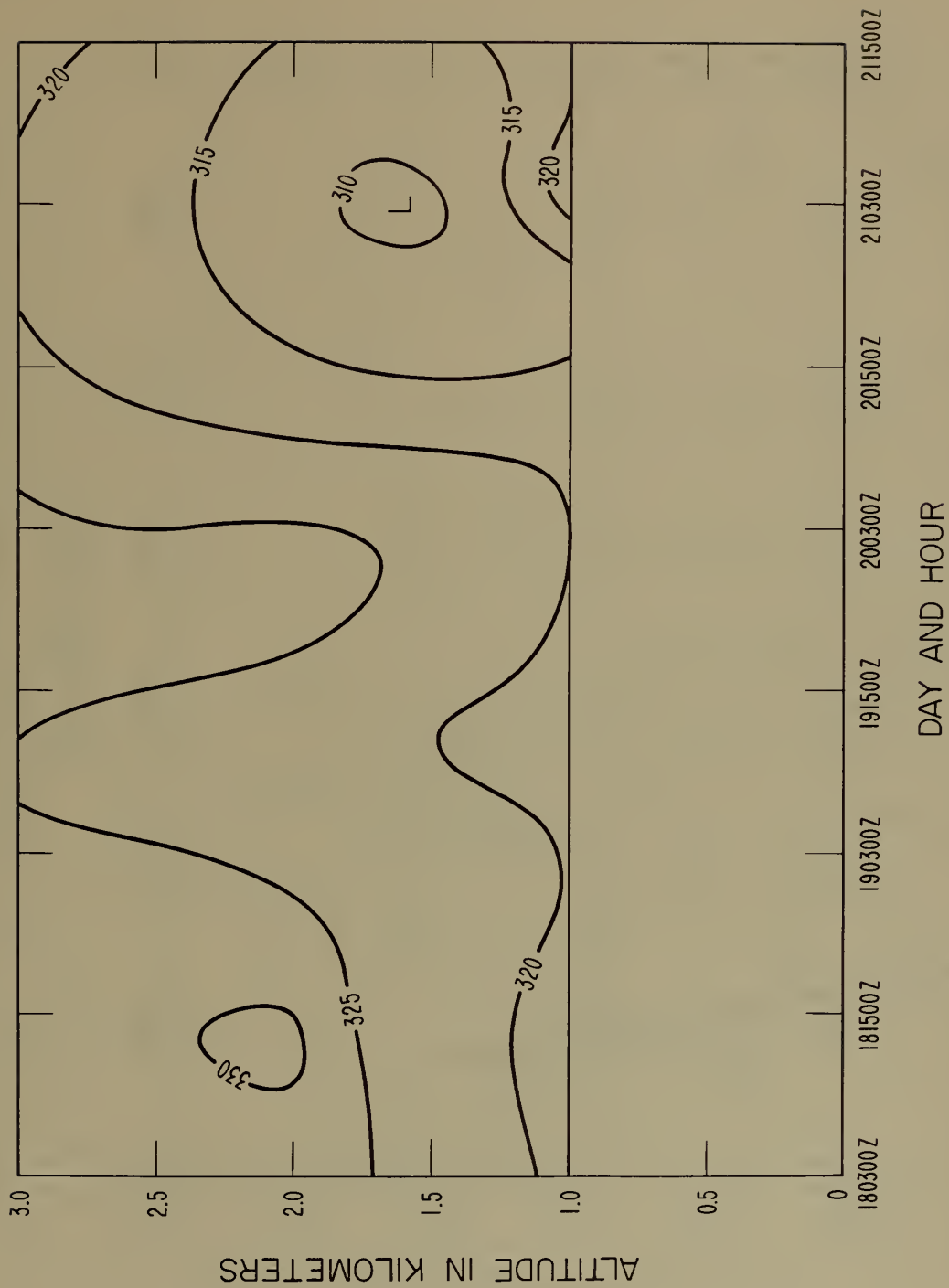


Figure 56. Time Cross-Section, Rapid City, South Dakota, in A Units

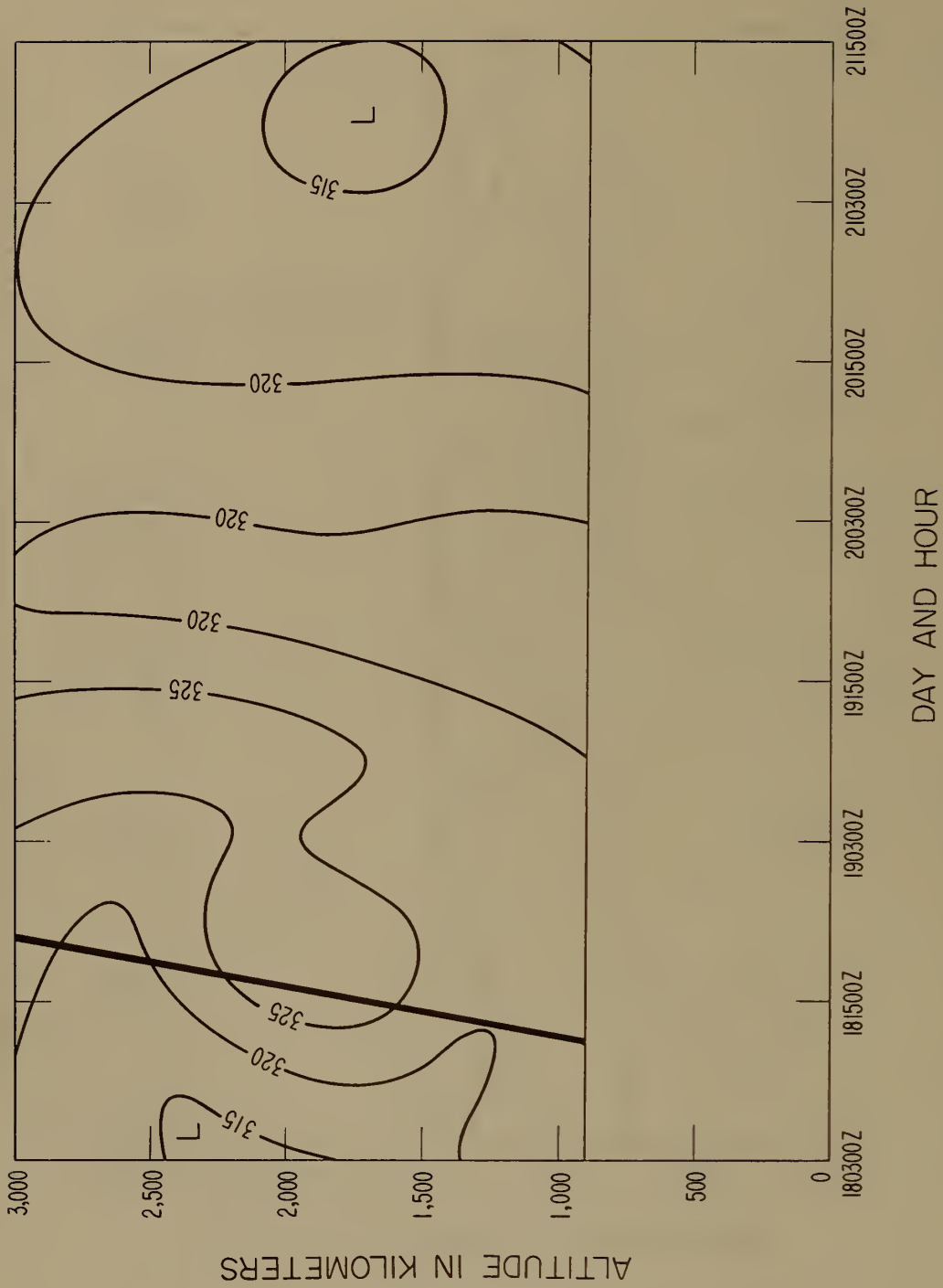


Figure 57. Time Cross-Section, North Platte, Nebraska, in A Units

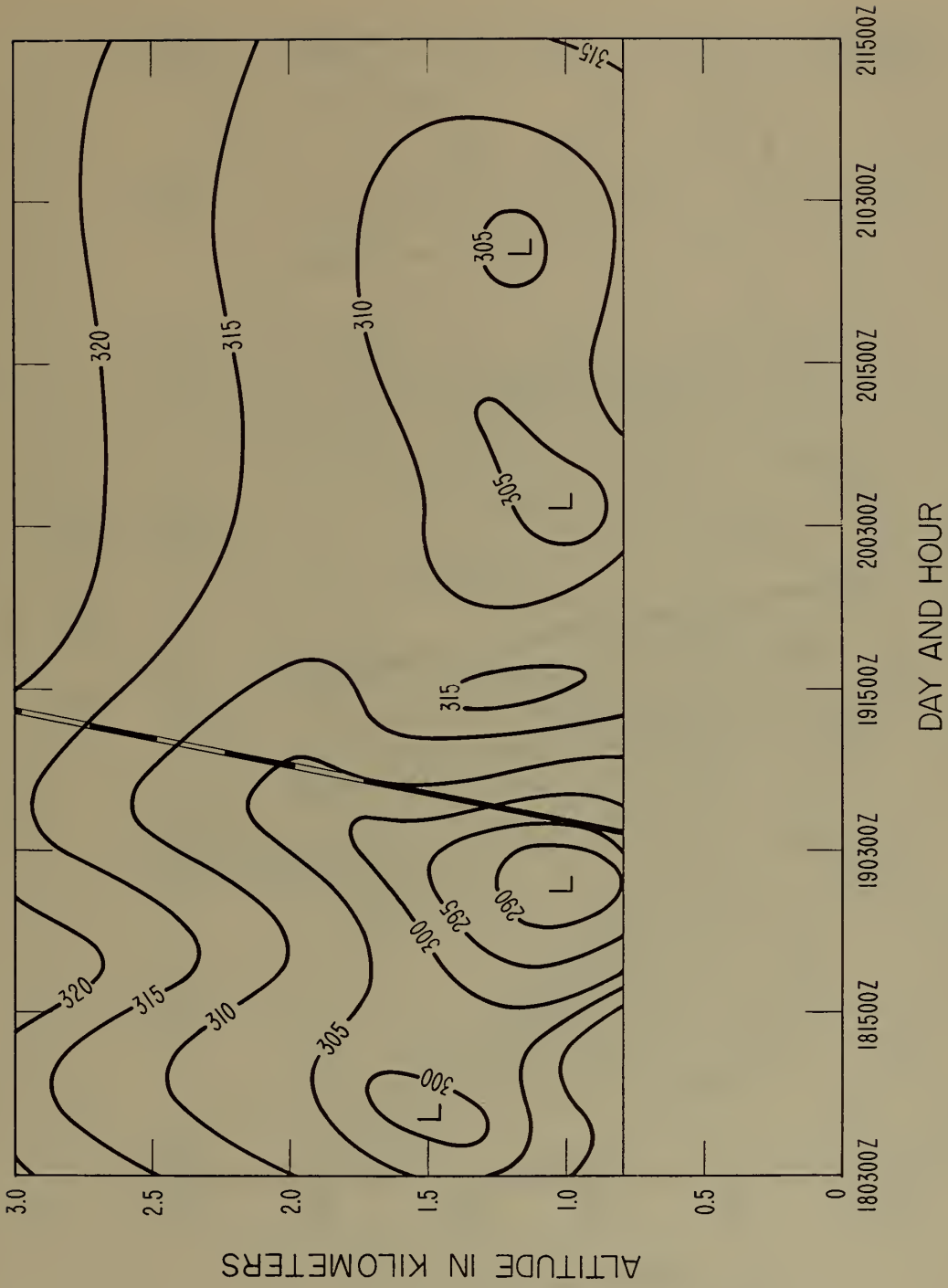


Figure 58. Time Cross-Section, Dodge City, Kansas, in A Units

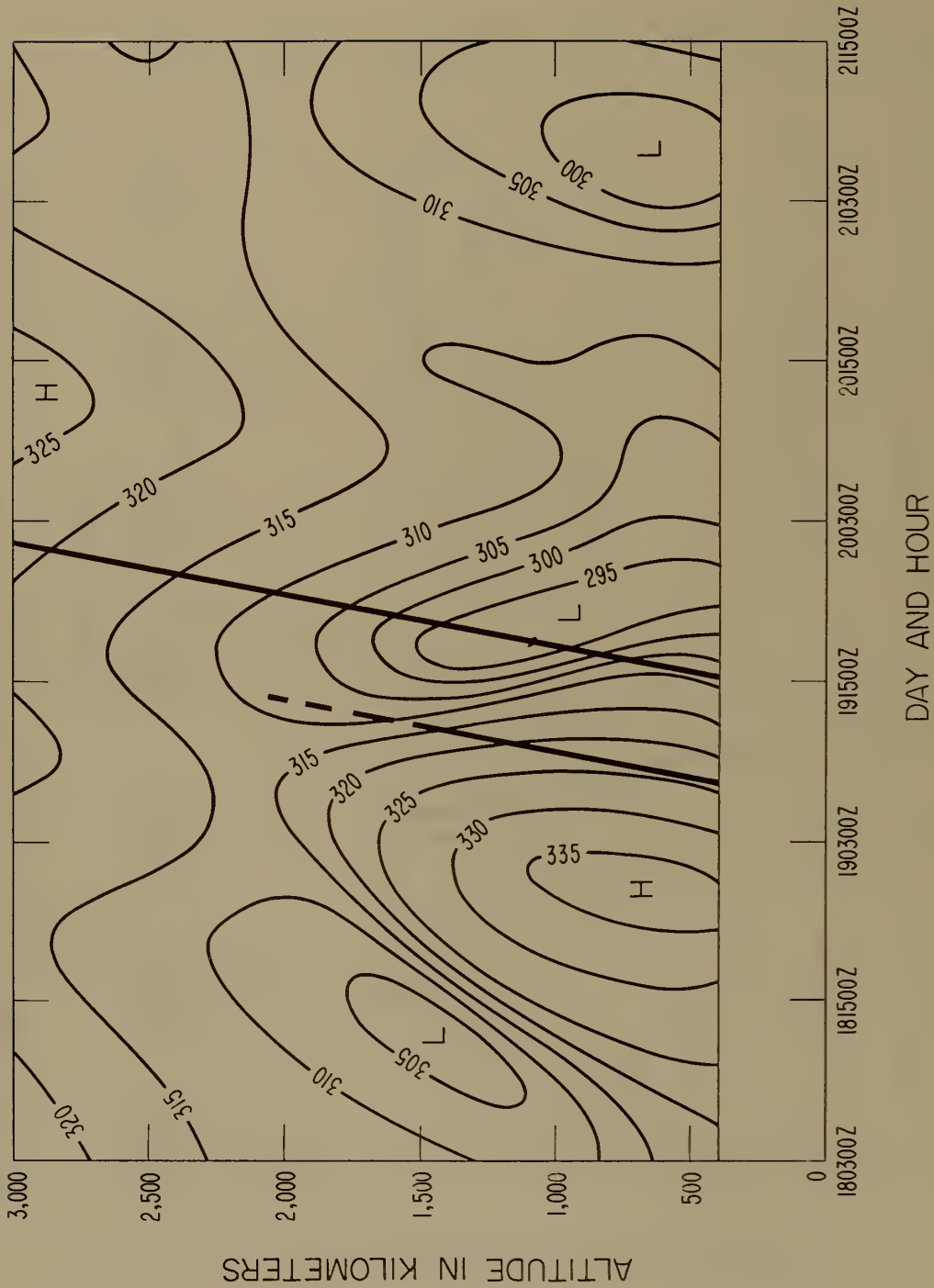


Figure 59. Time Cross-Section, Oklahoma City, Oklahoma, in A Units

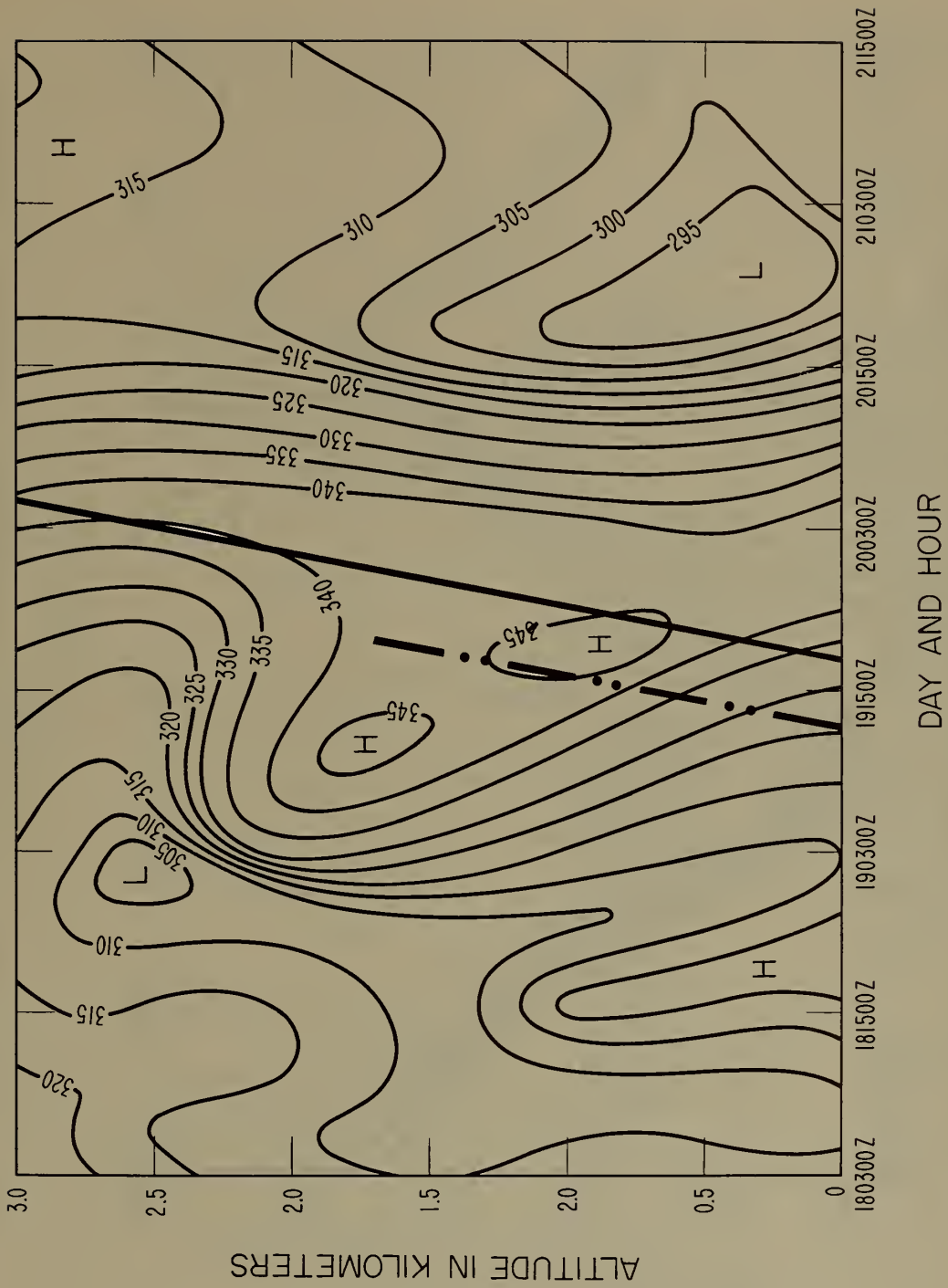


Figure 60. Time Cross-Section, Little Rock, Arkansas, in A Units

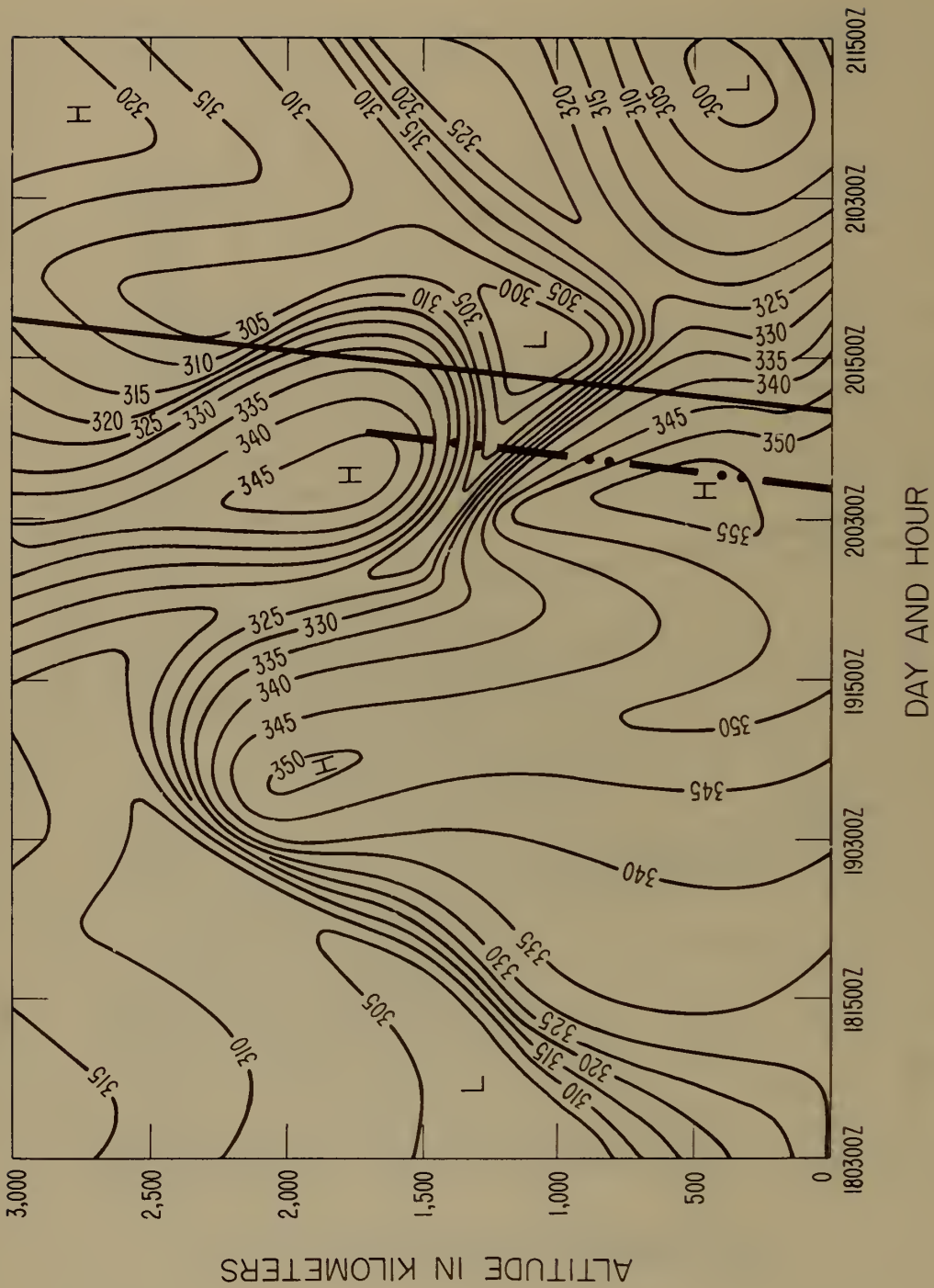


Figure 61. Time Cross Section, Lake Charles, Louisiana, in A Units

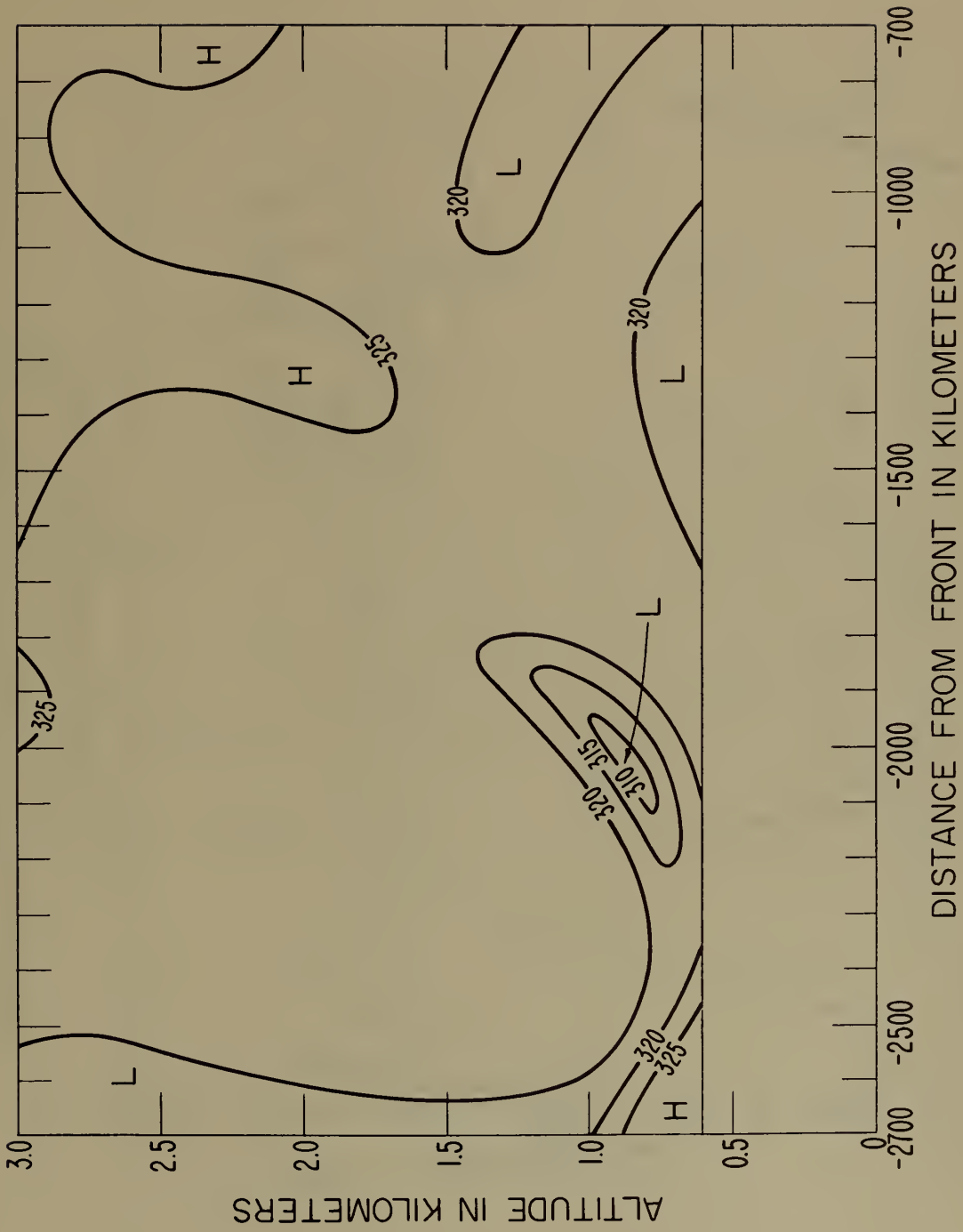


Figure 62. Epoch Chart, Glasgow, Montana, in A Units

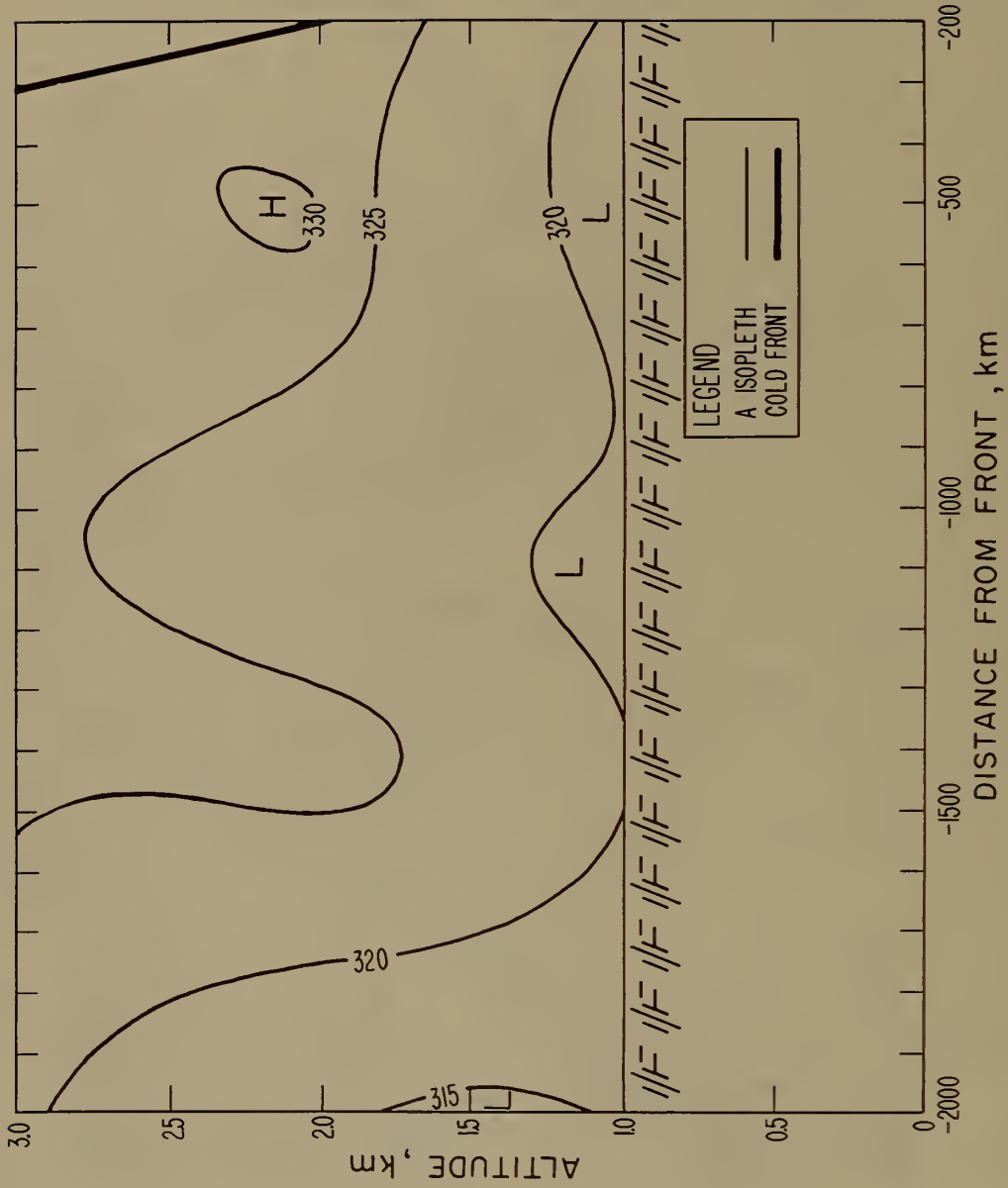


Figure 63. Epoch Chart, Rapid City, South Dakota, in A Units

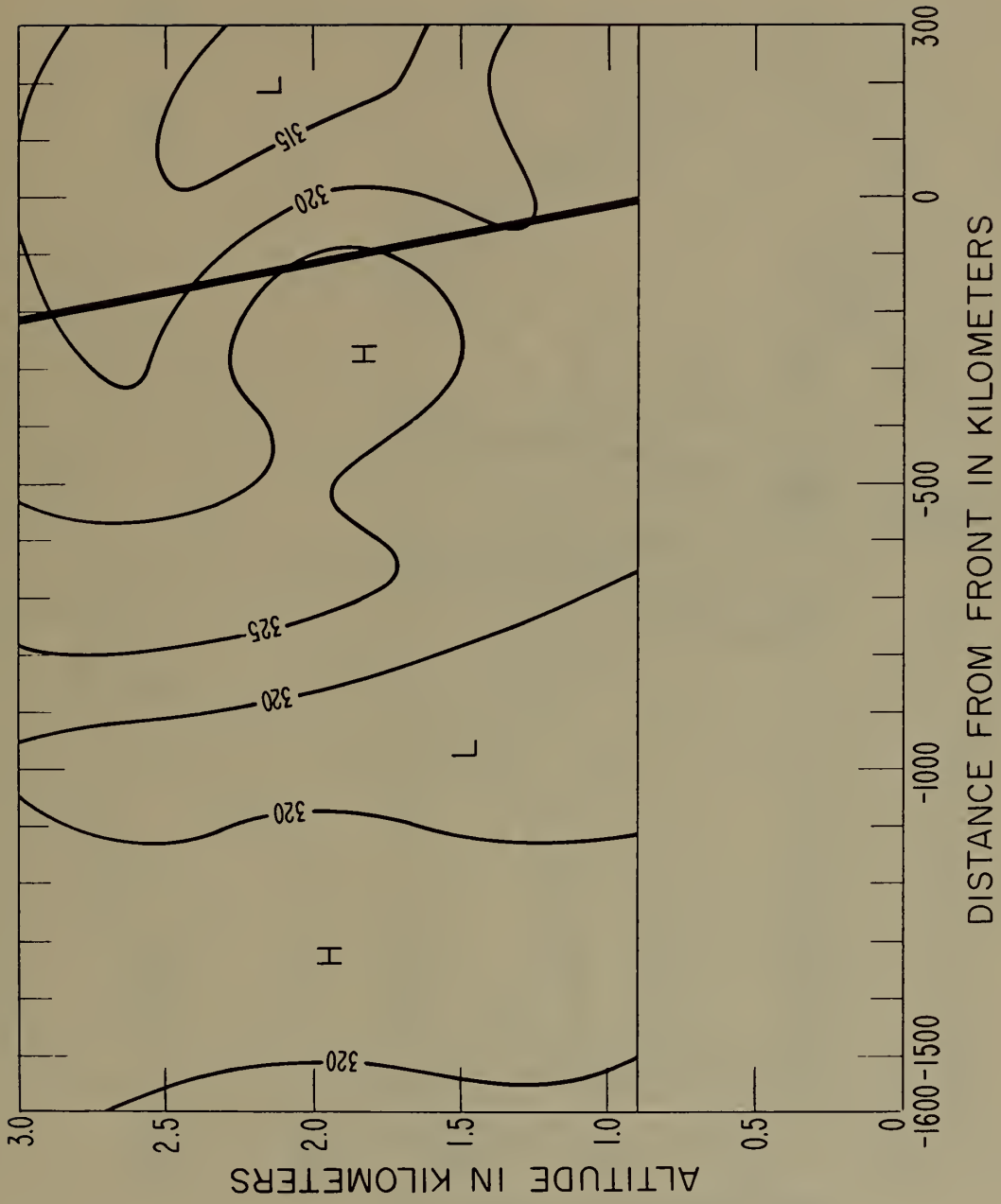


Figure 64. Epoch Chart, North Platte, Nebraska, in A Units

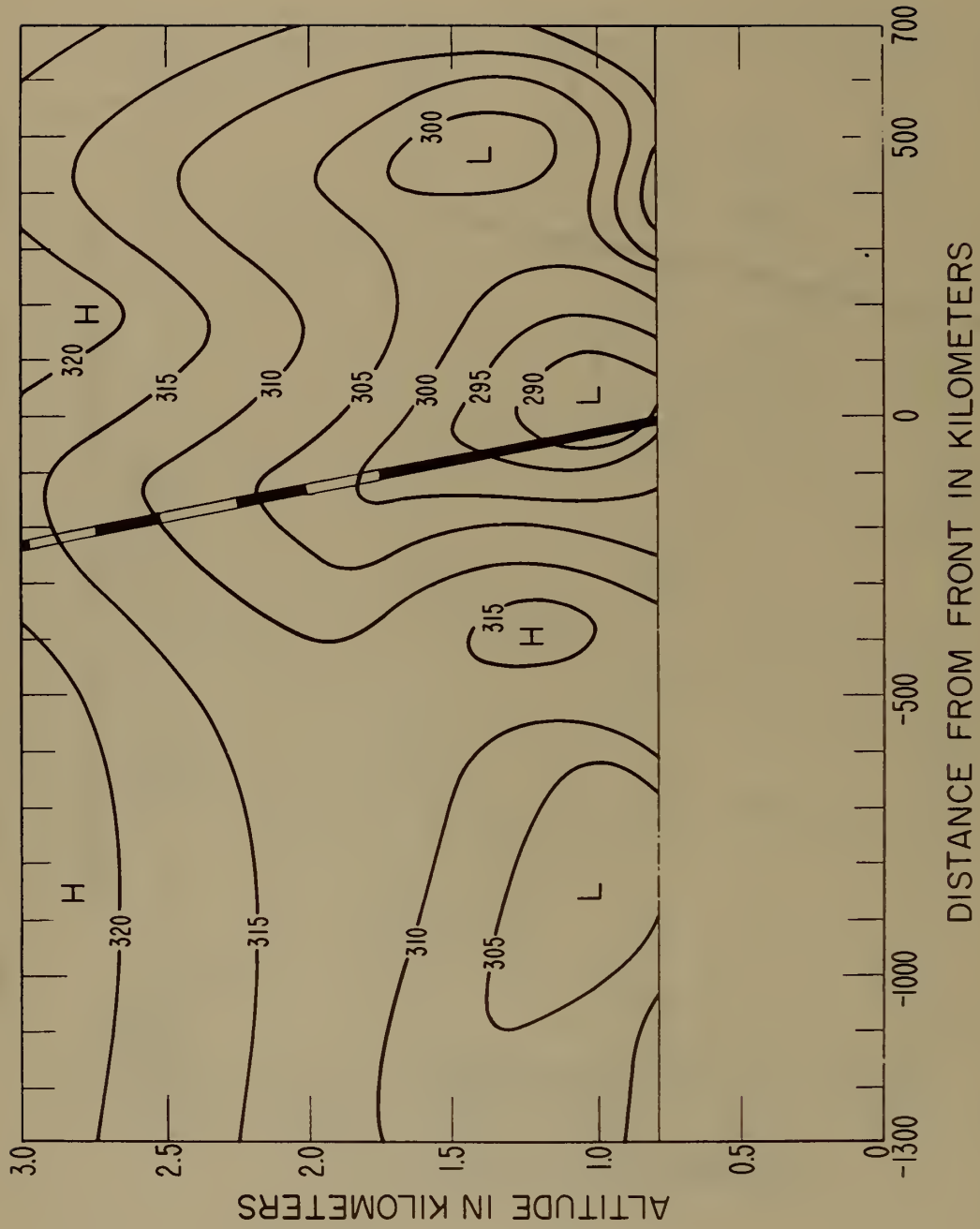


Figure 65. Epoch Chart, Dodge City, Kansas, in A Units

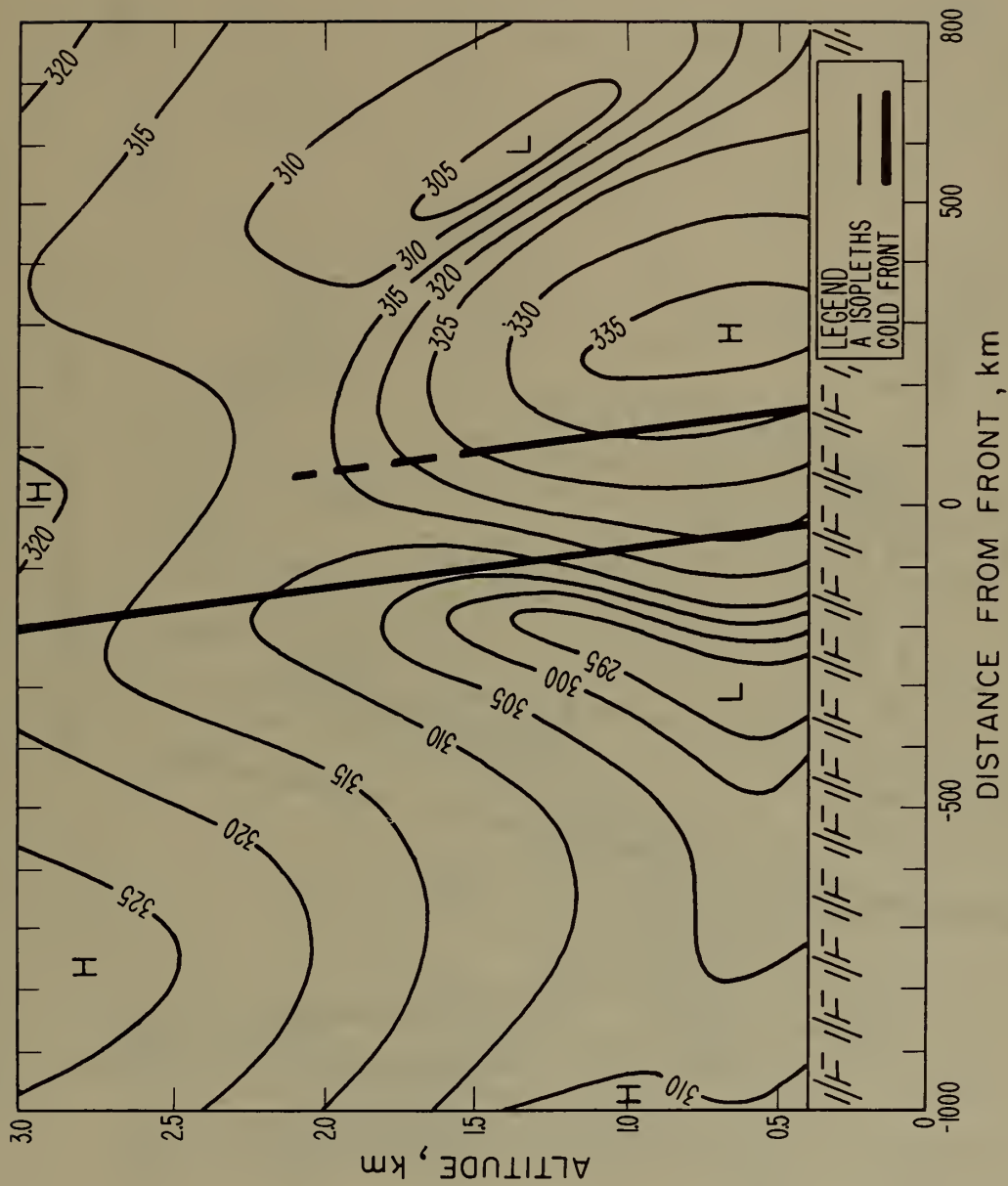


Figure 66. Epoch Chart, Oklahoma City, Oklahoma, In A Units

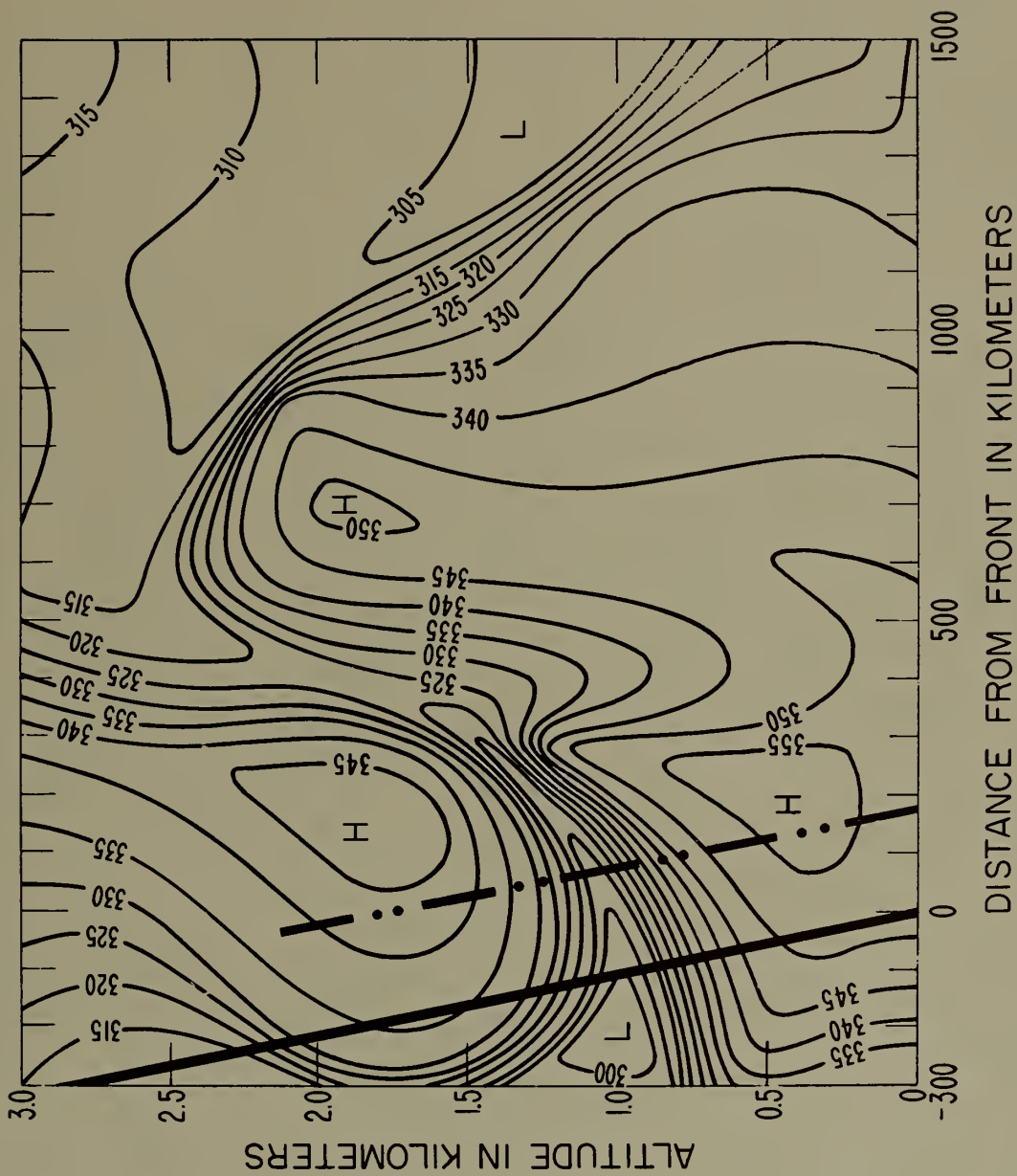


Figure 68. Epoch Chart, Lake Charles, Louisiana, in A Units



NATIONAL BUREAU OF STANDARDS

A. V. Austin, Director

THE NATIONAL BUREAU OF STANDARDS

The scope of activities of the National Bureau of Standards at its major laboratories in Washington, D.C., and Boulder, Colorado, is suggested in the following listing of the divisions and sections engaged in technical work. In general, each section carries out specialized research, development, and engineering in the field indicated by its title. A brief description of the activities, and of the resultant publications, appears on the inside of the front cover.

WASHINGTON, D. C.

Electricity. Resistance and Reactance. Electrochemistry. Electrical Instruments. Magnetic Measurements. Dielectrics. High Voltage.

Metrology. Photometry and Colorimetry. Refractometry. Photographic Research. Length. Engineering Metrology. Mass and Scale. Volumetry and Densimetry.

Heat. Temperature Physics. Heat Measurements. Cryogenic Physics. Equation of State. Statistical Physics.

Radiation Physics. X-ray. Radioactivity. Radiation Theory. High Energy Radiation. Radiological Equipment. Nuclear Instrumentation. Neutron Physics.

Analytical and Inorganic Chemistry. Pure Substances. Spectrochemistry. Solution Chemistry. Standard Reference Materials. Applied Analytical Research. Crystal Chemistry.

Mechanics. Sound. Pressure and Vacuum. Fluid Mechanics. Engineering Mechanics. Rheology. Combustion. Lenses.

Polymers. Macromolecules: Synthesis and Structure. Polymer Chemistry. Polymer Physics. Polymer Characterization. Polymer Evaluation and Testing. Applied Polymer Standards and Research. Dental Research.

Metallurgy. Engineering Metallurgy. Microscopy and Diffraction. Metal Reactions. Metal Physics. Electrolysis and Metal Deposition.

Inorganic Solids. Engineering Ceramics. Glass. Solid State Chemistry. Crystal Growth. Physical Properties. Crystallography.

Building Research. Structural Engineering. Fire Research. Mechanical Systems. Organic Building Materials. Codes and Safety Standards. Heat Transfer. Inorganic Building Materials. Metallic Building Materials.

Applied Mathematics. Numerical Analysis. Computation. Statistical Engineering. Mathematical Physics. Operations Research.

Data Processing Systems. Components and Techniques. Computer Technology. Measurements Automation. Engineering Applications. Systems Analysis.

Atomic Physics. Spectroscopy. Infrared Spectroscopy. Far Ultraviolet Physics. Solid State Physics. Electron Physics. Atomic Physics. Plasma Spectroscopy.

Instrumentation. Engineering Electronics. Electron Devices. Electronic Instrumentation. Mechanical Instruments. Basic Instrumentation.

Physical Chemistry. Thermochemistry. Surface Chemistry. Organic Chemistry. Molecular Spectroscopy. Elementary Processes. Mass Spectrometry. Photochemistry and Radiation Chemistry.

Office of Weights and Measures.

BOULDER, COLO.

Cryogenic Engineering Laboratory. Cryogenic Equipment. Cryogenic Processes. Properties of Materials. Cryogenic Technical Services.

CENTRAL RADIO PROPAGATION LABORATORY

Ionosphere Research and Propagation. Low Frequency and Very Low Frequency Research. Ionosphere Research. Prediction Services. Sun-Earth Relationships. Field Engineering. Radio Warning Services. Vertical Soundings Research.

Radio Propagation Engineering. Data Reduction Instrumentation. Radio Noise. Tropospheric Measurements. Tropospheric Analysis. Propagation-Terrain Effects. Radio-Meteorology. Lower Atmosphere Physics.

Radio Systems. Applied Electromagnetic Theory. High Frequency and Very High Frequency Research. Frequency Utilization. Modulation Research. Antenna Research. Radiodetermination.

Upper Atmosphere and Space Physics. Upper Atmosphere and Plasma Physics. High Latitude Ionosphere Physics. Ionosphere and Exosphere Scatter. Airglow and Aurora. Ionospheric Radio Astronomy.

RADIO STANDARDS LABORATORY

Radio Physics. Radio Broadcast Service. Radio and Microwave Materials. Atomic Frequency and Time-Interval Standards. Radio Plasma. Millimeter-Wave Research.

Circuit Standards. High Frequency Electrical Standards. High Frequency Calibration Services. High Frequency Impedance Standards. Microwave Calibration Services. Microwave Circuit Standards. Low Frequency Calibration Services.

NBS